

UNIVERSIDAD SAN FRANCISCO DE QUITO USFQ

COLEGIO DE CIENCIAS E INGENIERÍAS

**Mechanical, mineralogical, morphological and  
computational characterization of Ecuadorian  
Soil: A nationwide first data baseline**

Artículo académico

Paula Rafaela Betancourt Campuzano

Ingeniería Civil

Trabajo de titulación presentado como requisito para la obtención del título  
de Ingeniero Civil

Quito, 14 de mayo de 2018

UNIVERSIDAD SAN FRANCISCO DE QUITO

COLEGIO DE CIENCIAS E INGENIERÍAS

HOJA DE CALIFICACIÓN DE TRABAJO DE  
TITULACIÓN

**Mechanical, mineralogical, morphological and  
computational characterization of Ecuadorian  
Soil: A nationwide first data baseline**

*Paula Rafaela Betancourt Campuzano*

Ingeniería Civil

Calificación:

Nombre del Profesor:                      Ing. Fernando Romo, MSc.

---

Quito, 14 de mayo de 2018

## Derechos de Autor

Por medio del presente documento certifico que he leído todas las Políticas y Manuales de la Universidad San Francisco de Quito USFQ, incluyendo la Política de Propiedad Intelectual USFQ, y estoy de acuerdo con su contenido, por lo que los derechos de propiedad intelectual del presente trabajo quedan sujetos a lo dispuesto en esas Políticas.

Asimismo, autorizo a la USFQ para que realice la digitalización y publicación de este trabajo en el repositorio virtual, de conformidad a lo dispuesto en el Art. 144 de la Ley Orgánica de Educación Superior.

|                      |                                    |
|----------------------|------------------------------------|
| Firma:               | _____                              |
| Nombres y apellidos  | Paula Rafaela Betancourt Campuzano |
| Codigo:              | 00110861                           |
| Cédula de identidad: | 1716469521                         |
| Lugar y fecha:       | Quito, 14 de mayo de 2018          |

## Abstract

We introduce a first attempt to generate a nationwide data baseline of the mechanical, mineralogical and morphological characterization of Ecuadorian soil. With this aim, the analysis of unaltered soil samples corresponding to the capitals of twenty-three provinces and six other significant locations in Ecuador is performed as follows: First, the gradation and Atterberg limits allow us to obtain each sample's classification according to the Unified Soil Classification System (USCS), which provides important information regarding soil's mechanical behavior. Second, unconsolidated undrained (UU) tri-axial tests are carried out in order to determine soil's strength, i.e., internal friction angle and cohesion. Third, chemical and mineralogical features are inferred by means of energy dispersive spectroscopy (EDS) in a scanning electron microscope (SEM). Fourth, the morphology of the grains that furnish the fabric of each given soil sample is obtained by calculating parameters such as roundness, sphericity, grain volume, and grain surface area. Through 3D X-ray computed tomography (3DXRCT) of the samples the actual shape of each grain is first retrieved, and then by turning the 3DXRCT voxel-based images into mathematical functions called level sets (LS) enable us to perform calculations on the morphology of the grains. Thus, a virtual database can be created in order to generate more accurate computer models with enhanced predictive capabilities and an improved evaluation of microstructure from a real physical sample. These are the first few steps in order to develop more sophisticated computational models, which could eventually replace both: the need for extensive and costly laboratory tests to understand real natural phenomena, and the use of phenomenological models that fail to incorporate micro-mechanical and morphological effects that are key when it comes to the materials behavior. However, much remains to be done...

---

Keywords: Characterization, Mechanical, Chemical, Computational, Morphology, Ecuador, Base-line.

## Resumen

Presentamos un primer intento de generar una línea base de datos a nivel nacional de la caracterización mecánica, mineralógica y morfológica del suelo ecuatoriano. Con este objetivo, el análisis de muestras de suelo inalteradas correspondientes a las capitales de veintitrés provincias y otros seis lugares significativos en Ecuador se realiza de la siguiente manera: Primero, el análisis de la distribución de tamaño de partículas y los límites de Atterberg nos permiten obtener la clasificación de cada muestra de acuerdo con el Sistema Unificado de clasificación de Suelo (USCS), que proporciona información importante sobre el comportamiento mecánico del suelo. En segundo lugar, se llevan a cabo ensayos tri-axiales no drenados no consolidados con el fin de determinar la resistencia del suelo, es decir, el ángulo de fricción interna y la cohesión. En tercer lugar, las características químicas y mineralógicas se obtienen por medio de la espectroscopia de energía dispersiva (EDS) en un microscopio electrónico de barrido (SEM). En cuarto lugar, la morfología de los granos se obtiene calculando parámetros tales como redondez, esfericidad, volumen de grano y área de superficie del grano. A través de la tomografía computarizada de rayos-X 3D (3DXRCT) de las muestras. Se recupera primero la forma real de cada grano y luego se convierten las imágenes en funciones matemáticas llamadas 'Level Sets' (LS). Las mismas que nos permiten realizar cálculos sobre la morfología de los granos. Por lo tanto, se puede crear una base de datos virtual para generar modelos matemáticos más precisos con capacidades predictivas y una evaluación mejorada de la micro-estructura a partir de una muestra física real. Estos son los primeros pasos para desarrollar modelos computacionales más sofisticados, que eventualmente podrían reemplazar a ambos: la necesidad de extensas y costosas pruebas de laboratorio para comprender los fenómenos naturales, y el uso de modelos fenomenológicos que no incorporan mecanismos micro-mecánicos y morfológicos, efectos que son clave cuando se trata del comportamiento del material. Sin embargo, queda mucho por hacer ...

---

Palabras clave: Caracterización, Mecánico, Químico, Computacional, Morfología, Ecuador, Línea base

## Table of Contents

|          |   |           |
|----------|---|-----------|
| <b>1</b> | <b>Introduction</b>                                       | <b>8</b>  |
| <b>2</b> | <b>Sampling points and Mineralogical characterization</b> | <b>11</b> |
| 2.1      | Mineralogical characterization (EDS-SEM)                  | 12        |
| <b>3</b> | <b>Mechanical characterization</b>                        | <b>17</b> |
| 3.1      | USCS classification                                       | 17        |
| 3.2      | Shear strength  | 22        |
| <b>4</b> | <b>Morphological characterization</b>                     | <b>31</b> |
| <b>5</b> | <b>Conclusion</b>   | <b>37</b> |
|          | <b>References</b>   | <b>40</b> |
| <b>A</b> | <b>Appendix</b>   | <b>45</b> |
| A.1      | Cuenca  | 45        |
| A.2      | Guaranda  | 47        |
| A.3      | Azogues   | 49        |
| A.4      | Tulcán  | 51        |
| A.5      | Riobamba  | 53        |
| A.6      | Latacunga   | 55        |
| A.7      | Cotopaxi  | 57        |
| A.8      | Machala   | 59        |
| A.9      | Esmeraldas  | 61        |
| A.10     | Pedernales  | 63        |
| A.11     | Guayaquil   | 65        |
| A.12     | Durán   | 67        |
| A.13     | Ibarra  | 69        |
| A.14     | Loja  | 71        |
| A.15     | Babahoyo  | 73        |
| A.16     | Portoviejo  | 75        |
| A.17     | Jaramijó  | 77        |
| A.18     | Manta   | 79        |
| A.19     | Macas   | 81        |
| A.20     | Tena  | 83        |
| A.21     | Puerto Franciso de Orellana                               | 85        |
| A.22     | Puyo  | 87        |
| A.23     | Quito   | 89        |
| A.24     | Santa Elena   | 91        |
| A.25     | Santo Domingo   | 93        |
| A.26     | Nueva Loja  | 95        |
| A.27     | Zamora  | 97        |
| A.28     | Baños   | 99        |
| A.29     | Ambato  | 101       |

## List of Tables

|   |  |    |
|---|--|----|
| 1 | Locations where the samples were taken . . . . . | 15 |
| 2 | Geological features and description . . . . .    | 16 |
| 3 | Results . . . . .                                | 19 |

## List of Figures

|    |  |    |
|----|--|----|
| 1  | Process for the generation of the first nationwide database . . . . .                          | 10 |
| 2  | Exact locations of sampling points . . . . .   | 13 |
| 3  | Cumulative Distribution curves . . . . .   | 21 |
| 4  | Cumulative Distribution curves for two cities with the same amount of sand and fines . . . . . | 22 |
| 5  | Friction angle for all the samples . . . . .   | 23 |
| 6  | Stress-strain curves: a) Babahoyo, b) Latacunga, c) Riobamba, and d) Tena . . . . .            | 25 |
| 7  | Coulomb's envelope: a) Babahoyo, b) Latacunga, c) Riobamba, and d) Tena. . . . .               | 26 |
| 8  | Cohesion for all the samples . . . . .   | 28 |
| 9  | Stress-strain curves:a) Loja, b) Santa Elena, c) Latacunga, and d) Macas. . . . .              | 29 |
| 10 | Coulomb's envelope:a) Loja, b) Santa Elena, c) Latacunga, and d) Macas. . . . .                | 30 |
| 11 | 3DXRCT image slice of Jaramijó's soil sample . . . . .   | 32 |
| 12 | 8 Level Set grains avatar from Jaramijó's soil sample. . . . .                                 | 33 |
| 13 | umulative particle size distribution curve from Jaramijó's soil sample . . . . .               | 34 |
| 14 | Grain diameters distribution . . . . .   | 34 |
| 15 | Aspect ratio distributio . . . . .   | 35 |
| 16 | Roundness distribution . . . . .   | 36 |
| 17 | Minimum principal directions distribution . . . . .  | 36 |
| 18 | Volume-surface ratio distribution . . . . .  | 37 |
| 19 | Sphericities distribution . . . . .  | 37 |
| 20 | Sphericities distribution . . . . .  | 38 |

# Mechanical, mineralogical, morphological and computational characterization of Ecuadorian Soil: A nationwide first data baseline

Paula R. Betancourt<sup>1</sup>, Alex X. Jerves<sup>1\*</sup> Carlos F. Ávila<sup>2</sup> and Maurizio Mulas<sup>3</sup>

<sup>1</sup> *College of Science & Engineering, Universidad San Francisco de Quito, Quito Pichincha 1712841 Ecuador*

<sup>2</sup> *Departamento de Ingeniería Civil y Ambiental, Escuela Politécnica Nacional, Quito, Pichincha 170517, Ecuador,*  
*carlos.avila@epn.edu.ec, http://www.epn.edu.ec*

<sup>3</sup> *Facultad de Ingeniería en Ciencias de la Tierra, Escuela Superior Politécnica del Litoral, Guayaquil, Guayas*  
*09015863, Ecuador, mmulas@espol.edu.ec, http://www.espol.edu.ec*

## 1 Introduction

Soil is one of the world's most important natural resources [1]. It plays a fundamental role in society with crucial uses and applications in agriculture, mining, urban architecture and civil engineering constructions, among others. This novel material has been broadly studied since ancient times but it keeps offering numerous challenges, most of which arise from natural occurring phenomena. Thus, a proper testing and comprehension of soil characteristics is of uttermost importance given its heterogeneous nature and the sophisticated knowledge needed to comprehend it [2]. In the same way, the understanding of soil behavior has become a priority in countries that are susceptible to geological hazards such as earthquakes, volcanic eruptions, landslides and floods. In particular, Ecuador, a South-American country is located on a hazard-prone zone known as the "Pacific Ring of Fire". Consequently, the country has a long history of strong earthquakes, large landslides and explosive volcanic eruptions which in the past have had fatal repercussions for Ecuadorian people, socio-economic systems, environment and infrastructure.

Despite the high risk of natural disasters in Ecuador, there is currently no complete study containing fundamental soil properties of the entire country. Previous efforts have been made to generate soil maps with reliable information of soil mechanical characteristics (i.e., seismic microzoning), agricultural soil science (i.e., chemical and biological composition of soils) and soil classification (i.e., soil taxonomy). However, these studies are non-consistent, have been displayed

\*Corresponding author. E-mail: ajerves@usfq.edu.ec (Alex X. Jerves)



separately, or have not yet been performed across the entire Ecuadorian territory due to the complexity of data collection, lack of standardized procedures and high costs of soil exploration. Hence, the generation of a standard and complete database of Ecuadorian soils characteristics is essential. It will provide new perspectives for civil engineering, mining, agriculture and more importantly computer simulations applied to prediction and prevention of life losses and infrastructure damage in case of natural catastrophes.

Thus, in the present work, we propose a first attempt to generate a nationwide data base-line about the mechanical, mineralogical and morphological characterization of Ecuadorian soil. To begin with the development of such a database, twenty nine points of interest were selected throughout Ecuador's continental territory. With this aim, population density, existing infrastructure as well as previous catastrophic events were taken into account. Then, samples were obtained and thoroughly analyzed. With this data, risk prevention maps can be tailored as well as more accurate mathematical models and computational simulations with predictive capabilities that can include micro-structural properties of real soil samples.

For the generation of the aforementioned database, once the undisturbed soil samples are extracted from the proposed locations, the rest of characterization process follows the algorithmic scheme depicted by Figure 1. First, we obtained the mechanical properties of the samples by performing different geomechanical tests. For instance, each sample is classified according to the Unified Soil Classification System (USCS) [3], developed by Arthur Casagrande (1947), which is based on three fundamental characteristics: (i) predominant particle size range, (ii) Atterberg limits, and (iii) particle size distribution. Then, we perform unconsolidated undrained (UU) triaxial tests to determine the soil's cohesion ( $c$ ) and internal friction angle ( $\Phi$ ). These parameters define the shear strength of the soil being tested according to the *Mohr-Coulomb failure criterion* (MC)[4]. Second, each sample went through an Energy Dispersive Spectroscopy (EDS) analysis process on a Scanning Electron Microscope (SEM), and we inferred it's mineralogical composition. Third, given the importance of the role played by grain morphology in soil's behavior [5], we determined the morphological properties of the grains that constitute the samples. The real shapes of the soil grains are obtained by 3D X-ray computed tomography (3DXRCT), and these 3D images are turned into mathematical functions called Level Sets (LS) [6]. With these digitalized grains we can obtain morphological parameters such as sphericity and roundness, which are particularly useful

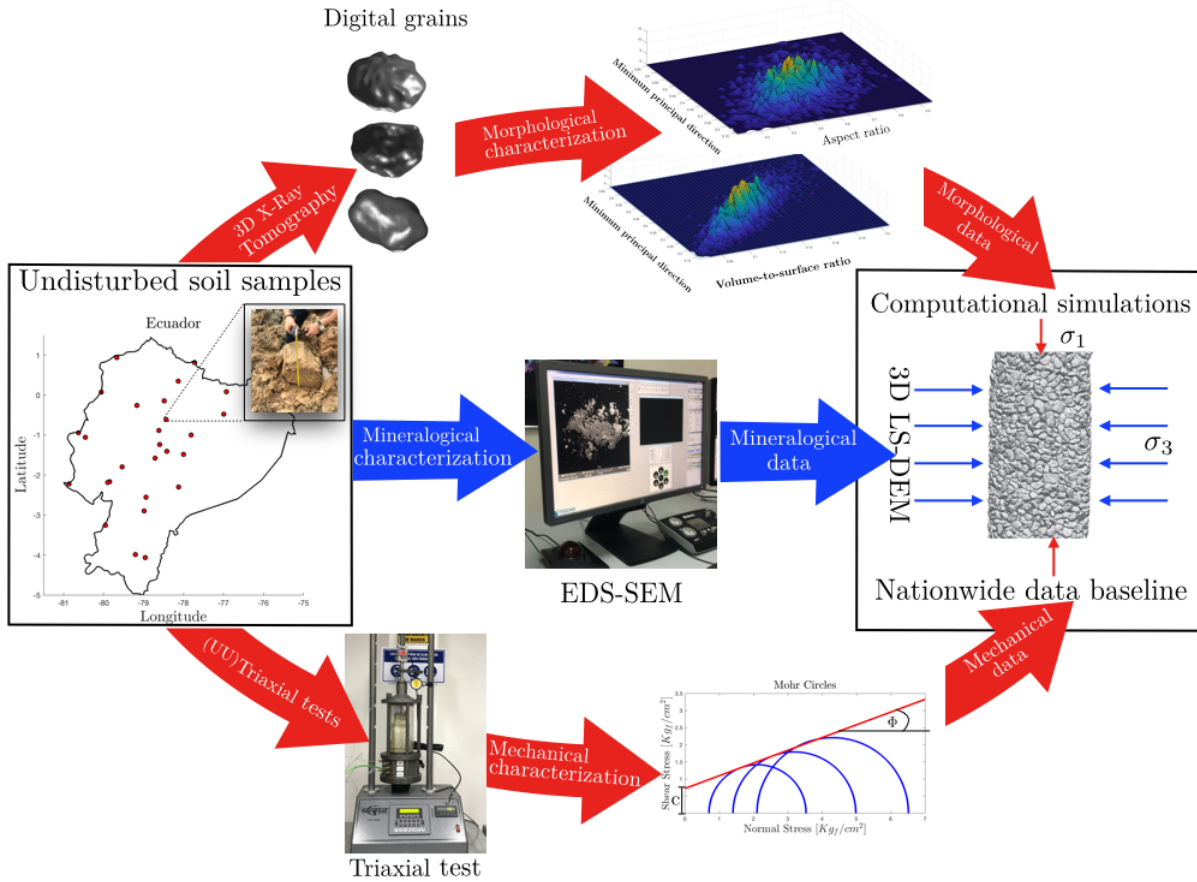


Figure 1: Generation of the first nationwide data baseline of Ecuadorian soil characteristics. First, undisturbed samples are taken from 29 strategic locations in Ecuador which are then put through: (i) geomechanical tests to establish parameters related to soil’s shear strength (i.e., internal friction angle  $\Phi$ , cohesion  $c$ ) and USCS soil classification, (ii) energy dispersive X-Ray spectroscopy on a scanning electron microscope in order to analyze the constitutive minerals of each sample, (iii) 3D X-Ray Tomography to obtain digitized grains for morphology measurements to be calculated (e.g., roundness, sphericity), and computational simulations with DEM schemes. Finally, the mechanical, mineralogical and morphological data serve as input for computational simulations and risk prevention / prediction of natural disasters.

given their widespread use within soil mechanics [5].

With the output from the three characterization processes previously described, the nationwide database is generated by gathering all the mechanical, mineralogical and morphological information, which in turn will be used for computational simulations with Level Set discrete element method (LS-DEM) and other important applications in science, industry and construction [5, 7–9]. This will potentially allow a faster and less expensive way to study different soil phenomena that affect infrastructure, as well as an important contribution to the risk prevention of natural disasters.

Finally, it is important to highlight the fact that this is only a first step within the creation of a complete database of Ecuadorian soil characteristics. This database is intended to contribute to the optimization of soil exploration, and provide with sufficient data for the generation of maps with geographic information systems (GIS). Moreover, the creation of these maps and the obtained characterization parameters will facilitate effective disaster risk identification, prevention, preparedness and response. Although the current database has been initially built out of twenty nine location points, the ultimate goal is to add as many sampling points as possible to improve the accuracy and effectiveness of the mechanical, mineralogical and morphological Ecuadorian soil characterization.

## 2 Sampling points and Mineralogical characterization

Continental Ecuador can be divided into three large regions: the Coastal Plain, the Andean Highlands and the Amazon Region [10]. Each one of these presents a very distinct geography, which in turn led to unique soil formations with distinctive characteristics. The soil sampling locations were selected according to population density and existing infrastructure such as roads, bridges, water supply networks, sewers, electrical grids and telecommunications, since these places will suffer the most serious consequences in case of a natural disaster. Thus, following this sampling criterion, the capitals of the 23 provinces of Ecuador were sampled, as close as possible to the city center, and 6 other locations of high importance. The exploration method used for sample recovery was test pits [11] which allowed us to get all of the 29 undisturbed samples. Thus, a representative portion of soil that retains its basic conditions such as mineralogical composition, consolidation, structure and water content was obtained. Blocks of thirty by thirty [cm] were cautiously extracted. The sampling process consisted in removing the organic layer of soil, which is approximately of eleven to forty-four [cm] [12, 13], then manually a block was carved until the required size was reached. For the sample not to lose its properties (i.e. water content [%] and structure) it was covered with plastic, labeled and carefully transported. The exact locations of the sampling points are shown in Figure 2 as well as the geological formations where those samples were taken, while the names of the cities corresponding to each number, geological formation's legend and coordinates (UTM WGS84) are shown in Table 1.

The city of Pedernales, located in the province of Manabí, in the Coastal Plain region, was

sampled considering that a historic 7.8  $M_W$  (moment magnitude) earthquake left the city in ruins the past April 16 of 2016 and aftershocks continue to hit the zone. Most of the buildings after the earthquake were marked for demolition and the human losses added up to approximately 602 [14]. Likewise, Manta is the most populated metropolitan area of Manabí and it possesses one of the most important international ports of the country. Therefore, it has a strong dynamic economy where nine out of the ten largest companies of the province are located. On the other hand, the city of Jaramijó was chosen as a checking point that served to calibrate equipment as well as carry out the whole algorithmic procedure described by Figure 1 for first time. Moreover, in the province of Guayas the city of Durán located by the Guayas river was sampled taking into account that it is the second most populated area in its province after Guayaquil.

## 2.1 Mineralogical characterization (EDS-SEM)

The mineralogical composition of soil has a direct relation with its shear strength, especially for fine-grained soils as a result of the importance of inter-particle forces and the shape of the grains. The cementation between grains can be due to chemical bonds or physico-chemical bonds [16]. Therefore, the chemical analysis of the 29 proposed locations was carried out with energy dispersive spectroscopy (EDS) on a scanning electron microscope (SEM). This is a chemical microanalysis technique that detects X-Rays emitted from the soil samples in order to obtain its elemental composition.

Clay particles are the smallest of all ( $< 2 \mu\text{m}$ ) and consist of kaollinite, illite and smectite. Kaollinite clay is usually found in moist climates like tropical rainforest zones and in Ecuador the Amazon region is mostly tropical rainforest which agrees with the fact that most of the cities located there have a USCS classification of CL (see, section 3). Hence cities such as Nueva Loja, Puerto Francisco de Orellana, Tena and Zamora were sampled. While silts (0.0039-0.0625 mm), mostly found in the Andean Highlands, are composed of quartz, feldspars, chlorites, micas, and are mostly carbonates. Clays present more cohesion than silts because they are formed from thin plate-shaped particles that are adhered by van der Waals forces and hydrogen bonds [17].

The soil matrix is usually more stable when calcium carbonates or magnesium carbonates are present due to the improvement of inter-particulate bonding [18]. Thus, calcium-rich soils were found in Azogues and Santa Elena and magnesium-rich soils were found in Manta and Pedernales.

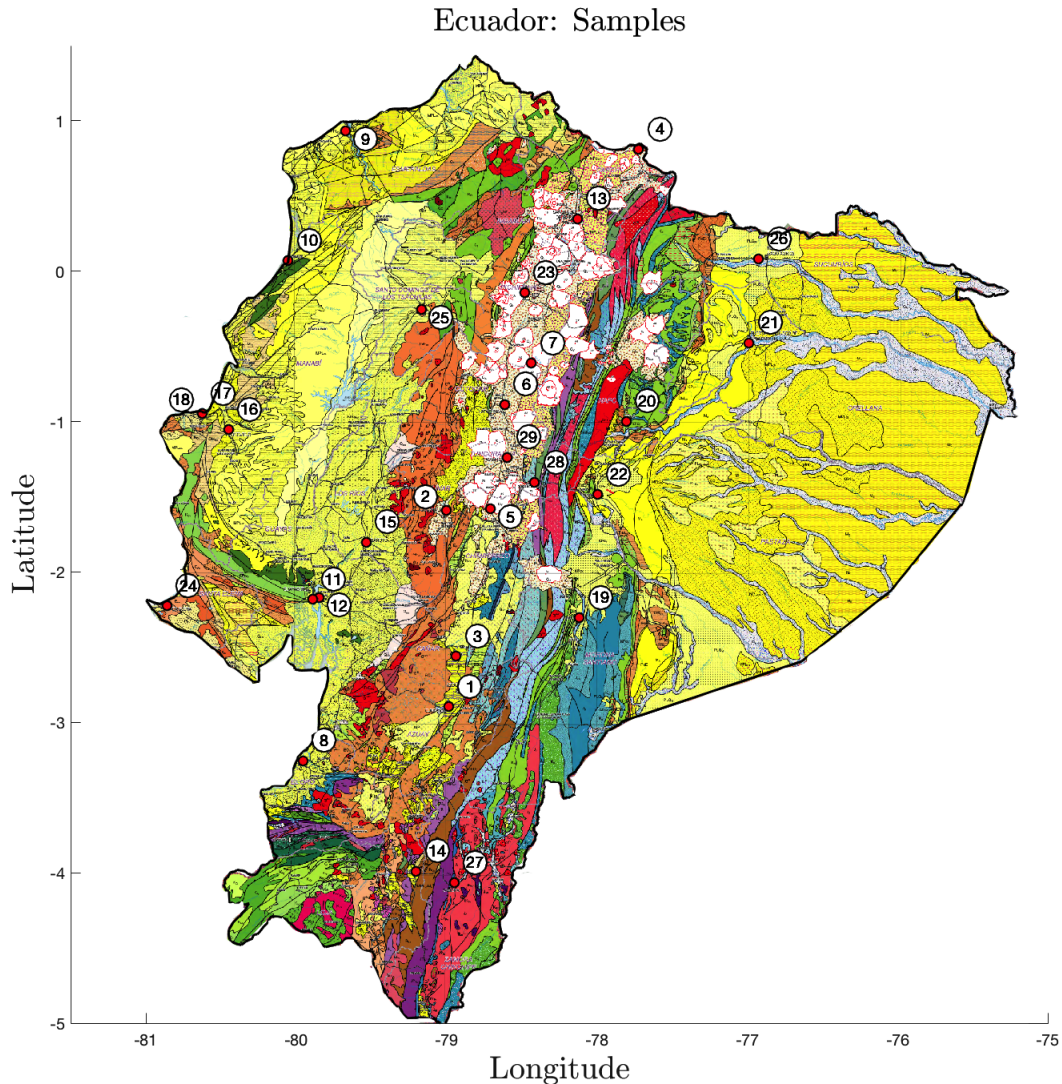


Figure 2: Exact locations of the 29 sampled points and corresponding geological formations [15].

Iron and Aluminum are two elements acting as binding agents that are key in soil aggregation and structural formation and they were found in abundance in the Amazon region. Furthermore, titanium oxides are commonly found in silts and sands as a mineral from igneous rocks and this element is found in Guaranda and Cotopaxi.

Sodium Chloride ( $NaCl$ ) has an important effect on engineering properties of soil. According to Durotoye et al. [19] the optimum moisture content, liquid limit as well as the plastic limit decrease when there is an increase in  $NaCl$ . Consistently, soils near the Pacific Ocean are expected to have higher content of  $NaCl$ . Moreover, Ecuador is a country that has 27 still active volcanoes [20], which represent an imminent risk for population in case of any volcanic hazard such as lahars, lava

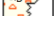
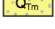
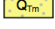
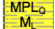
flows, partial collapse of the volcanic edifice, pyroclastic density currents among others. Taking this into account, samples of volcanic soil were extracted from the Andean region cities and from the hillside of the Cotopaxi volcano which is covered by abundant ice and is located eastward of Latacunga in the province of Cotopaxi [21], considering that in case of any hazard the populated zone of Los Chillos valley will be directly exposed to its threats. In addition, in the Andean Highlands the city of Baños was also sampled considering it is one of the most touristic places of the country and the Tungurahua volcano is only 8.8 [km] away.

Although at least one sampling point per province is not representative at all, more points will be added over time. The main objective is to start generating a database of Ecuadorian soil's characteristics which does not currently exist. This first nationwide database is not only experimental (i.e. mechanical properties, chemical analysis) but also computational. It includes real images of the grains used for determining its morphology and for simulations in DEM (Discrete element method). Furthermore, these virtual grains are to be reproduced in large quantities by means of a cloning algorithm [6].

The geologic features found throughout Ecuador determine the type of soil found in specific locations. Thus, in Table 2, the formation found in each point sampled is listed and accompanied by a brief description [15]. According to this table, the cities of the Andean Highlands are mainly distal facies formed by primary and reworked pyroclasts, debris avalanche, lahars as well as lava flow. This, in fact, is expected, considering that the area is surrounded by volcanoes. Moreover, the north part of this zone is dominated by a USCS classification of silts, verified by the composition of pyroclasts mostly fine ashes and tuffs. In addition, these fine grains are cemented by amorphous clay material, silica, iron oxide and calcite. The cementing properties of this type of soil confirm the high values of cohesion of the Andean region  $c_{mean} = 1.5 [Kg_f/cm^2]$  and also  $\Phi_{mean} = 21^\circ$ . This pyroclastic projections are characteristics of quaternary volcanism, and reached a large extension which covers approximately a third of the country [22].

Also, the locations of Azogues (ML), Cuenca (MH) and Loja (SM) in the southern Andean region are the oldest geological formations. For instance, Cuenca has boulders and sands as part of an alluvial deposit, while Azogues and Loja are composed by a group of formations which include mostly sandstones, shales and tuffs. On the other hand, 50 % of the locations sampled in the Amazon region correspond to the Mera formation. However, all formations from these specific

Table 1: Locations where the samples were taken corresponding to the numbers exhibited in Figure 2, the geological formation legend and their exact UTM coordinates (WGS84, zone 17S).

| Location No. | Location              | Legend  | Easting [UTM] | Northing [UTM] |
|--------------|-----------------------|---|---------------|----------------|
| 1            | Cuenca                |    | 723807        | 9679649        |
| 2            | Guaranda              |    | 722322        | 9824078        |
| 3            | Azogues               |    | 729323        | 9716750        |
| 4            | Tulcán                |    | 196889        | 10089584       |
| 5            | Riobamba              |    | 755014        | 9825106        |
| 6            | Latacunga             |    | 765494        | 9901893        |
| 7            | Cotopaxi              |    | 785233        | 9932464        |
| 8            | Machala               |    | 615899        | 9640101        |
| 9            | Esmeraldas            |    | 647689        | 10103051       |
| 10           | Pedernales            |    | 605031        | 10007816       |
| 11           | Guayaquil             |    | 622935        | 9758640        |
| 12           | Durán                 |    | 628051        | 9760125        |
| 13           | Ibarra                |    | 819358        | 10038708       |
| 14           | Loja                  |    | 699452        | 9558774        |
| 15           | Babahoyo              |    | 662962        | 9800740        |
| 16           | Portoviejo            |    | 560919        | 9883569        |
| 17           | Jaramijó              |  | 541346        | 9895403        |
| 18           | Manta                 |  | 541408        | 9895403        |
| 19           | Macas                 |  | 820647        | 9745075        |
| 20           | Tena                  |  | 187536        | 9889495        |
| 21           | Pto. Fco. de Orellana |  | 278556        | 9947395        |
| 22           | Puyo                  |  | 166571        | 9835661        |
| 23           | Quito                 |  | 780446        | 9984238        |
| 24           | Santa Elena           |  | 515497        | 9753993        |
| 25           | Santo Domingo         |  | 703623        | 9971736        |
| 26           | Nueva Loja            |  | 285432        | 10008841       |
| 27           | Zamora                |  | 727328        | 9550379        |
| 28           | Baños                 |  | 787620        | 9844655        |
| 29           | Ambato                |  | 767392        | 9863062        |

locations are constituted, up to some point, by shale, which is a clastic sedimentary rock built up of a mix of clay minerals and silt sized grains. Consistently, the predominant soil type of the zone is clay and it has the highest percentage of cohesion contribution to shear strength (see, subsection 3.2). Furthermore, the sampling points in the Coastal Plain region such as Guayaquil and Durán

are located in the Cayo formation, which is formed by greywacke and basaltic mantles, that are characterized by their hardness. Specifically, the soil sample from Guayaquil has a  $\Phi = 28.2^\circ$ , one of the largest. Moreover, Jaramijó and Manta, both correspond to the Tablazo formation and are mainly old terraces formed by skeletal fossil fragments found in sedimentary rocks. Both soil samples have a low friction angle of  $0.27^\circ$  and  $0.18^\circ$  respectively and a low value of cohesion of  $0.28 [Kg_f/cm^2]$  and  $0.18 [Kg_f/cm^2]$ . Furthermore, the cities of Machala (SM), Pedernales (SC), and Babahoyo (MH) are marine terraces constituted of estuarine marine clays, where Pedernales is the location with highest content of clay.

Table 2: Geological features and description according to all 29 sampled locations.

| Location No. | Geological feature             | Description                                 |
|--------------|--------------------------------|---|
| 1            | Quaternary alluvial deposit    | Blocks, boulders and sands                  |
| 2            | Chimborazo volcano deposits    | Primary and reworked pyroclasts             |
| 3            | Azogues group                  | Clays and sandstones                        |
| 4            | Chaquilulo volcano deposits    | Distal primary and reworked pyroclasts      |
| 5            | Chimborazo volcano deposits    | Distal primary and reworked pyroclasts      |
| 6            | Cotopaxi volcano deposits      | Distal primary and reworked pyroclasts      |
| 7            | Cotopaxi volcano deposits      | Median primary and reworked pyroclasts      |
| 8            | Quaternary marine deposits     | Marine terrace                              |
| 9            | Borbón formation               | Tuffaceous sandstones                       |
| 10           | Quaternary marine deposits     | Estuarine marine clays                      |
| 11           | Cayo formation                 | Greywacke, shales, basaltic mantles         |
| 12           | Cayo formation                 | Greywacke, shales, basaltic mantles         |
| 13           | Imbabura volcano deposits      | Median primary and reworked pyroclasts      |
| 14           | Quillollaco group              | Conglomerates, shales, sandstones and tuffs |
| 15           | Quaternary marine deposits     | Estuarine marine clays and clayey silts     |
| 16           | Onzole formation               | Shales, siltstones                          |
| 17           | Tablazo formation              | Bioclastic marine terraces                  |
| 18           | Tablazo formation              | Bioclastic marine terraces                  |
| 19           | Mera formation                 | Terraces: conglomerates, sands and shales   |
| 20           | Tena formation                 | Shales, red layers                          |
| 21           | Alluvial deposit               | Blocks, boulders and sands                  |
| 22           | Mera formation                 | Terraces: conglomerates, sands and shales   |
| 23           | Pichincha volcano deposits     | Median primary and reworked pyroclasts      |
| 24           | Azúcar formation               | Sand and shales                             |
| 25           | San Tadeo formation            | Median primary and reworked pyroclasts      |
| 26           | Mera formation                 | Terraces: conglomerates, sands and shales   |
| 27           | Quaternary alluvial deposit    | Blocks, boulders and sands                  |
| 28           | Tungurahua volcano deposits    | Median primary and reworked pyroclasts      |
| 29           | Charihuairazo volcano deposits | Distal primary and reworked pyroclasts      |



### 3 Mechanical characterization

#### 3.1 USCS classification

The Unified Soil Classification System (USCS) allows us to categorize the soils from the proposed locations according to their mechanical properties following the *ASTM D2487-11* standard [3]. First, this method requires to establish if the soil is highly organic. If it is not, particle size analysis must be performed based on the *ASTM D422-17* standard [23] and the corresponding gradation curve is obtained. Second, the amount of material passing the sieves of 3 (in), No.4 (4.75 mm) and No.200 (75  $\mu\text{m}$ ) will define if the soil is either gravel, sand, silt or clay. If more than 50 % of the particles are retained on the No.200 then the soil is known as coarse-grained and most of the classification will follow from the gradation curve and it is then catalogued as gravel (G) or sand (S) either well (W) or poorly (P) graded (SW-SP-GW-GP). A soil can be considered well graded if it meets the criteria for the coefficient of uniformity  $C_u$  (defined as the ratio of particle diameter at sixty percent finer to the diameter at ten percent finer on the cumulative particle-size distribution curve ( $C_u = D_{60}/D_{10}$ )), and the coefficient of curvature  $C_c$  (which compares the slope of the curve that represents the smaller particles to the slope of the curve above it ( $C_c = (D_{30})^2/(D_{10})(D_{60})$ )). Thus for a gravel to be well graded:  $C_u > 4$  and  $1 < C_c < 3$ , while for a sand:  $C_u \geq 6$  and  $1 < C_c < 3$ . Otherwise, they will be classified as poorly graded [3].

On the other hand, if 5 % or more of the particles pass the No. 200 sieve both grain size distribution and soils plasticity have an important effect. Hence, the so-called, Atterberg Limits i.e. plastic limit (roll and thread method) and liquid limit (Casagrande's method) must be obtained following the *ASTM D4318-17* standard [24]. For instance, coarse-grained soils are now accompanied by a second symbol that can be M-silty or C-clayey. If more than 50 % of the samples value passes the No. 200 sieve, then the soil is considered fine-grained. These soils are classified by 3 group symbols of first order M-predominantly silt, C-predominantly clay and O-organic, and then accompanied by second order symbols such as L-low plasticity and H-high plasticity. Soils having a liquid limit (LL) over 50 % are highly plastic and will have the symbol H, while soils that have a LL less than 50 % are known as soils with low plasticity and are accompanied by the symbol L. Finally, the plasticity index (PI) which indicates the magnitude of water content range over which the soil remains plastic, allows to make a distinction between silts and clays or in some specific

cases it assigns a dual designation such as CL-ML [2].

In the case of the 29 samples considered in this study, we have found that majority of samples are considered to be fine-grained soils due to the fact that 69 % of them are made up of 50 % of fines or more, as it is shown in Table 3. The remaining 31 % of the samples have a larger percent of sand than fines and gravel. Consistently, the most common soil classification is inorganic silt, either with high (MH) or low (ML) plasticity making up the 48 % of the total, clay (CL) corresponds to 21 % and sands (SM or SC) 31 % of the total. For clays and silts (fine-grained soils) the shape of the particles, rather than their size, has greater influence on engineering properties such as internal friction angle and permeability, considering that gravity forces lose importance in face of chemical-physical forces [25], and therefore further analysis are required. The complete USCS classification for every location is shown in Table 3 as well as values of water content, liquid limit, plasticity index and percentage of gravel, sand and fines.

Thus, as can be concluded from Table 3, there are three regional trends in terms of the type of soil analyzed. For instance, the northern and southern Coastal Plain region exhibit a predominance of clayey sands (SC) and silty sands (SM), while the Andean region has a majority of silts either of high plasticity (MH), or with slight plasticity (ML). The Amazon region has a marked tendency of clayey soil (CL). Moreover, taking into account the plasticity index (PI) and considering that soil strength and stiffness behavior are correlated to the plastic consistency, it is observed (see, Table 3) that the Andean region has the lower values of PI meaning Andean soils have harder consistency, while the Amazon and Coastal Plain regions have larger and similar values.

Consistency is the property of soils defined as their resistance to flow, which is, in turn, directly related to strength. For fine-grained soils water content is a major factor to be considered due to the fact that the arrangement of grains can easily change. Consequently, as water content decreases soils shrink and gain strength while when it increases soils expand and lose strength [26]. Furthermore, fine-grained soils have higher specific surface area (SSA), a morphological feature that has significant influence on their physical and chemical properties and it varies notably with mineralogy and particle size distribution (see volume-to-surface ratio distribution of Jaramijó's sample (CL). in section 4. Clays are the ones that contribute with more SSA to soil [27] and change their consistency dramatically with small variations in water content. Being the amount of water of high importance it is obtained based on the *ASTM D2216-10* standard [28], considering

Table 3: Results of the particle sieve analysis where the percentages of gravel (G), sand (S) and fines (F) are determined (*ASTM D422-17*), liquid limit (LL) and plasticity index (PI) (*ASTM D4318-17*), water content (W) (*ASTM D2216-10*), USCS classification (*ASTM D2487-11*), internal friction angle ( $\Phi$ ) and cohesion ( $c$ ) for each one of the samples.

| Location No. | W[%]   | LL     | PI    | G [%] | S [%] | F [%] | USCS | $\Phi$ [°] | $c$ [ $Kgf/cm^2$ ] |
|--------------|--------|--------|-------|-------|-------|-------|------|------------|--------------------|
| 1            | 87.11  | 110.58 | 33.89 | 0     | 2     | 98    | MH   | 6.689      | 0.25               |
| 2            | 12.23  | 48.45  | 19.26 | 0     | 19    | 81    | ML   | 11.43      | 0.84               |
| 3            | 8.29   | 26.97  | 4.24  | 0     | 42    | 58    | ML   | 29.96      | 3.92               |
| 4            | 12.58  | 25.33  | 3.9   | 0     | 54    | 46    | SC   | 20.44      | 0.599              |
| 5            | 5.31   | 0      | 0     | 0     | 35    | 65    | ML   | 14.82      | 0.148              |
| 6            | 8      | 0      | 0     | 4     | 50    | 46    | SM   | 29.08      | 1.61               |
| 7            | 7      | 0      | 0     | 17    | 70    | 13    | SM   | 25.44      | 0.197              |
| 8            | 5.42   | 0      | 0     | 4     | 83    | 3     | SM   | 30.686     | 0.45               |
| 9            | 24     | 0      | 0     | 0     | 82    | 18    | SC   | 8.82       | 0.36               |
| 10           | 20     | 44     | 25    | 6     | 46    | 48    | SC   | 3.43       | 0.32               |
| 11           | 39.78  | 76.23  | 28.23 | 0     | 5     | 95    | MH   | 28.2       | 1.21               |
| 12           | 46.14  | 56.2   | 16.28 | 0     | 60    | 40    | SM   | 12.46      | 0.105              |
| 13           | 3.14   | 24.21  | 0.95  | 0     | 42    | 58    | ML   | 34.17      | 3.51               |
| 14           | 12.03  | 27.31  | 2.82  | 2     | 57    | 41    | SM   | 35.74      | 4.33               |
| 15           | 16.77  | 60.7   | 23.27 | 0     | 4     | 96    | MH   | 44.58      | 2.59               |
| 16           | 102.13 | 119.63 | 42.43 | 0     | 14    | 86    | MH   | 20.43      | 0.72               |
| 17           | 27.16  | 43.44  | 19.17 | 0     | 33    | 67    | CL   | 3.22       | 0.264              |
| 18           | 55.37  | 70.84  | 43.68 | 0     | 21    | 79    | CH   | 6.63       | 0.18               |
| 19           | 132.31 | 150.89 | 33.09 | 0     | 4     | 96    | MH   | 10.19      | 0.09               |
| 20           | 41.81  | 24     | 17.8  | 0     | 3     | 97    | CL   | 0.439      | 0.12               |
| 21           | 22     | 49     | 38    | 0     | 39    | 61    | CL   | 6.45       | 0.297              |
| 22           | 132.11 | 164.43 | 66.99 | 0     | 6     | 94    | MH   | 25.52      | 0.45               |
| 23           | 40.54  | 63.92  | 16.17 | 0     | 27    | 73    | MH   | 18.16      | 0.88               |
| 24           | 14.52  | 0      | 0     | 5     | 86    | 9     | SM   | 42.5       | 2.93               |
| 25           | 49.36  | 60.62  | 13.01 | 0     | 42    | 58    | MH   | 16.05      | 0.38               |
| 26           | 20     | 38     | 18    | 0     | 27    | 73    | CL   | 20.73      | 0.47               |
| 27           | 26.09  | 48.97  | 21.2  | 0     | 45    | 55    | CL   | 5.19       | 0.31               |
| 28           | 137.05 | 167.29 | 55.69 | 2     | 30    | 68    | MH   | 7.78       | 0.504              |
| 29           | 10.06  | 0      | 0     | 0     | 25    | 75    | ML   | 17.54      | 0.907              |

that soil behaves like a solid, semi-solid, plastic, and liquid depending on the amount of water present. The boundaries of these soil consistencies, where the soil's behavior changes, are known as the Atterberg limits and are specific for every type of soil. The LL for all locations analyzed is specified in Table 3, while the plastic limit (PL) is not shown because the plasticity index (PI) by

definition is the difference between the liquid limit and the plastic limit [24]. Both the LL and PL have a direct relation with the amount of clay present, therefore, a soil with high clay content will exhibit larger values of LL and PL[29].

According to Table 3, the lowest value of LL for the CL classification corresponds to Nueva Loja 38 %, and the highest to Puerto Francisco de Orellana 49 %. Only Manta has a CH classification and the LL has a value of 70.84 %. On the other hand, the lowest LL for silts with low plasticity (ML) is 0 % for Riobamba and Ambato, and the highest LL is 48.45 % from Guaranda. Furthermore, silts with high plasticity (MH) have a lowest LL of 60.62 % corresponding to Santo Domingo's sample and a highest value of 167.29 % corresponding to Baños. Clays present a LL mean of 49 % while for MH is 108 %, which is 2.44 larger. However, when obtaining the average LL of silts considering both MH and ML, it goes down to 76.7 %, which is still 1.6 larger than the average of 49% of clays. In addition, according to Burmister's classification of clays (1949) [30], Manta (CH) is the location where the soil is very high plastic ( $PI > 40$ ), while Zamora (CL) and Puerto Francisco de Orellana (CL) are high plastic and Jaramijó, Nueva Loja and Tena are classified as medium plastic [31]. When soils are at their liquid limit, they exhibit very low shearing strength, and by looking at the water content of each location, none of the samples reach the percentage of moisture to be at the LL. It can be seen that 34 % of the samples analyzed have a water content less than the one for the soil to be considered in a plastic state, for it can be said that the soil from these locations are either in a semi-solid or solid state while the rest are in a plastic state. Moreover, the majority of samples of the Andean region (75 %) exhibit a water content lower than 15 %, that corresponds to a though consistency [2]. Overall, the samples with harder consistency belong to the Andean Highlands.

Following this analysis, the particle-size distribution curve of Portoviejo (MH) showed in Figure 3-b), represents the most common gradation curve of the entire country, where most grains are of the same size. Therefore, it is called a uniformly graded soil also known as poorly graded soil, which has a high void ratio. Conversely, the gradation curve in Figure 3-a) is less steeper than the curve in b). Thus, it is a representation of a better graded soil classified as a silty sand (SM) from the city of Santa Elena, where the void ratio decreases due to the existence of varying particle sizes that fill the voids and greater particle interlocking enables it to support heavier loads. Hence, load distribution will be better than poorly graded soil as a result of grains being fitted and therefore

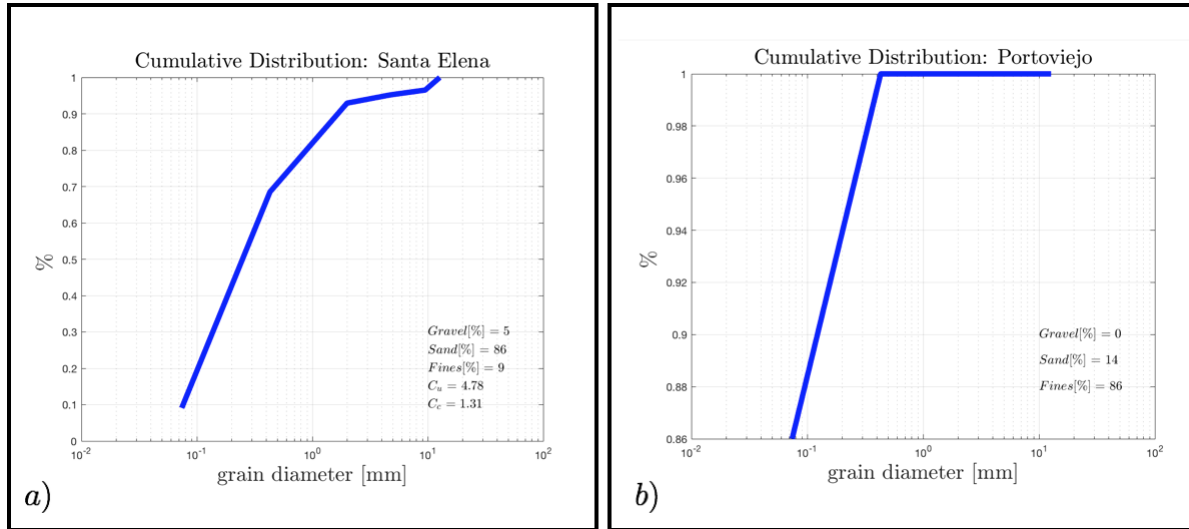


Figure 3: a) Cumulative Distribution curve of Santa Elena, an example of a better graded soil. b) Cumulative Distribution curve of Portoviejo, an example of a poorly graded soil.

there is small tendency for their displacement. However, in accordance with the USCS [3] for a sand to be well graded the coefficient of uniformity and the coefficient of curvature must meet the aforementioned specific criteria and the cumulative distribution curve of Santa Elena does not. A  $C_u$  of 1 establishes that the particles of soil are almost the same size, however the value obtained of 4.78 confirms the several sizes of particles found in Santa Elena's sample. On the other hand  $C_c$  meets the criteria, but its value is closer to the lowest boundary of 1, and since this coefficient depends on the influence of the smaller particle size on the engineering properties it can be said that all sizes that contribute to the  $C_u$  are equally represented [32].

There are soils that exhibit the same percentage of gravel, sand and fines but have different particle-size distribution curves, therefore, they will differ in engineering behavior [32]. For instance, as shown on Table 2 the samples from Santo Domingo, Azogues and Ibarra have the same amount of sand and fines, but from Figure 4 it is evident that their cumulative distribution curves vary. The difference lies on that for Santo Domingo only 1 % is retained in No.40 sieve while for Ibarra 11 % is retained. This demonstrates that even though both samples are constituted of the same percentage of sand and fines, Ibarra has a wider variety of particle sizes than Santo Domingo. As a consequence Ibarra will have better particle interlocking and a lower void ratio, overall it will exhibit a higher load bearing capacity as will be shown in subsection 3.2.

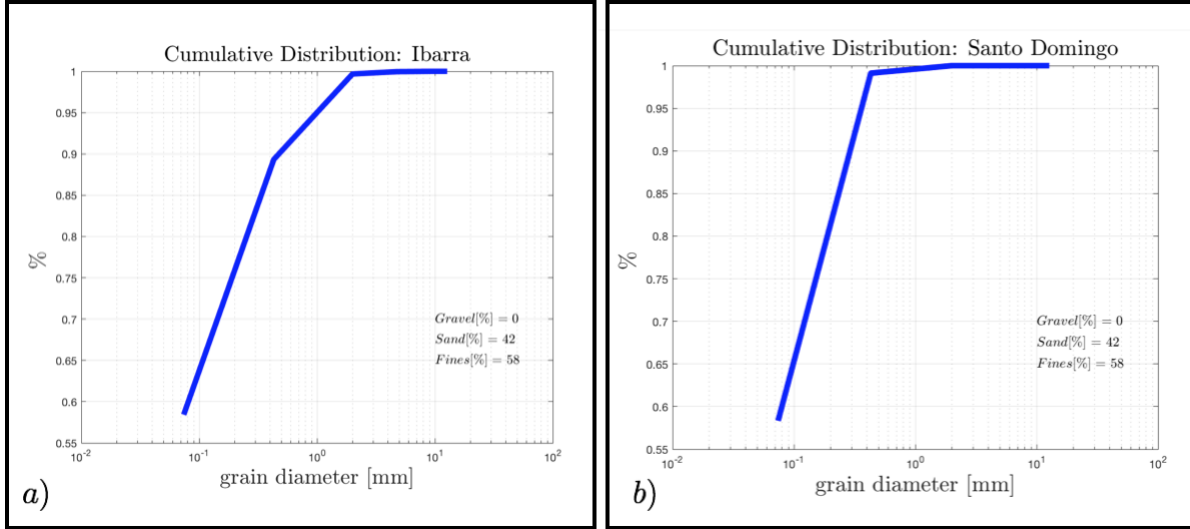


Figure 4: Cumulative Distribution curves for two cities having the same amount of sand and fines  
a) Ibarra b) Santo Domingo.

### 3.2 Shear strength

Shear strength of soil depends on several factors such as inter-particle bonds, fabric, deformation history and the pressure exerted by the fluid that fills its voids. Friction angle  $[\circ]$  and cohesion  $[Kg_f/cm^2]$  are the most common and general measures of shear strength in geomechanics. Thus, they are obtained for the 29 samples through (UU) triaxial testing based on the *ASTM D 2850-03a* standard [33], and the corresponding results are presented on Table 3.

Stability problems require a deep understanding of soil's shear strength, defined as the internal resistance per unit area that the mass of soil has to maintain before reaching failure [34]. The particular relationship between shearing stress and confining / normal stress is expressed as a linear equation:

$$\tau = \sigma \tan(\Phi) + c \quad (1)$$

where,  $c$  is the cohesion,  $\Phi$  is the angle of internal friction,  $\sigma$  normal stress on the failure plane, and  $\tau$  is the shear strength. Cohesion is a constant that equals shear strength when the compressive stress is zero, and while the angle of internal friction is linearly dependent on external stress cohesion is not [35, 36]. Therefore, equation (1) is represented in the Mohr diagram as a straight line inclined by  $\Phi$  to the normal stress axis ( $\sigma$ ). This failure envelope (see, Figures 7, 10) is tangent to the Mohr circles at different hydrostatic pressures ( $\sigma_3$ ), which in our case were of 0.5 - 1 - 2  $[Kg_f/cm^2]$  for

the (UU) triaxial testing. The Mohr Coulomb failure criterion can also be represented in principal stresses space [37] as:

$$(\sigma_1 - \sigma_3) = (\sigma_1 + \sigma_3) \sin \Phi + 2(c) \cos \Phi \quad (2)$$

Where,  $\sigma_3$  is the minor principal stress (hydrostatic pressure of the chamber) and  $\sigma_1$  is the major principal stress, which is the stress at failure plus the chamber pressure [33]. The stress at failure is the highest stress of the UU triaxial test stress-strain curve (see, Figure 5). The Mohr's circle diameter is by definition  $(\sigma_1 - \sigma_3)$  and the location of the center of the circle in the normal stress axis is given by  $(\sigma_1 + \sigma_3)/2$ . Thus, drawing the Mohr circles corresponding to the aforementioned hydrostatic pressures, Coulomb's envelope can be generated on the  $\sigma, \tau$  plane [37].

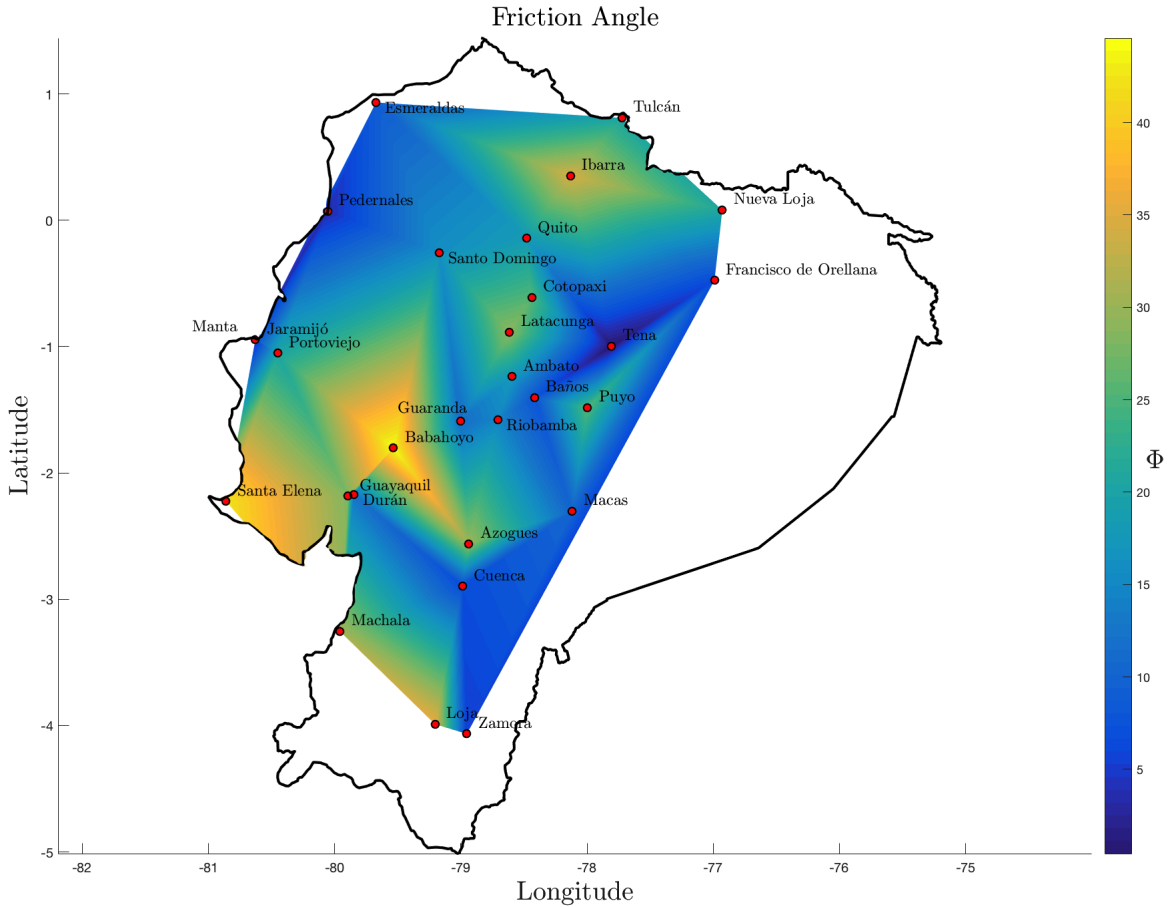


Figure 5: Friction angle  $\Phi$  [ $^{\circ}$ ] corresponding to the samples taken from the 23 capitals of the provinces plus other 6 locations of interest.

In Figure 5, the internal friction angle ( $\Phi$ ) of each soil sample is plotted according to its exact location, and a multilinear fitting is applied. Note that the lowest friction angle of  $0.44^{\circ}$  corresponds

to the city of Tena in the Amazon region while the largest of  $44.58^\circ$  is found in the Coastal Plain region in the city of Babahoyo (see, Table 3). Moreover, by looking at specific areas of the country, several trends can be derived. For instance, on the Coastal Plain region around the area of the provinces of Guayas, Santa Elena and the south part of Manabí the values of  $\Phi$  range from approximately thirty to forty degrees, which are represented in yellow. Also, the predominant type of soil of this region according to the USCS classification is silty sand (SM) and plastic silt (MH) and it is known that these areas of the littoral are dry and semi-desertic [38]. On the other hand, the samples of the cities located in the Amazon region and at the north-western part of the country, near the Pacific Ocean, exhibit the lowest friction angles, and therefore the dominant color is dark blue. The soil of these two zones mentioned have a dominant USCS classification of clay (CL) and clayey sand (SC) (see, Table 3). Furthermore, in the Andean Highlands, in terms of soil classification, the zone is dominated by silts and the samples analyzed have friction angles that range from  $7.78^\circ$  in Baños to  $35.74^\circ$  in Loja. A variation of  $27.96^\circ$  is obtained from soils of the same region which shows how varied Ecuadorian soils are. It must be considered that the northern part of the country is surrounded by volcanoes down to the province of Chimborazo, the ones that have had a strong influence in the type of soil of the zone due to the fact that soils developed on volcanic ash are considered evolved soils and geologically young. Conversely, the southern part of the country does not have active volcanoes and is characterized by old soil [38]. Consequently, there is a strong relation between the type of soil and the internal friction angle. The mean of  $\Phi$  for the Andean region is  $21^\circ$ , the Coastal Plain region is  $20^\circ$  and for the Amazon region  $11^\circ$ .

The soil has different types of behavior under stress (i.e. elastic, plastic, viscous and brittle), which control the percentage of deformation that will be achieved before failure. Figure 6 exhibits the stress-strain curves corresponding to four Ecuadorian cities. For instance, Figure 6-b) shows the stress-strain curves of the city of Latacunga, and it depicts a typical behavior for sands, this is consistent since the USCS classification for this location is silty sand (SM). Regardless of the confinement pressure, it can be seen that in all three curves failure of the specimen is reached approximately at a strain ( $\epsilon$ ) of 2.1 % and the ultimate stress ( $\sigma$ ) that soil resists for a confinement pressure of 2 [ $Kgf/cm^2$ ] is 9.2 [ $Kgf/cm^2$ ]. On the other hand, in Figure 6-a), city of Babahoyo, the stress-strain curves show that the specimen failed because it reached critical state, where without any increment in axial load the soil continued to deform, all curves exhibit the same behavior,



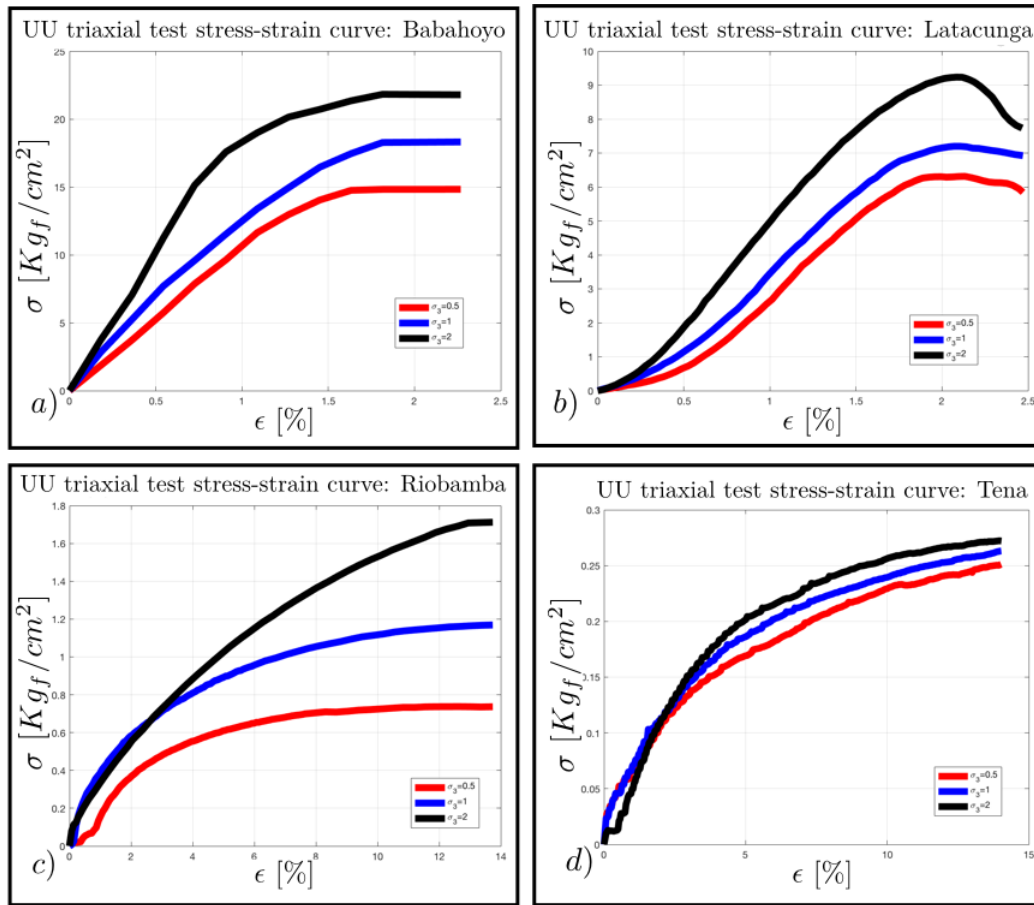


Figure 6: Stress-strain curves corresponding to the samples taken at the locations: a) Babahoyo, b) Latacunga, c) Riobamba, and d) Tena. The different confinement pressures used are represented by different colors: red curve = 0.5  $[Kg_f/cm^2]$ , blue curve = 1  $[Kg_f/cm^2]$  and black curve = 2  $[Kg_f/cm^2]$ .

and the ultimate stress ( $\sigma$ ) is 23.82  $[Kg_f/cm^2]$ , which is more than twice the ultimate stress of Latacunga. Conversely, Figure 6-d) corresponding to Tena shows the lowest value of ultimate stress, i.e., 0.275  $[Kg_f/cm^2]$ , and the stress-strain curve shows a typical clay behavior where the slope gradually tends to zero as failure is reached, and it is 21.54  $[Kg_f/cm^2]$  less than the ultimate stress of Babahoyo. This shows a considerable difference from a soil where silt predominates (Babahoyo) to a mostly clay soil (Tena). However, the soil sample of Tena has a water content close to reaching the liquid limit, while the one from Babahoyo suggests it is in a semi-solid state. In addition, Figure 6-c) shows Riobamba's stress-strain curve where soil achieves failure when subjected to 0.5  $[Kg_f/cm^2]$  and 1  $[Kg_f/cm^2]$  of confinement pressure. Note that it gradually flattens down as for the Tena's sample.

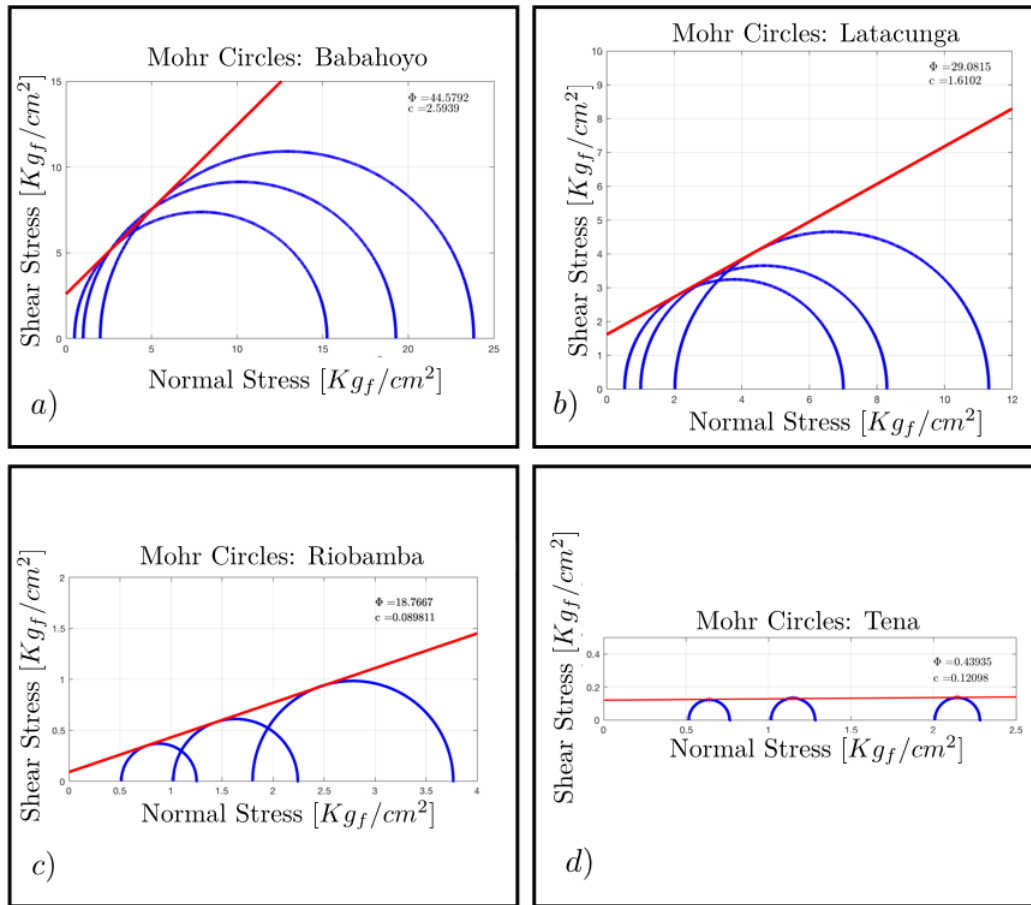


Figure 7: Coulomb's envelope for the samples taken at the locations: a) Babahoyo, b) Latacunga, c) Riobamba, and d) Tena.

Taking into account that the geometry of grains is a factor that directly relates with shear strength, sands that tend to be fine, poorly graded and well rounded will exhibit lower friction angles compared to well graded angular sands [39]. Moreover, as grains are more regular they reach compaction at lower pressures and it implies less strength [5]. Figure 7 shows the Mohr's circles and Coulomb's failure envelope (see, equations 1) and (2) obtained for the same four Ecuadorian cities previously analyzed. Babahoyo with a USCS classification of plastic silt (MH) (Figure 7-a), located in the Coastal Plain region, has the highest value of friction angle ( $\Phi = 44.57^\circ$ ). It may be due to the geology of the region which is constituted by marine terraces formed of marine clays and clayey silts of estuarine origin [15] and the semi-solid sample's consistency considering that the water content is less than the PL. Conversely, the soil from the city of Tena (CL) (Figure 7-d)), in the Amazon region, shows an almost perfect horizontal Coulomb's failure envelope with

$\Phi = 0.44$ . This suggests that the soil might have been fully saturated since it presents an important strength feature for cohesive soils that meet this condition (full saturation). Even though confining pressure changes the axial stress at failure is the same. As a consequence the shear strength of this type of soil is equal to the radius of the Mohr circle,  $\tau = c$ . This feature of  $\Phi = 0$  is only displayed by saturated clays and silts [2]. The geology of this zone is mainly constituted by lutite (sedimentary rock composed by clay/silt size sediment) [15]. In a distance of only 212 [km] in straight line from Babahoyo to Tena exists a difference of  $44.13^\circ$  in friction angle, which once again prove the variability of Ecuadorian soil. Furthermore, (Figure 7 b)-c)) are two cities (Latacunga (SM) and Riobamba (ML)) from the Andean region which have friction angles that are not too high or too low, in fact they represent 50 % and the 75 % of the value of friction angles from all the samples of the country, and they are  $10^\circ$  apart. Latacunga's soil is constituted mainly by volcanic ash of andesitic composition alternating with pumice, cementitious materials of sands and silts, as consequence of lahars deposits produced by the last eruptions of the Cotopaxi volcano [40]. Similarly, Riobamba's soil is of volcanic origin which does not register the presence of water table [41].

Clays exhibit an important strength characteristic which is a direct relation between the friction angle and the plasticity index (PI). The friction angle tends to decrease with an increase in plasticity index [32]. Nonetheless, by looking at Table 3, it is evident that the PI of Tena is 17.8 while its  $\Phi = 0.439$  and for Zamora, which has a PI of 21.2, the friction angle is supposed to be lower, but it is of  $5.19^\circ$ . However, Tena has a high content of fines 97 % while Zamora has 55 %. Now, when analyzing Nueva Loja (PI = 18 ,  $\Phi = 20.73$ ) with respect to Puerto Francisco de Orellana (PI = 38,  $\Phi = 6.45$ ), which have almost the same amount of fines, the PI increases in 20 % and the friction angle decreases in  $14.28^\circ$ , which was empirically expected. Moreover, according to Skempton [42] the PI increases linearly when the percentage of clay fraction increments. In addition, Laskar, A. et al. [43] established that the grain size determines plasticity, therefore when there is an increment in sand content the inter-molecular attraction forces decrease. As it is shown on Table 3, the locations where the amount of sand is higher, the plasticity index is either zero (mostly cities from the Andean region) or as low as 3.9 for Tulcán with 54 % of sand, and 2.82 for Loja with 57 % of sand. Conversely for the locations with high percent of fines such as Puyo (94 %) the PI is 66.99.

As it can be observed in Figure 8 the largest values of cohesion are located in the Andean

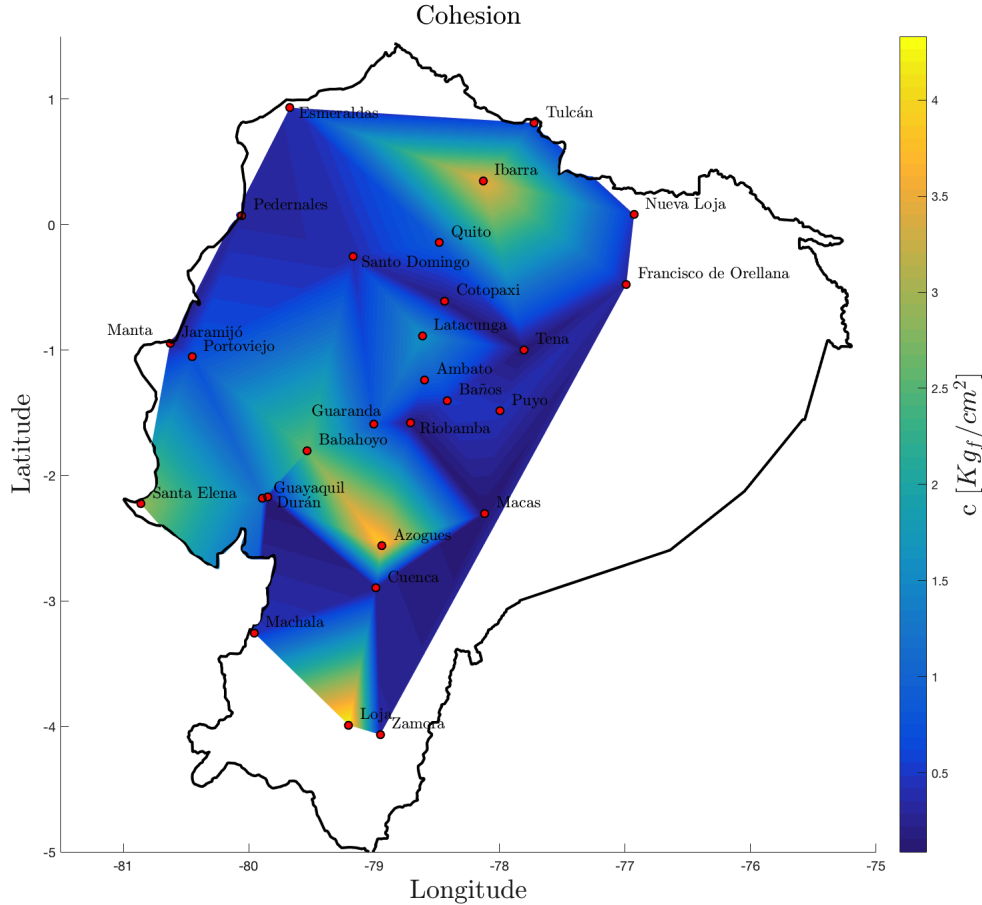


Figure 8: Cohesion  $c$  [ $Kg_f/cm^2$ ] corresponding to the samples taken from the 23 capitals of the provinces plus other 6 locations of interest.

region, specifically in the cities of Loja (SM), Azogues (ML) and Ibarra (ML), which are mainly composed by silts and have a low index of plasticity. While, the lowest values are located in the Amazon region and in the north-western part of the country where the USCS classification of CL is predominant. Furthermore, the average cohesion (see, Table 3) for the Coastal Plain region reaches a value of  $0.9$  [ $Kg_f/cm^2$ ], for the Andean region the average  $c$  is  $1.5$  [ $Kg_f/cm^2$ ] and for the Amazon region where clays predominate is  $0.3$  [ $Kg_f/cm^2$ ].

In addition, in Figure 9 the UU triaxial stress-strain curves for four cities (Loja, Santa Elena, Latacunga and Macas) are shown. For the cities of Loja and Santa Elena the curves reach failure approximately at a strain of  $1.6\%$ . Note that the behavior of these two soil samples is similar and at confinement pressure of  $2$  [ $Kg_f/cm^2$ ] their ultimate stresses are  $22.58$  [ $Kg_f/cm^2$ ] and  $21.71$  [ $Kg_f/cm^2$ ] respectively. On the other hand the stress-strain curves of Latacunga reach failure at

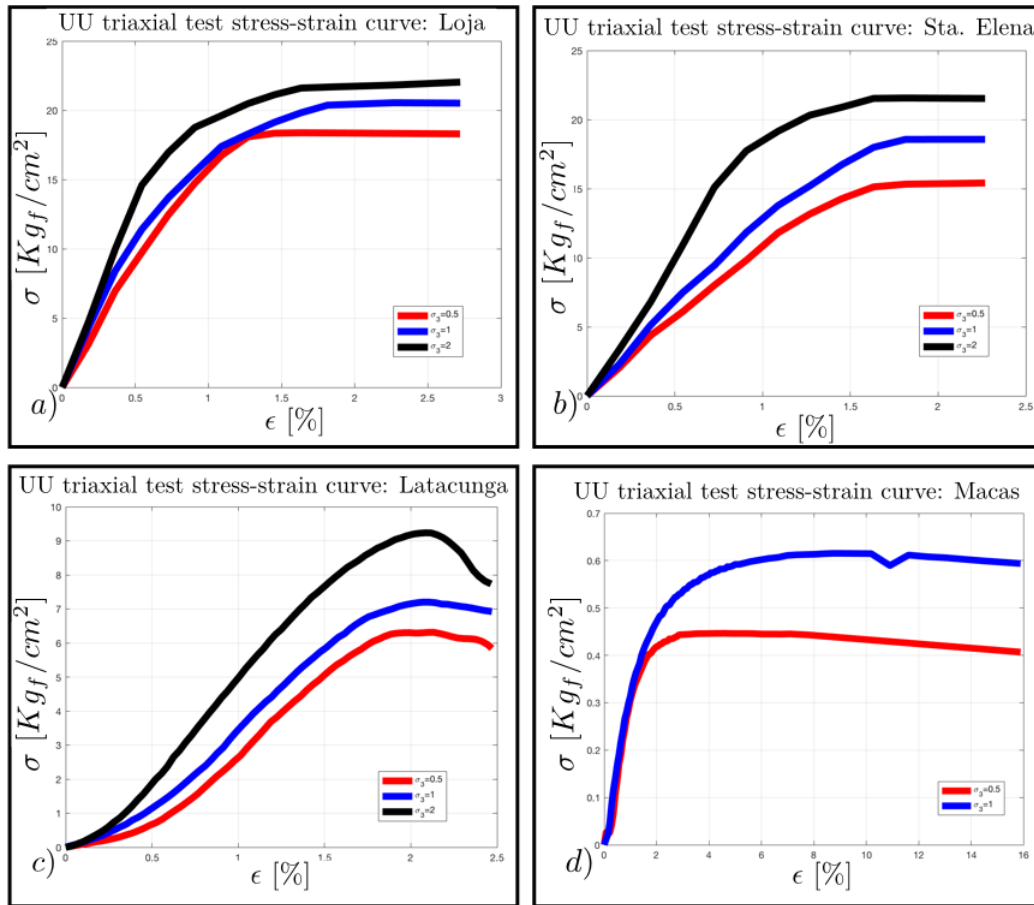


Figure 9: Stress-strain curves corresponding to the samples taken at the locations: a) Loja, b) Santa Elena, c) Latacunga, and d) Macas. The different confinement pressures used are represented by different colors: red curve =  $0.5 [Kg_f/cm^2]$ , blue curve =  $1 [Kg_f/cm^2]$  and black curve =  $2 [Kg_f/cm^2]$ .

2.1 % of axial strain, after which the curves display softening, and the curves corresponding to the city of Macas reach maximum strength of axial strain at about 2.5 %.

Figure 10 shows the Mohr circles and corresponding Coulomb's failure envelope of the four cities aforementioned, which have the highest, lowest, 50 % and 75 % values of cohesion among all the samples taken. The city of Loja (SM), located in the Andean region, has the highest  $c = 4.33 [Kg_f/cm^2]$ , which is 48 times larger than the cohesion of the city of Macas (MH) located in the Amazon region. As depicted by Table 3, Macas has a larger content of fines than Loja, and therefore, a higher PI. Furthermore, Santa Elena (SM) located near the Pacific Ocean has a high content of sand and only 9 % of fines, and this location displays a 75 % of the highest value of  $2.93 [Kg_f/cm^2]$ . On the other hand Latacunga's (SM) cohesion of  $1.61 [Kg_f/cm^2]$  is  $1.32 [Kg_f/cm^2]$

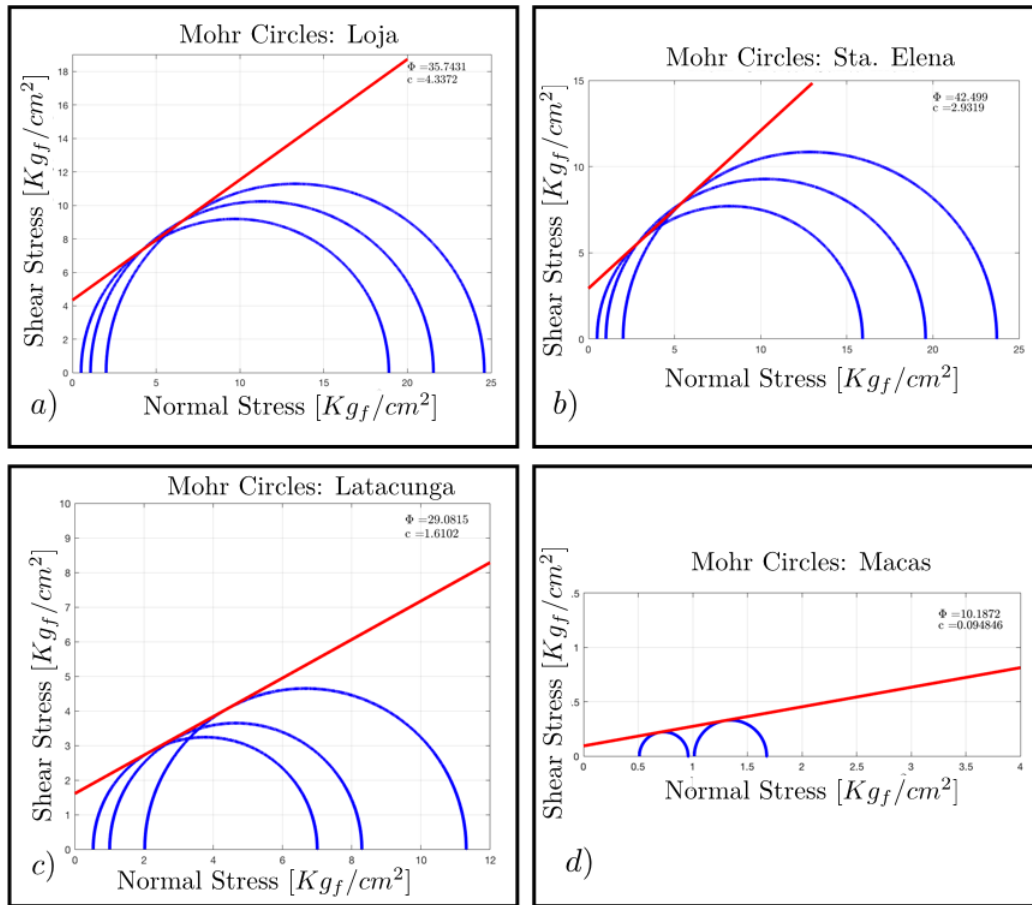


Figure 10: Coulomb's envelope for the samples taken at the locations: a) Loja, b) Santa Elena, c) Latacunga, and d) Macas.

less than Santa Elena. Note that three out of the four soil samples analyzed are silty sands and only the lowest value corresponds to silt of high plasticity. According to Adunoye [44], an increment in the percentage of fines will increase cohesion in soils. However, when looking at the data shown by Figure 10, the three locations with higher cohesion have higher percentage of sand than fines and Macas which displays the lowest cohesion (almost 0 [ $Kg_f/cm^2$ ] cohesion) has 4 % of sand.

Finally, in order to compare the percentage of soil's strength given by the internal friction angle and cohesion, the peak stress from the stress-strain curve with a confinement pressure of 2 [ $Kg_f/cm^2$ ] was selected. This maximum value, where the sample reached failure, represents 100 % of soil's stress. The value of cohesion is determined by the intersection of Coulomb's failure envelope with the shear stress axis of the Mohr circles diagram and the percentage of cohesion in the aforementioned peak stress value is then obtained. Thus, the remaining percentage corresponds to

internal friction. This procedure was repeated for all the 29 samples, and the mean was calculated for the different types of soil. As a result for Ecuadorian clayey soils the contribution of cohesion in shear strength is of 28 %, for silty soils is 19 %, and for sandy soils is 17 %. Furthermore, when analyzing the cohesion contribution per region, the Coastal Plain displays 19 % of cohesion, the Andean region 20 % of cohesion, and the Amazon shows the highest value with 23 %. The data corroborates the study of Akayuli et al. [45], who found that for clayey soils the contribution of cohesion in shear strength is higher than for sandy soils, while friction angle decreases with increasing clay content. In addition, it can be shown with these results that there is a general increase in cohesion with clay content, taking into account that the small size of clay particles allow them to fill the voids of sandy materials and, therefore, they generate an increment in interlocking behavior [46]. On the other hand, an increment of sand gives the soil a more frictional behavior (as long as the sand is angular). Thus, by looking at Table 3, the soils with a USCS classification of either SM or SC have larger friction angles than those CL,CH, ML and MH.

## 4 Morphological characterization

The physical behavior of soil and its strength are directly influenced by grain morphology [5]. As a result, not only the orientation and distribution of grains are the features that control macroscopic response, but the interaction between them are just as important [8]. Thus, in order to quantify and qualify grain morphology, parameters such as aspect ratio, roundness, sphericity, minimum principal direction, and volume-to-surface ratio were chosen since they are of general use in the field of soil mechanics and geomechanics [6]. In this work sphericity is defined as

$$S = \frac{r_{in,max}}{r_{cir,min}} \quad (3)$$

where,  $r_{in,max}$  is the maximum inscribable radius and  $r_{cir,min}$  is the minimum circumscribable radius of a given soil particle. Moreover, the definition for roundness is given by

$$R = \frac{\sum_1^N \frac{r_i}{N}}{r_{cir,min}} \quad (4)$$

where,  $r_i$  is the radius of curvature at the  $i$ th corner and  $N$  is total number of corners taken for the calculation.

With the aim of obtaining the aforementioned morphological measurements, 3D X-Ray Computed Tomography (3DXRCT) is used to get 3D images of the soil samples. However, these images are stored as voxels (just as a photographic picture), and they must be transformed through image processing methods into mathematical functions in order to allow for quantitative measurements. In the last few years the Level Set (LS) method has been used to generate mathematical functions which accurately describe the complex geometry of real grains and capture grain morphology [8, 47]. The soil sample from the city of Jaramijó was sent to Université Grenoble Alpes to Edward Andò's Laboratoire 3SR in order to get the three-dimensional images from 3DXRCT, and a slice from these raw images is shown in Figure 11. The 3D images have a resolution of  $1 \mu\text{m}/\text{pixel}$  edge, this means that the specimen of  $0.5 \text{ mm} \times 1 \text{ mm}$  has a total of  $500 \times 500 \times 1000$  voxels. Basic characteristics of the grains' geometry can be seen in Figure 11, and therefore we can affirm that the sample is composed mainly of cubic-angular shaped particles and flaky as well as elongated particles which are overall irregular. It is important to mention that due to the numerous challenges encountered with the image processing method the remaining soil samples are to be analyzed in a future publication.

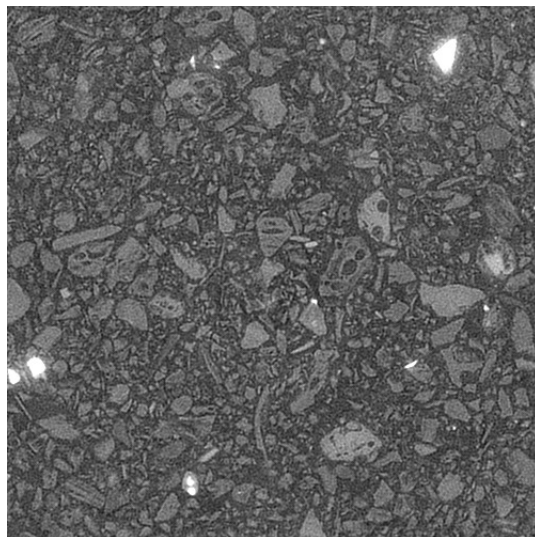


Figure 11: 3DXRCT image slice of Jaramijó's soil sample at a resolution of 1 micron per voxel obtained by the Université Grenoble Alpes.

To analyze the morphological features of the Jaramijó's sample, individual grains are identified



and extracted from the 3DXRCT images, then Level Set (LS) functions were computed for each one of them. Thus, for instance, the Level Sets of some grains from the sample are shown in Figure 12. According to this the digitalized soil particles are mostly angular, irregular and flaky elongated, which is consistent with the raw image depicted by Figure 11.

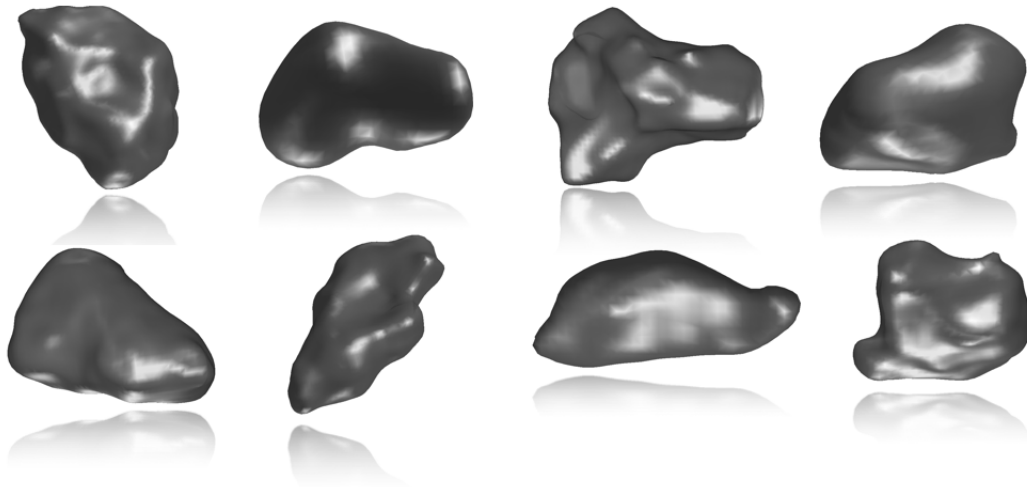


Figure 12: 8 Level Set grains avatar from Jaramijó's soil sample.

As previously mentioned, two main challenges were found in the process of obtaining the morphological characterization of the Ecuadorian soil samples. First, the scanning of the sample is a complex process which takes long time to be completed. It has to be taken into account that samples must be shipped abroad in order to get the 3DXRCT images. Second, we realized that the image processing methods proposed by Ivan Vlahinić Ivan et. al. [8, 47] do not give accurate results when having scattered particle-size distributions, as it is the case of the Jaramijó's soil sample. The image processing procedures are challenging due to the complex shapes that grains can take and the difficulty to separate them from other grains and voids. This becomes even more arduous when having to deal with a varied gradation, since small particles must be identified as well as larger ones. Clearly, the image processing method fails to take into account small particles and as it can be seen on Figure 13, where a experimental soil gradation curve is compared to the one obtained from the Level Sets retrieved from the aforementioned image processing. The curve from the digitalized grains has grains with larger diameters than the curve obtained by a laser scattering particle size distribution analyzer. Moreover, for the grain's diameter distribution, note from Figure 14 that it has a mean of 0.26 [mm] and a standard deviation of 0.07 [mm], which

implies that most of the grains fall in between 0.19 [mm] to 0.33 [mm]. In addition, note that the right tail is longer, suggesting that there might be a bias in the image processing from where the grains Level Sets are obtained, and therefore the smallest grains are not being captured by it.

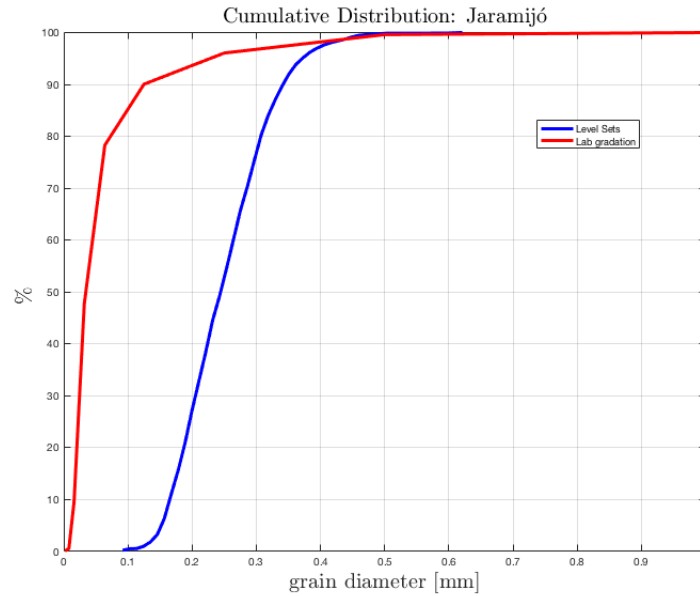


Figure 13: Cumulative particle size distribution curve from Jaramijó's soil sample. The line in blue represents the Level Set grains gradation, while the line in red corresponds to the experimental gradation with a laser scattering particle size distribution analyzer.

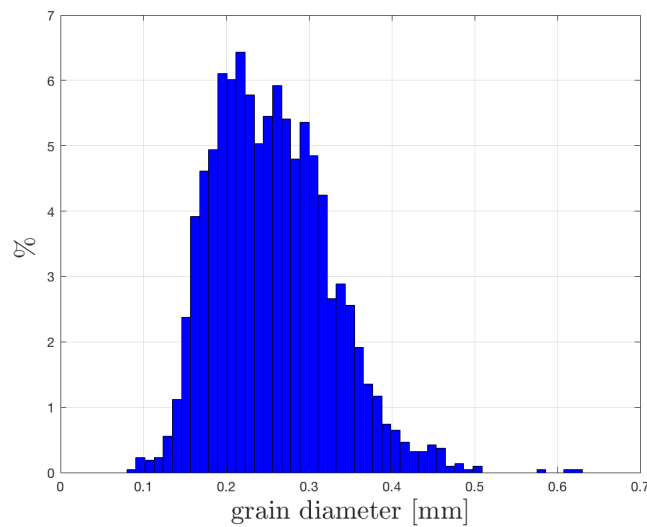


Figure 14: Grain diameters distribution corresponding to Jaramijó's sample containing 2145 grains.

Moreover, for aspect ratio, which is a measure of sphericity [6], Jaramijó's sample has a mean

of 0.57 with a standard deviation of 0.12. Note from Figure 15 that this seems to be a normal distribution where at least 68 % of the grains have aspect ratios between 0.45 and 0.69. Taking into account these values it can be said that the grains are mainly elongated. Furthermore, the values of roundness obtained by applying equation (4) are shown in Figure 16, with a mean of 0.72 and a standard deviation of 0.11. This implies that most of the grains have a roundness between 0.61 to 0.83, hence it can be concluded that the soil sample from Jaramijó is composed by both types of grains, mainly with edges and vertices and grains with smooth surfaces.

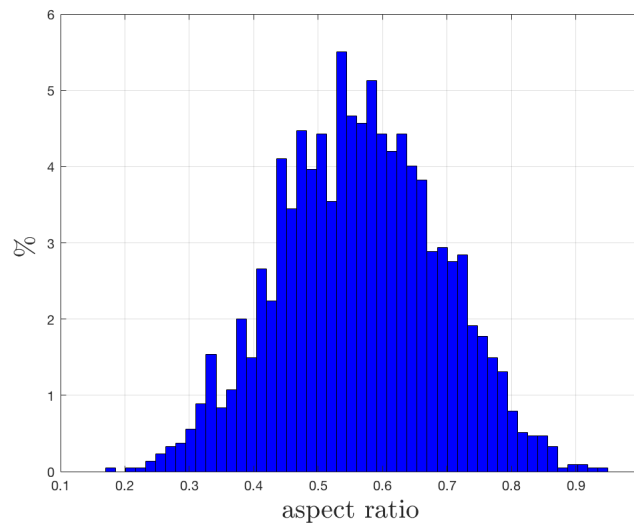


Figure 15: Aspect ratio distribution corresponding to Jaramijó’s sample containing 2145 Level Set avatar grains.

In addition, the grains’ minimum principal directions distribution with a mean of 0.07 [mm] and a standard deviation of 0.02 [mm] is shown in Figure 17. This suggests that most of the grains have their minimum diameter between 0.05 [mm] and 0.09 [mm]. Which suggests that the sample from Jaramijó is built up of silt (0.002-0.05 [mm]) and sand (0.05-2.0 [mm]) particles. Now, the distribution corresponding to volume-surface ratios is shown by Figure 18, with a mean of 0.02 and a standard deviation of 0.007, which indicates that most of the grains have volume-surface ratios between 0.013 and 0.027, confirming the fact that Jaramijó’s grains have edges and vertices and tend to be elongated. Moreover, note that the distribution has a longer right tail, indicating that most grains have lower values of volume-surface ratio.

Finally, for the distribution of sphericities, calculated using equation (3) and shown in Figure

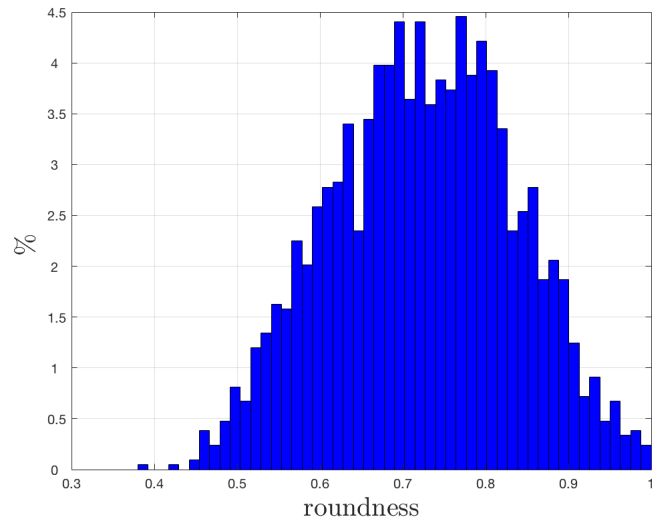


Figure 16: Roundness distribution computed from Jaramijó's sample containing 2145 Level Set avatar grains.

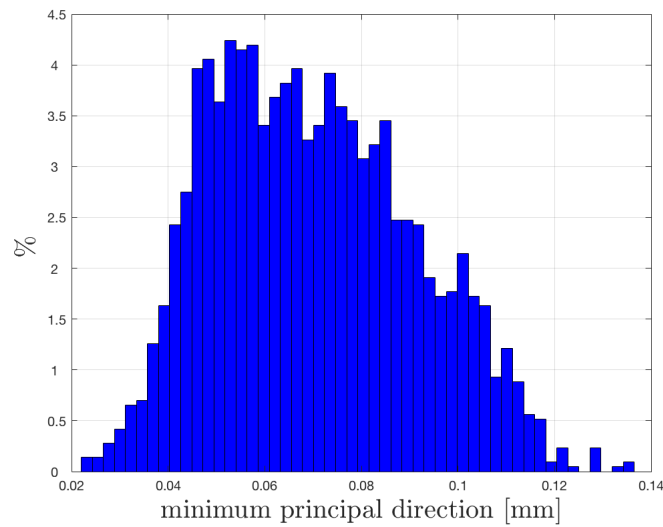


Figure 17: Minimum principal directions distribution obtained from Jaramijó's sample made of 2145 Level Set avatar grains.

19, note that the mean is 0.31 and the standard deviation 0.09. This means that most of the grains have a sphericity from 0.22 to 0.4, once again it is consistent with the fact that the grains are elongated. Moreover, note that in Figure 20 it is evident that a correlation between both parameters, aspect ratio and sphericity, exist. The aforementioned rela

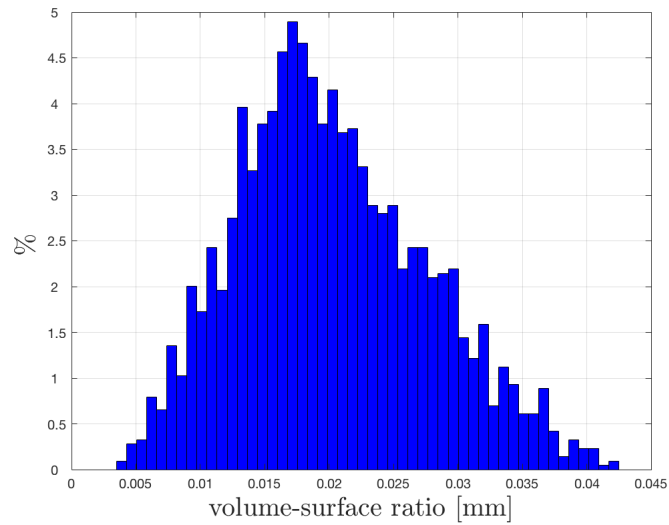


Figure 18: Volume-surface ratio distribution extracted from Jaramijó's soil sample containing 2145 Leve Set avatar grains.

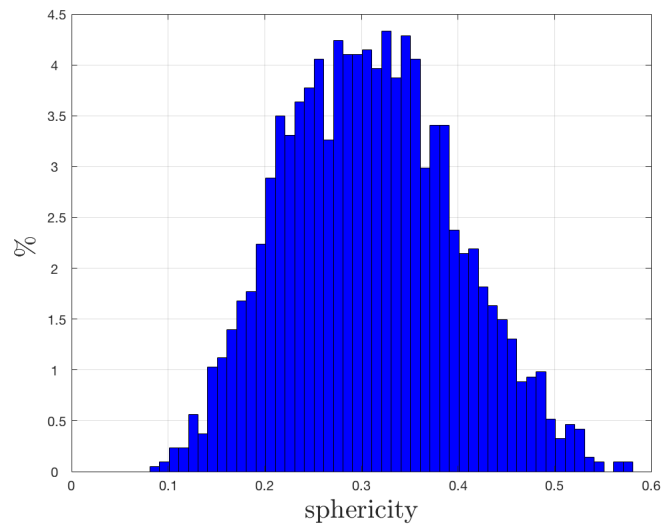


Figure 19: Sphericities distribution extracted from Jaramijó's soil sample containing 2145 Leve Set avatar grains.

## 5 Conclusion

We have introduced a first attempt to generate an experimental and computational nationwide data baseline of the mechanical, mineralogical and morphological characterization of Ecuadorian soils. This is a fundamental necessity provided that Ecuador is located in a hazard prone zone and currently there is no availability of such an important type of data. The twenty-nine locations sam-

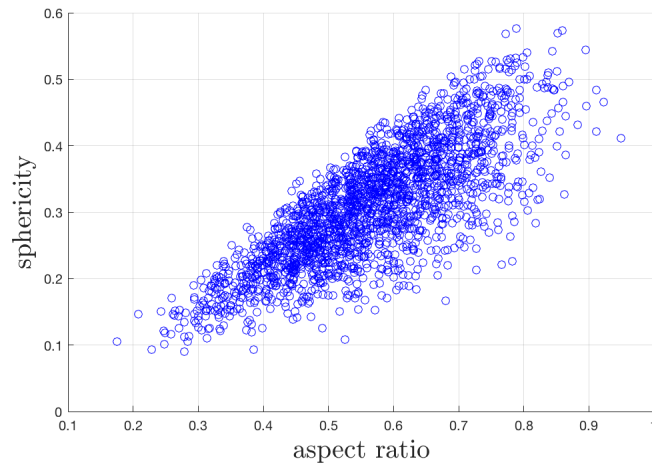


Figure 20: Sphericities distribution extracted from Jaramijó’s soil sample containing 2145 Leve Set avatar grains.

pled were selected taking into account that any natural disaster will generate serious consequences for population and infrastructure (see, Figure 2). However, more sampling points need to be added over time with the aim of improving the database’s accuracy and completeness.

Geomechanical laboratory tests were carried out in order to determine mechanical properties which define the soil’s shear strength. Moreover, by means of energy dispersive spectroscopy (EDS) on a scanning electron microscope (SEM), mineralogical characteristics were obtained for all samples and correlated to the aforementioned mechanical parameters. Furthermore, through 3D X-Ray tomography, the actual shapes of the sample’s grains allowed us to get morphological measurements such as roundness and sphericity. These digitalized grains are also used for computational simulations with LS-DEM schemes. Thus, since we are still working on obtaining the 3DXRCT images of all the 29 samples, as a proof of concept [6], we have included the morphological data and digitalized shapes from Jaramijó’s sample.

In terms of the particle size analysis of soils, most of the twenty-nine samples were determined to be poorly graded fine-grained soils after being classified by the USCS. Furthermore, three regional trends were evident in terms of type of soil (see, Table 2): In the Coastal Plain region we found the soil to be mostly sands, while in the Andean region the predominant soil type is silt and in the Amazon region the primary soil found is clay. In addition, water content is a major factor considered due to the notorious changes in soil behavior according to the amount of moisture present in the

samples. Hence, the samples from the Andean Highlands were found to be the ones with hardest consistency. On the other hand, the plasticity index (PI) increased when the percentage of clay fraction was higher, and with an increment of sand, the inter-molecular forces decreased, which is expected according to Skempton and Laskar [42, 43]. Moreover, relations between the USCS classification and shear strength parameters were observed. For instance, in soils with high content of clay the contribution of cohesion to shear strength is the highest while for sandy soils internal friction is dominant in the soil's strength. Therefore, there is a general increase in cohesion with increments in clay content and an increment in sand gives the soil a more frictional behavior.

Furthermore, the morphological parameters (i.e. aspect ratio, roundness, sphericity, minimum principal direction and volume-surface ratio) calculated for Jaramijó's soil sample is consistent with the fact that the grains are mostly irregular particles, cubic-angular shaped and flaky-elongated as it can be noticed from the 3DXRCT (see, Figure 11) raw images and the Level Sets (see, Figure 12). However, when comparing the cumulative particle size distribution of the Level Set avatar grains to the ones obtained through laboratory testing, it is evident that the image processing method is not taking into account smaller particles. For this reason, further analysis is required to improve the method.

On the other hand, the soil's mineralogical composition has a strong correlation with shear strength when considering the importance of inter-particle forces and shape of the grains for fine-grained soils. For instance, Kaollinite clay mostly found in tropical rainforests (the Amazon region) presented high cohesion because they are formed by plate-shaped particles adhered by Van der Waals forces and hydrogen bonds. Also, calcium carbonates and magnesium carbonates generate a more stable soil matrix due to the increment of inter-particle bonding. Consistently, calcium-rich soils from Azogues and Santa Elena have high values of both friction angle and cohesion, while magnesium-rich soils from Manta and Pedernales have a greater contribution of cohesion to shear strength. Moreover, geologic features in the country determine the type of soil which will be found in certain locations. Most of the soil in the Andean region is from volcanic origin and the south part of the country is constituted by the oldest geological formations.

Finally, it is key to note the high importance of generating the first standard and consistent database of soil characteristics that would have an impact in future studies regarding all the fields related and dependent on soil sciences, which have not been thoroughly developed and much work

remains to be done. For instance, biological parameters (i.e. soil microbiology) should be added to the database as well as other important specifications that will help with modern agriculture, water quality, land management and to overcome environmental challenges.

## References

- [1] Tapas Bhattacharyya and D. K. Pal. *Soil Science: An Introduction*. Indian Society of Soil Science, New Delhi, first edition, 2015.
- [2] Luis I González, Mercedes Ferrer, Luis Ortuño, and Oteo Carlos. *Ingeniería Geológica*. Pearson Prentice Hall, 2004.
- [3] ASTM D2487-11. *Standard Practice for Classification of Soils for Engineering Purposes (Unified Soil Classification System)*. ASTM International, West Conshohocken. PA, 2011.
- [4] A Hackston and E Rutter. The mohr–coulomb criterion for intact rock strength and friction – a re-evaluation and consideration of failure under polyaxial stresses. *Solid Earth*, 7:493–508, 2016.
- [5] Alex X. Jerves, Reid Y. Kawamoto, and José E. Andrade. Effects of grain morphology on critical state: a computational analysis. *Acta Geotech*, 11:493–503, 2015.
- [6] Alex X. Jerves, Reid Y. Kawamoto, and José E. Andrade. A geometry-based algorithm for cloning real grains. *Granular Matter*, 2017.
- [7] Reid Y. Kawamoto, E Andò, G Viggiani, and José E. Andrade. Level set discrete element method for three-dimensional computations with triaxial case study. *Journal of the Mechanics and Physics of Solids*, (91):1–13, 2016.
- [8] I Vlahinic, E Andò., G Viggiani, and José E. Andrade. Towards a more accurate characterization of granular media: extracting quantitative descriptors from tomographic images. *Granular Matter*, 2013.
- [9] Reid Y. Kawamoto, E Andò, G Viggiani, and José E. Andrade. All you need is shape: pre-



- dicting shear banding in sand with ls-dem. *Journal of the Mechanics and Physics of Solids*, 2017.
- [10] P.V.N. Henderson. *The Course of Andean History*. Diálogos Series. University of New Mexico Press, 2013.
- [11] Joseph E Bowles. *Foundation Analysis and Design*. McGraw-Hill, 1996.
- [12] X M. Fang, F S. Chen, S Z. Wan, Q P. Yang, and J M. Shi. Topsoil and deep soil organic carbon concentration and stability vary with aggregate size and vegetation type in subtropical china. *PLoS ONE*, 10(9), September 2015.
- [13] J E. Schoonover and J F. Crim. An introduction to soil concepts and the role of soils in watershed management. *Journal of Contemporary Water Research Education*, 154:21–47, 2015.
- [14] Área de Sismología Instituto Geofísico. Informe técnico del sismo de pedernales. quito-ecuador, 2016.
- [15] Arturo Egüez, Miguel Gaona, and Andrea Albán. Mapa geológico de la república del ecuador. 2017.
- [16] Muawia A. Dafalla. Effects of clay and moisture content on direct shear tests for clay-sand mixtures. *Advances in Materials Science and Engineering*, 2013:1–8, December 2012.
- [17] I. A. Oyediran and H. F. Durojaiye. Variability in the geotechnical properties of some residual clay soils from southwestern nigeria. *International Journal of Scientific Engineering Research*, 2(9), September 2011.
- [18] Keith B. Hodinott. *Physico-chemical Aspects of Soil and Related Materials*, volume 1905. ASTM International, 1990.
- [19] T.O Durotoye and J.O Akinmusuru. Effects of sodium chloride on the engineering properties of expansive soils. *International Journal of Research in Engineering and Technology*, 5(9), September 2016.
- [20] Vulcanología Instituto Geofísico. Red de observatorios vulcanológicos (rovig), 2018.

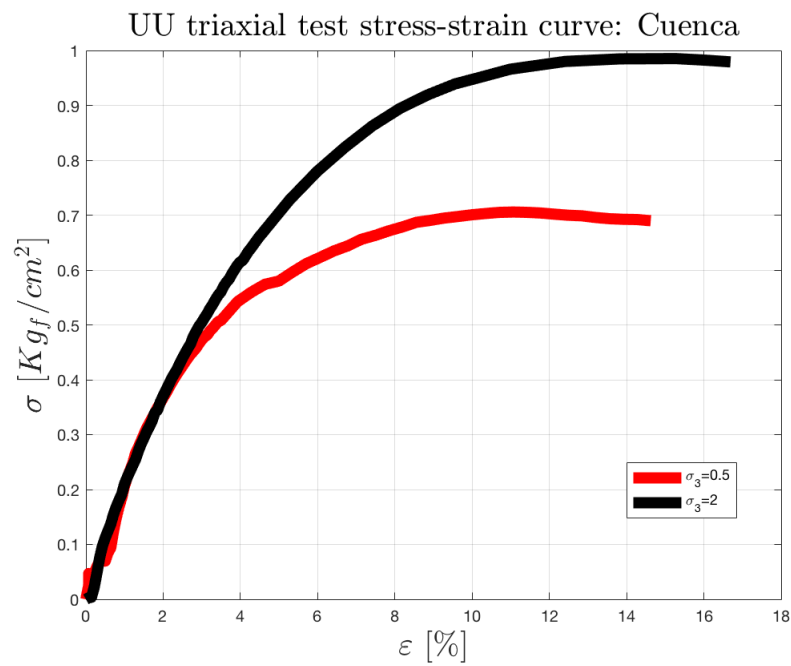
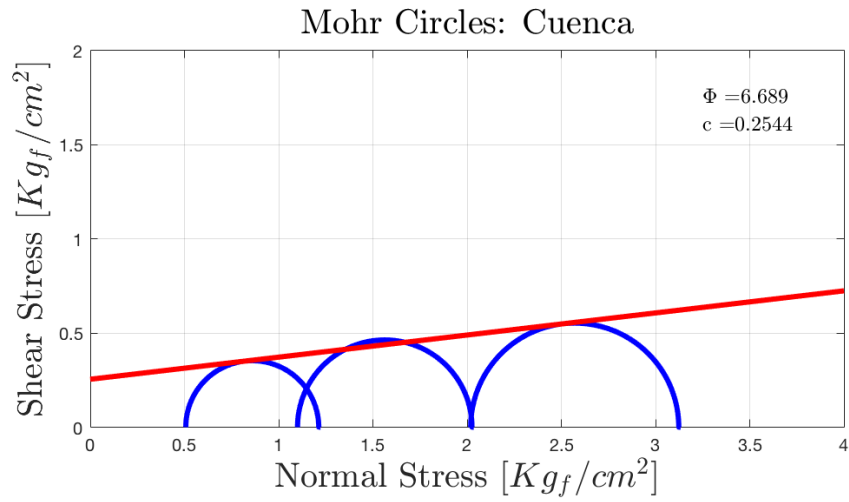
- [21] Patricia A. Mothes. *Lahars of Cotopaxi Volcano, Ecuador: hazard and risk evaluation*. Springer, Dordrecht, 1992.
- [22] Martín H Iriondo. *Cuaternario de Ecuador, Perú y Chile*. Moglia S.R.L, November 2012.
- [23] ASTM D422-17. *Standard Test Methods for Particle-Size Distribution (Gradation) of Soils Using Sieve Analysis*. ASTM International, West Conshohocken. PA, 2017.
- [24] ASTM D4318-17. *Standard Test Methods for Liquid Limit, Plastic Limit, and Plasticity Index of Soils*. ASTM International, West Conshohocken. PA, 2017.
- [25] J M. Rodriguez. Importance of the particle shape on mechanical properties of soil materials. Master's thesis, Luleå University of Technology, SE-97187 Luleå, Sweden, 2013.
- [26] R Surendra and K. Sanjeev. Role of geotechnical properties of soil on civil engineering structures. *Resources and Environment*, 7(4):103–109, 2017.
- [27] A B. Cerato and A J. Lutenegeger. Determination of surface area of fine-grained soils by the ethylene glycol monoethyl ether (egme) method. *Geotechnical Testing Journal*, 25(3), 2002.
- [28] ASTM D2216-10. *Standard Test Methods for Laboratory Determination of Water (Moisture) Content of Soil and Rock by Mass*. ASTM International, West Conshohocken. PA, 2010.
- [29] E Polidori. Relationship between the atterberg limits and clay content. *Soils and Foundations*, 47(5):887–896, October 2007.
- [30] Donald M. Burmister. Principles and techniques of soil identification. *Proceedings of the Highway Research Board*, page 420, 1949.
- [31] M Das Braja. *Geotechnical Engineering Handbook*. J. Ross Publishing, 2010.
- [32] R P. Long, K R. Demars, and A Covo. Conversion to the unified soil classification system. Technical report, Connecticut Cooperative Transportation Research Program, December 1987.
- [33] ASTM Standard D 2850-03. *Standard Test Method for Unconsolidated-Undrained Triaxial Compression Test on Cohesive Soils*. ASTM International, West Conshohocken. PA, 2003.

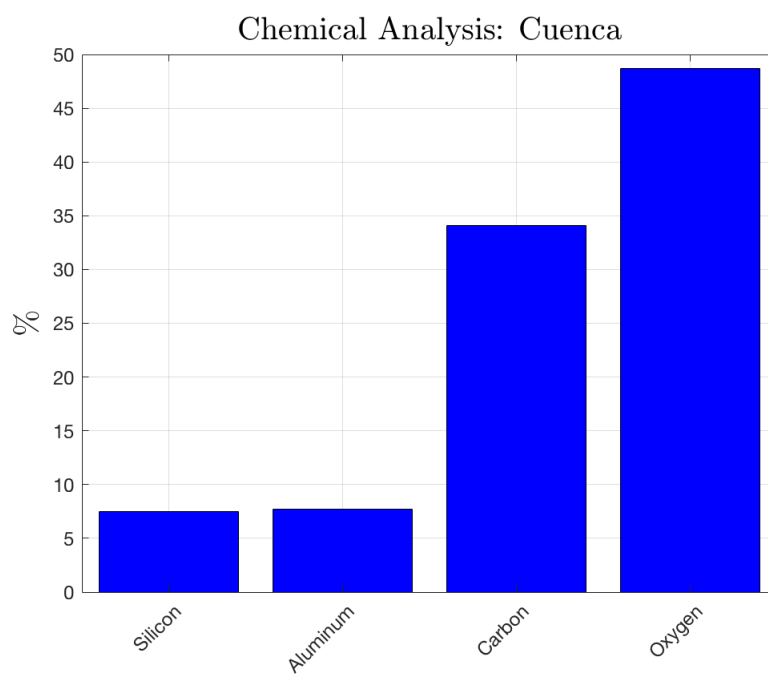
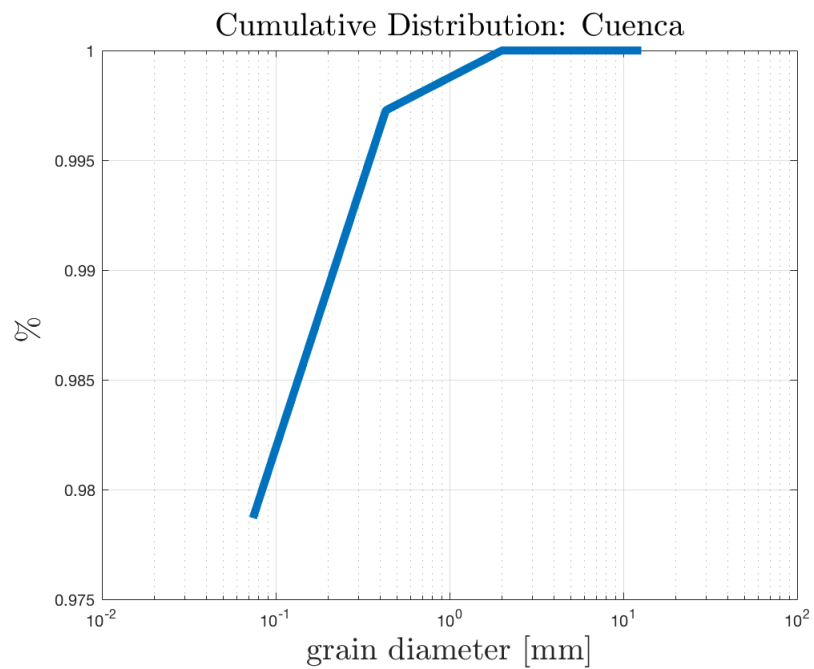
- [34] D C. Drucker and W Prager. Soil mechanics and plastic analysis or limit design. Division of Applied Mathematics 2, Brown University, 1951.
- [35] V Osipov. Friction and cohesion as multifaceted factors of soil shear resistance. *Soil Mech Found Eng*, 53(143), 2016.
- [36] H Yokoi. Relationship between soil cohesion and shear strength. *Soil Science and Plant Nutrition*, 14(3):89–93, 1968.
- [37] J F. Labuz and A Zang. Mohr–coulomb failure criterion. *Rock Mechanics and Rock Engineering*, 45(6):975–979, November 2012.
- [38] G Fontaine, I Narváez, and P Cisneros. *Capítulo IV Estado del suelo*. FLACSO-MAE-PNUMA, 2008.
- [39] C Bareither, T Edil, and et al. Geological and physical factors affecting the friction angle of compacted sands. *Journal of Geotechnical and Geoenvironmental Engineering*, 134(10), 2008.
- [40] M. Hall and P Mothes. The rhyolitic–andesitic eruptive history of cotopaxi volcano, ecuador. *Bull Volcanol*, 2007.
- [41] A Martinez and P Hernández. Caracterización y sectorización de las propiedades físicas y mecánicas del suelo en los barrios "la libertad y la florida" de la ciudad de riobamba. Master's thesis, Universidad Nacional de Chimborazo, 2013.
- [42] A.W Skempton. The colloidal activity of clays. volume 1 of *Soil Mechanics and Foundation Engineering*, pages 47–61, 1953.
- [43] A. Laskar and S.K. Pal. Geotechnical characteristics of two different soils and their mixture and relationships between parameters. *EJGE*, 17, 2012.
- [44] G.O Adunoye. Study of relationship between fines content and cohesion of soil. *British Journal of Applied Science Technology*, 4(4):682–692, 2014.
- [45] C. Akayuli, B. Ofofu, S Nyako, and K Opuni. The influence of observed clay content on shear strength and compressibility of residual sandy soils. *Int J Eng Res Appl*, 3(4), July-August 2013.

- [46] W Shanyoug, D Chan, and K.C Lam. Experimental study of the fines content on dynamic compaction grouting in completely decomposed granite of hong kong. *CONSTR BUILD MATER*, 23:1249 –1264, 2009.
- [47] Ivan Vlahinić, Reid Kawamoto, Edward Andò, Gioacchino Viggiani, and José E. Andrade. From computed tomography to mechanics of granular materials via level set bridge. *Acta Geotechnica*, 12:85–95, 2017.

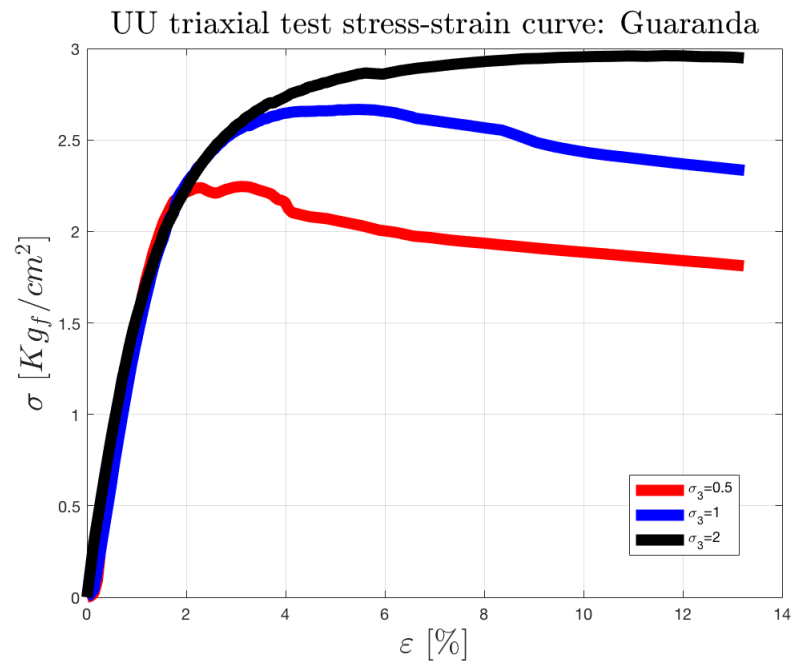
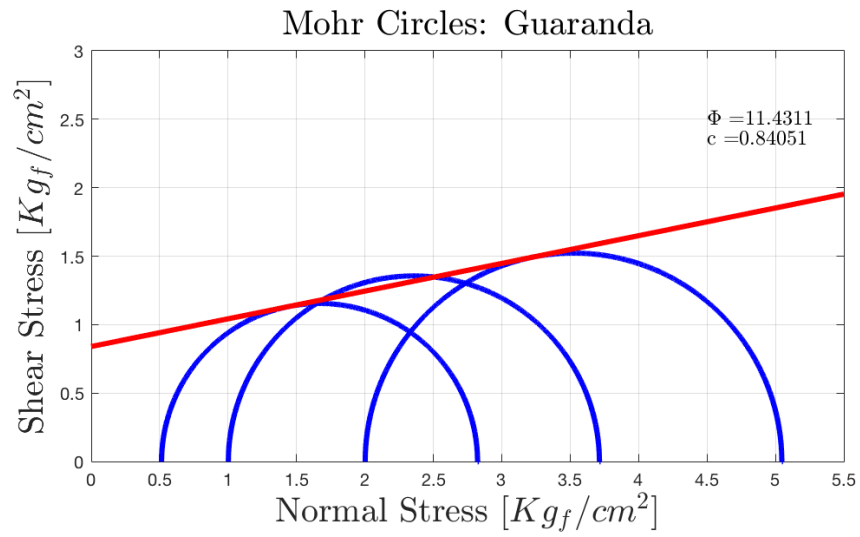
## A Appendix

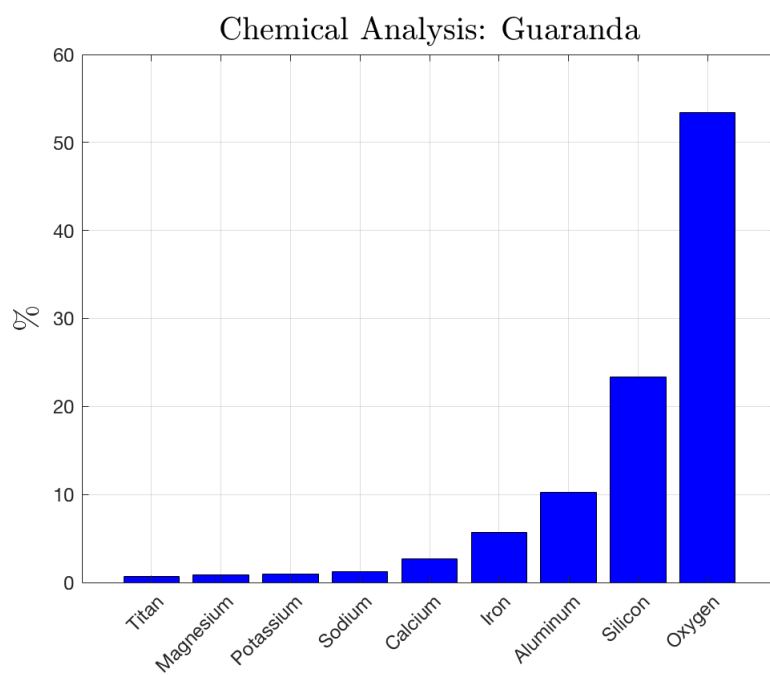
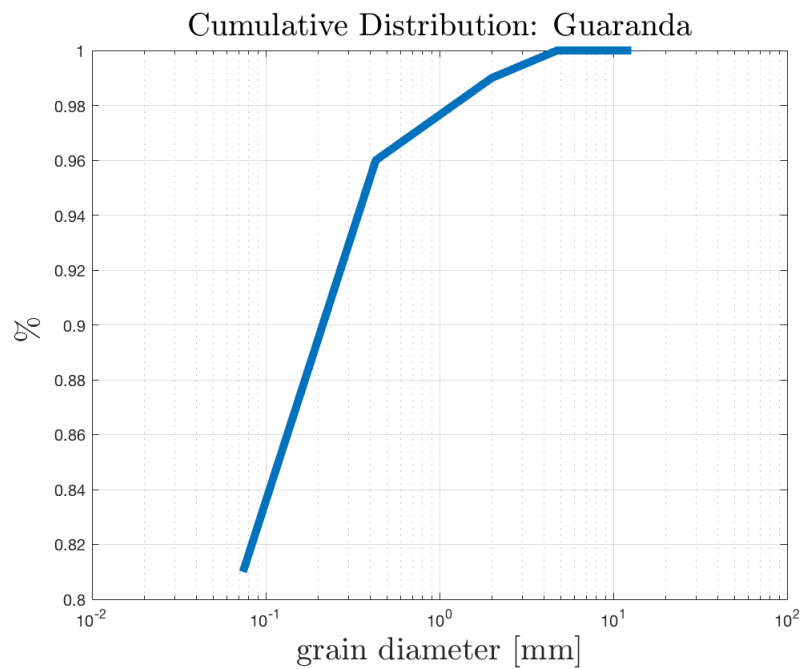
### A.1 Cuenca





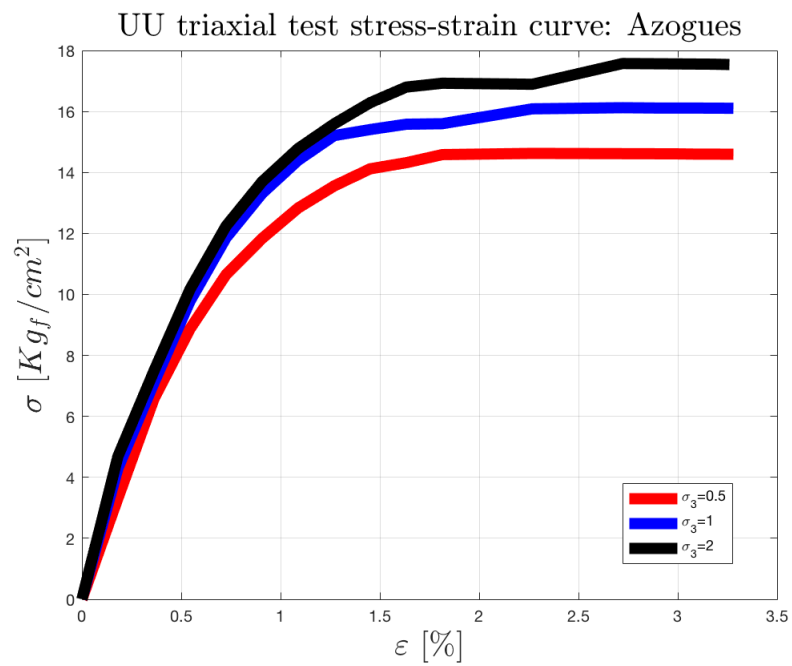
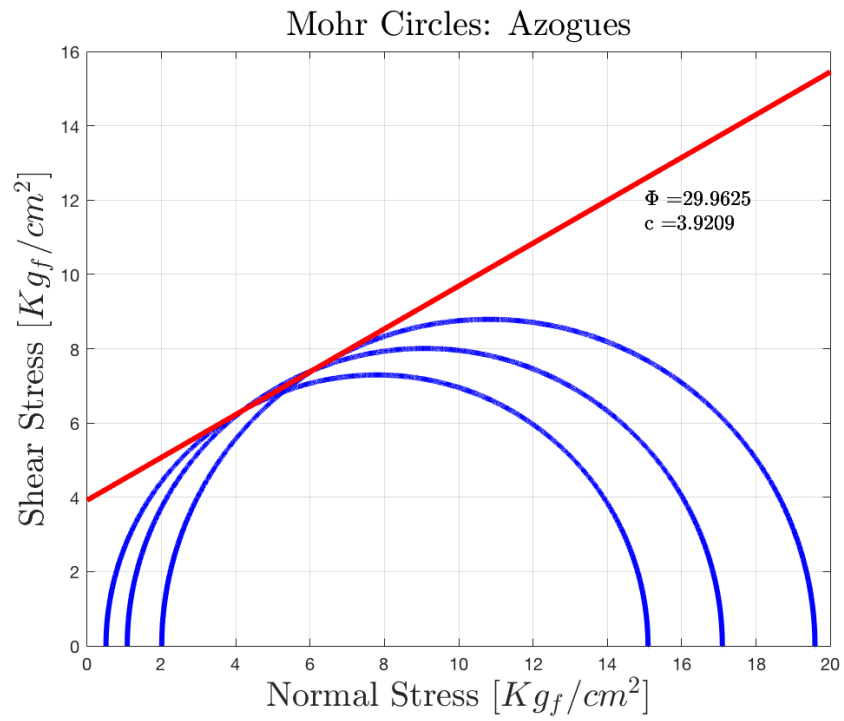
## A.2 Guaranda

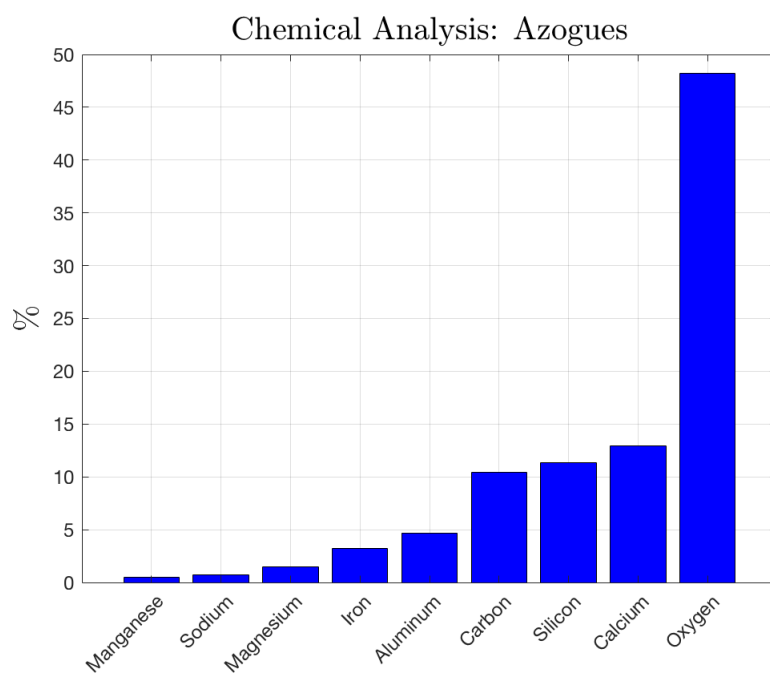
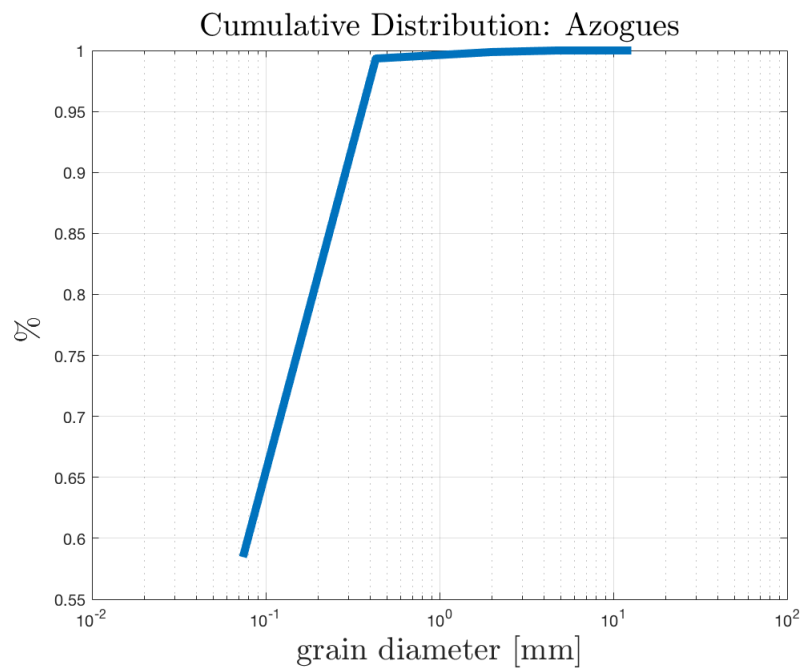




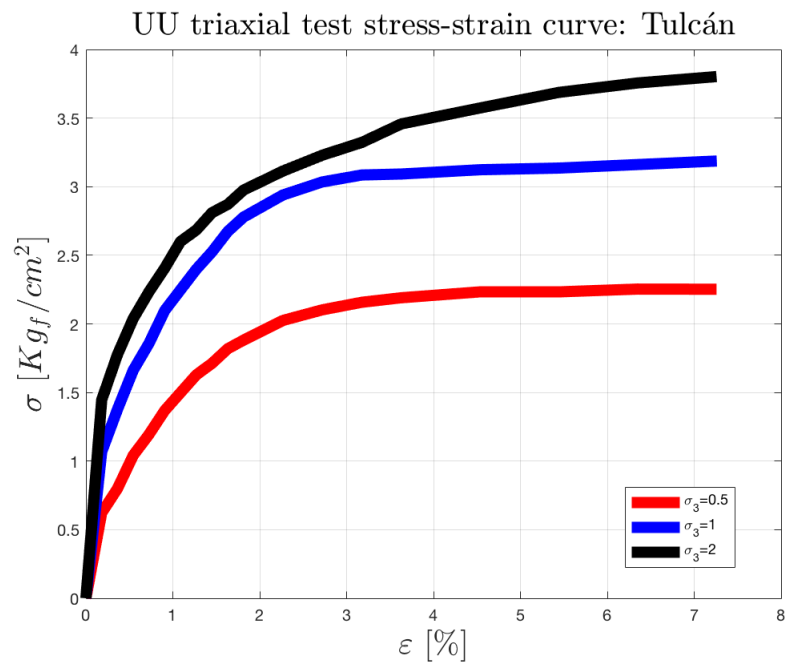
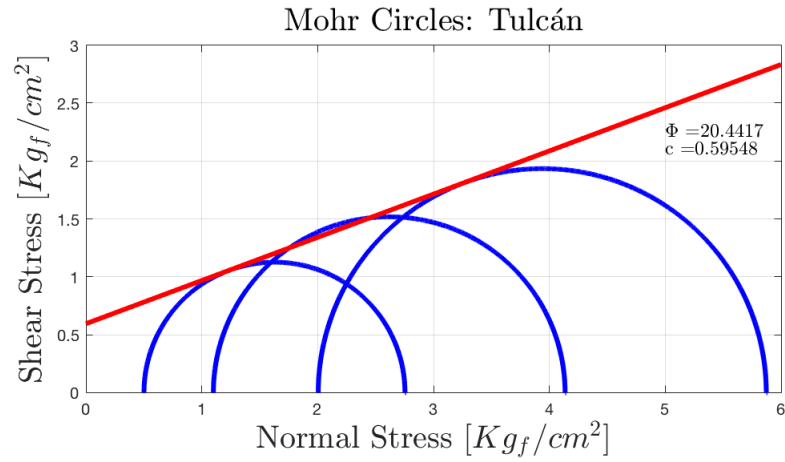


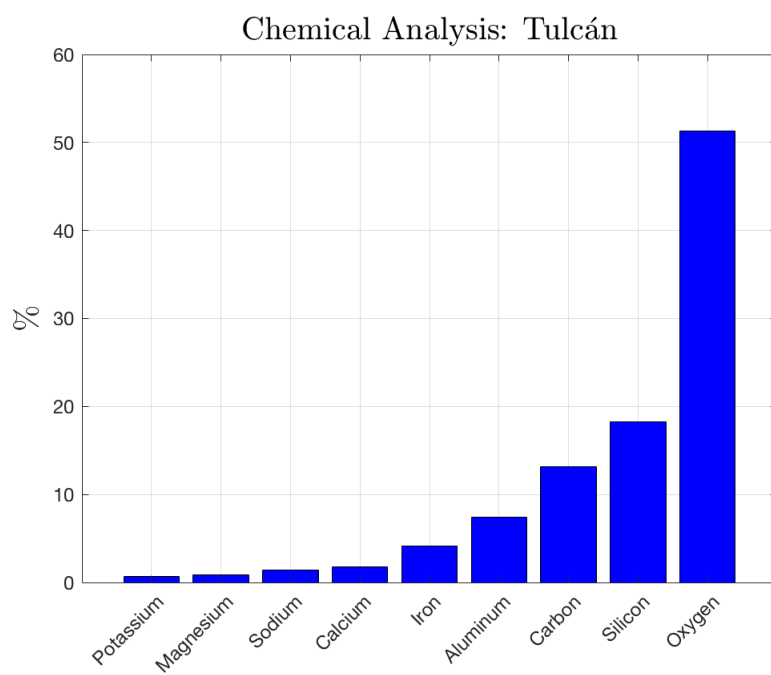
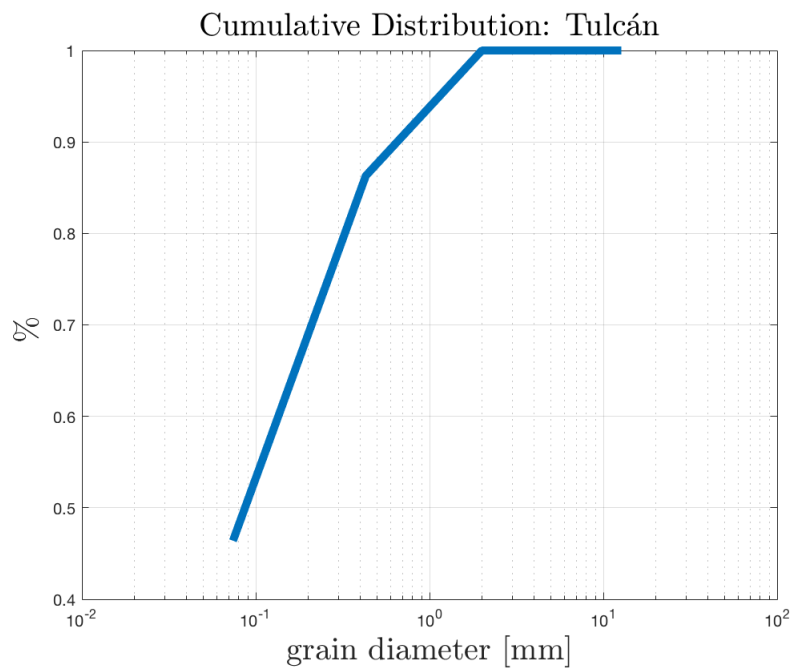
## A.3 Azogues



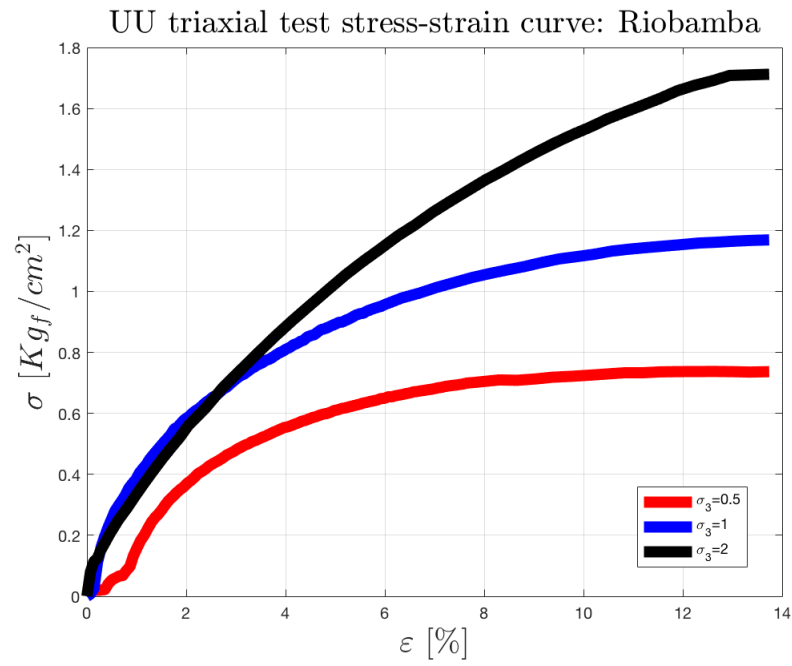
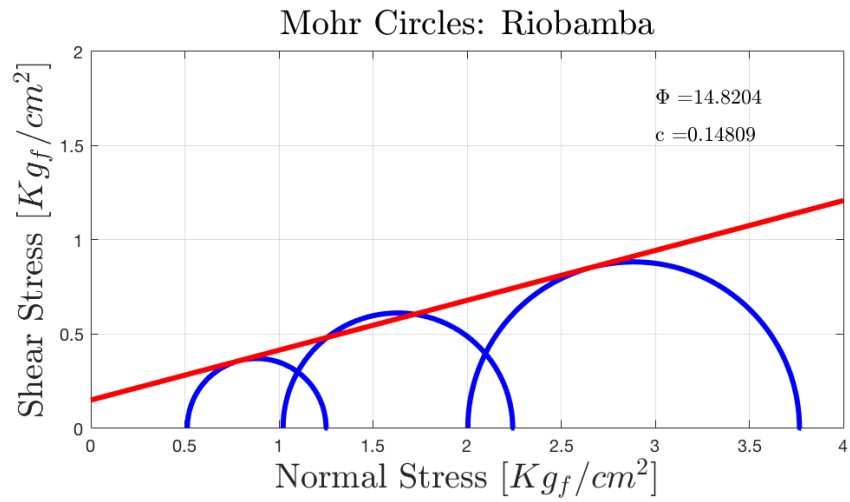


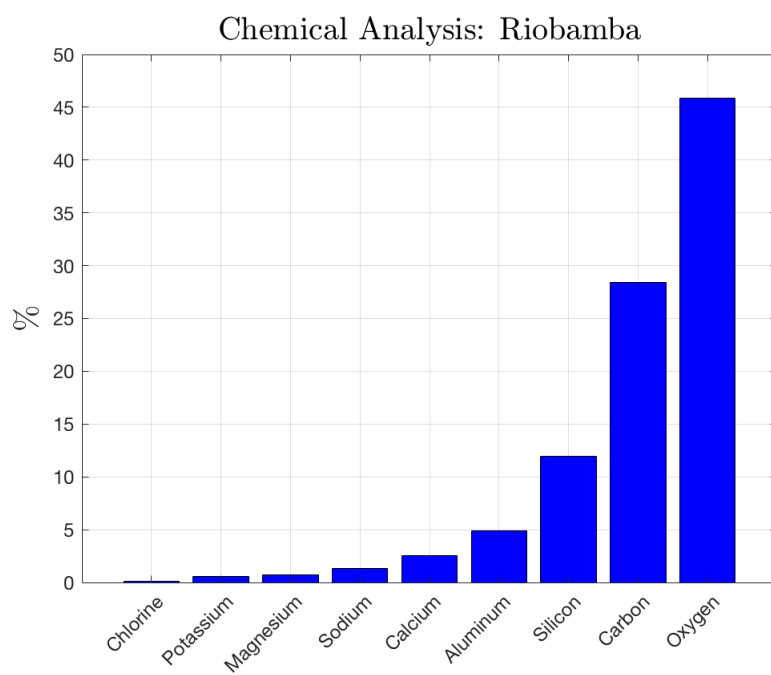
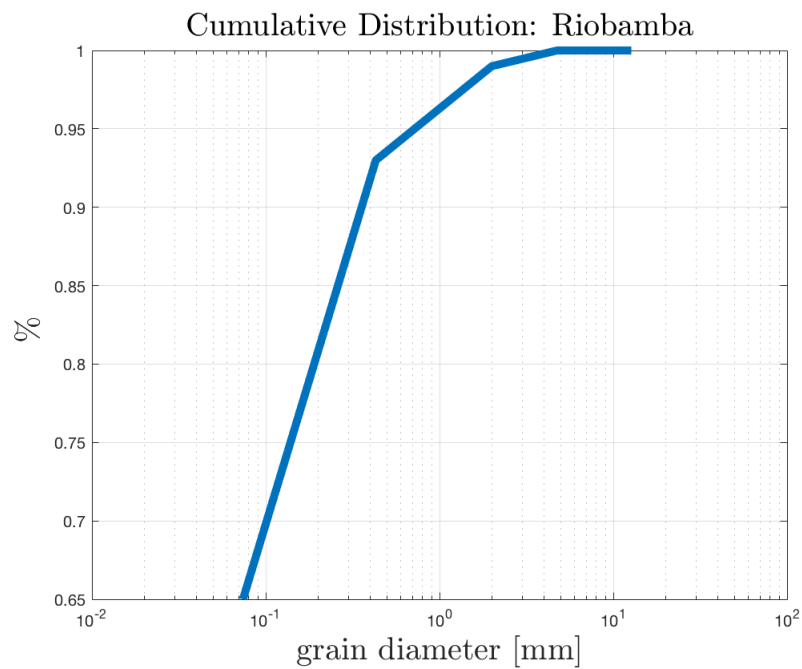
## A.4 Tulcán



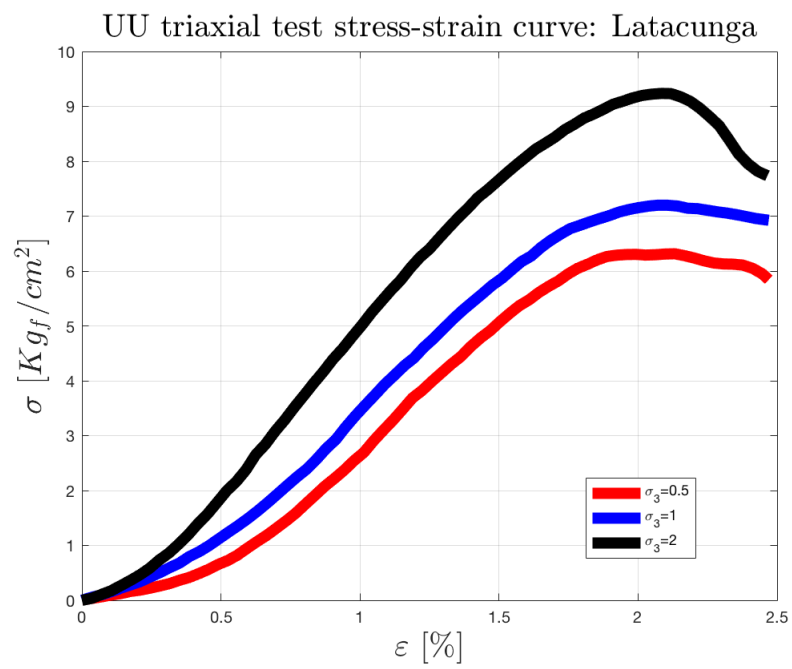
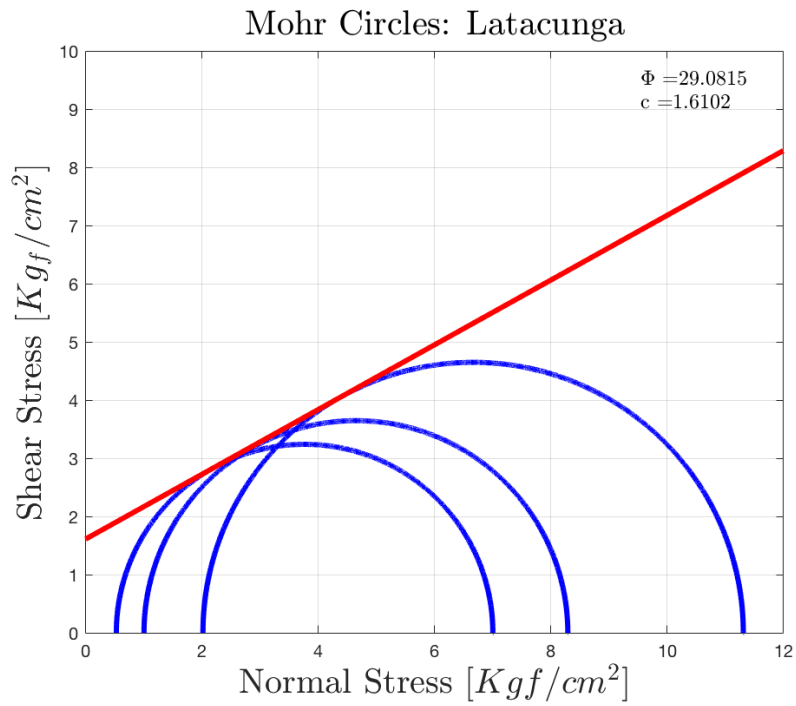


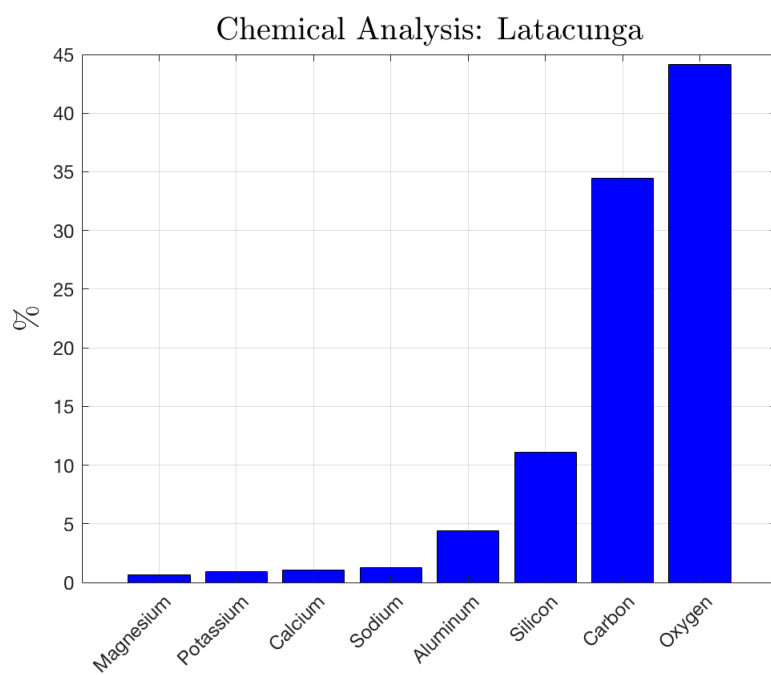
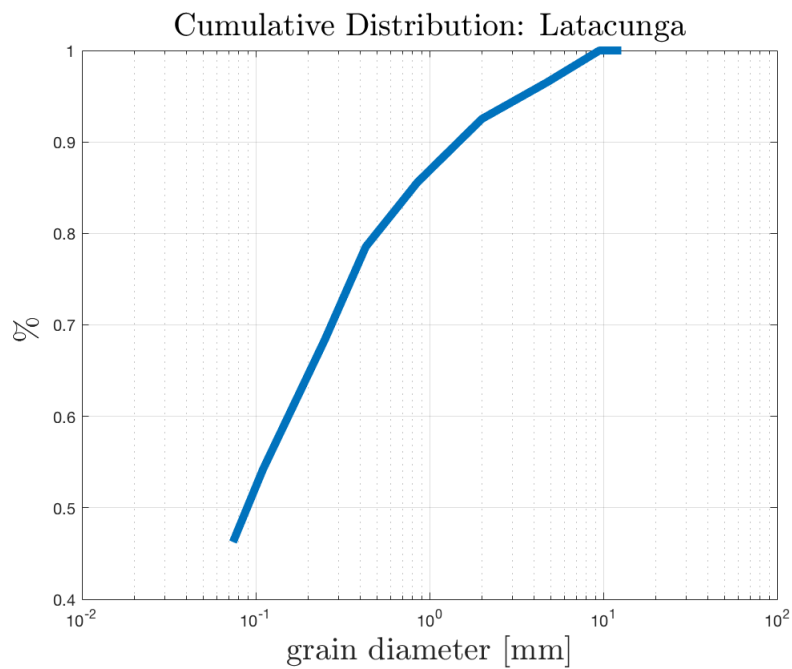
## A.5 Riobamba





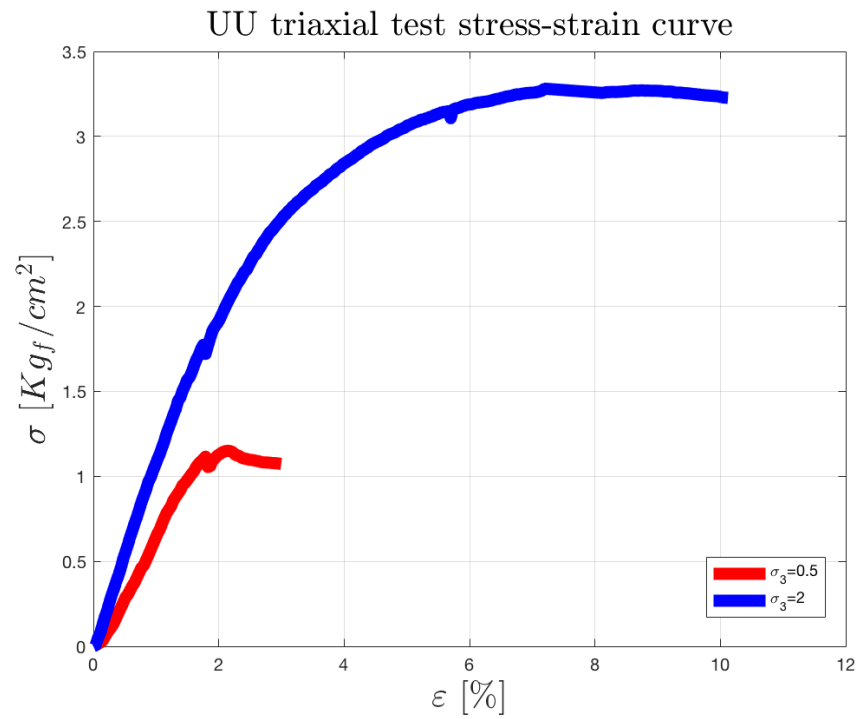
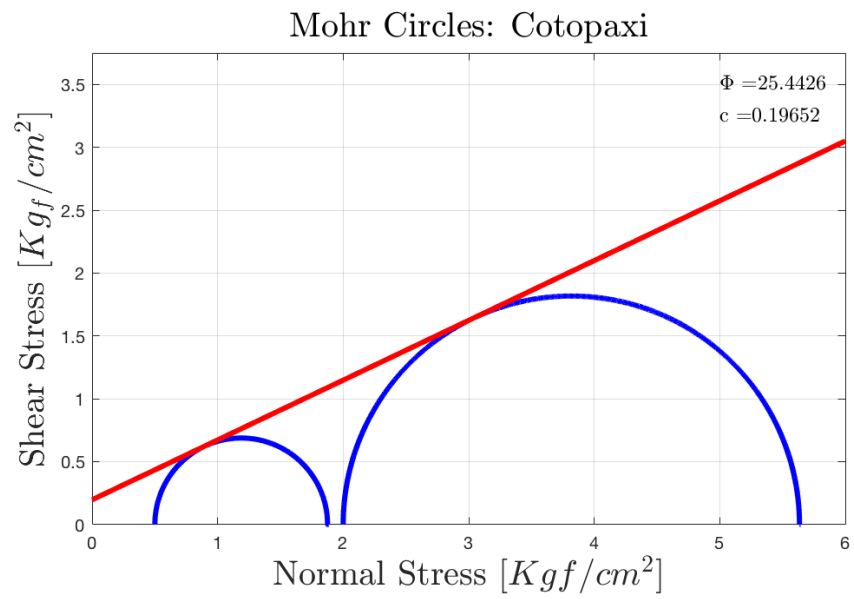
## A.6 Latacunga

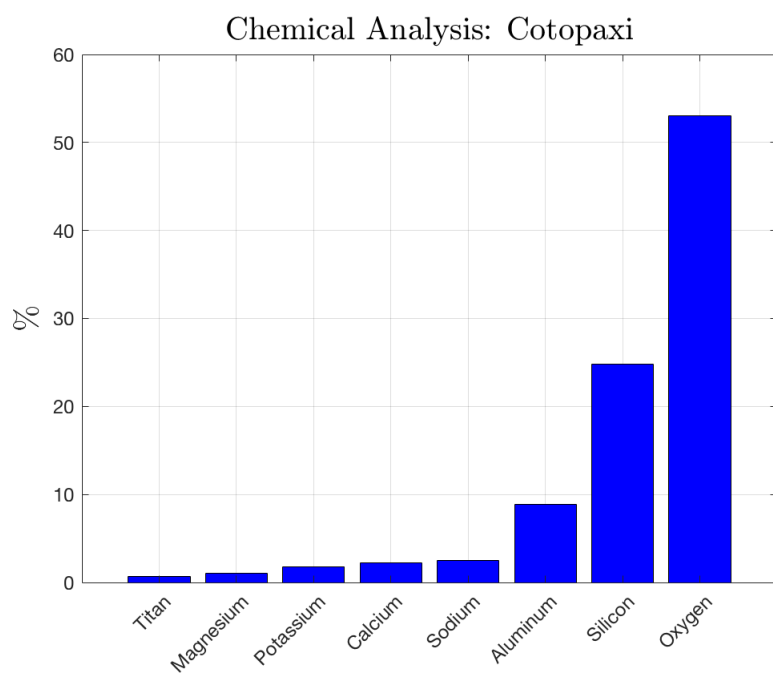
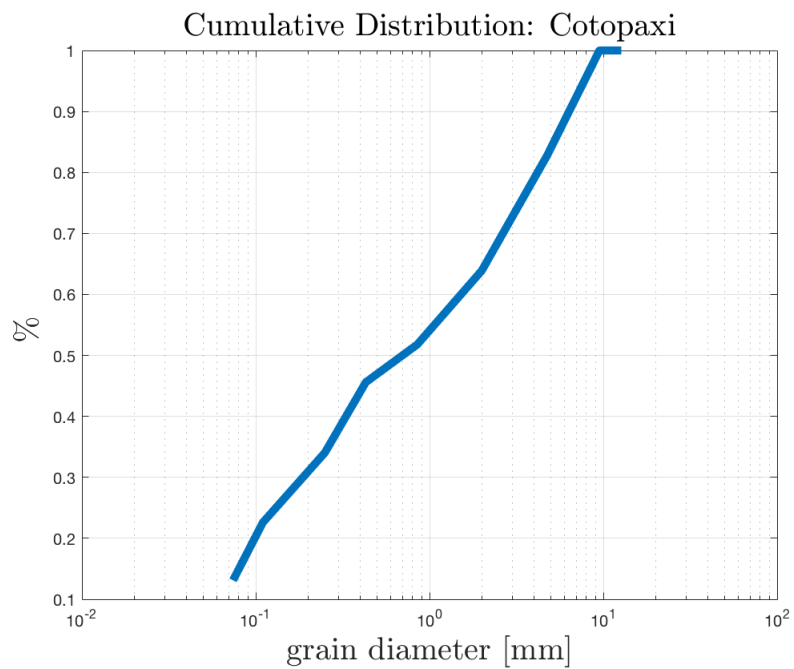




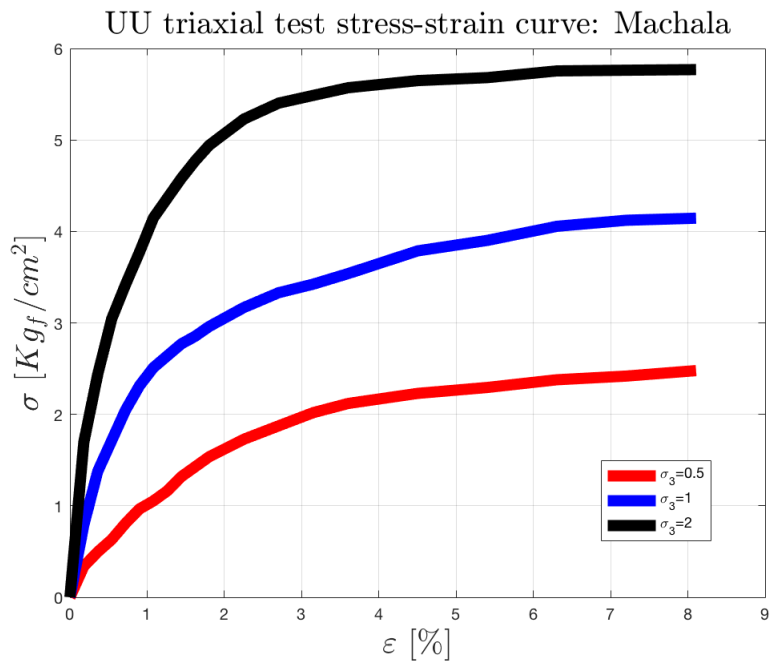
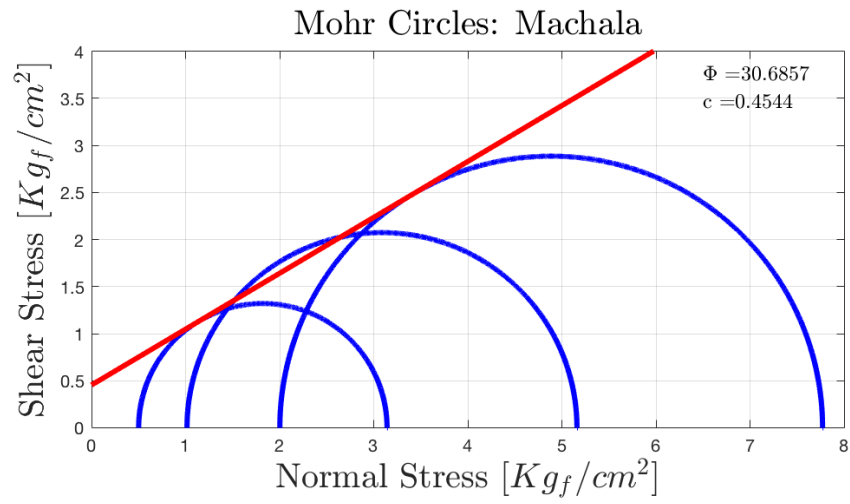


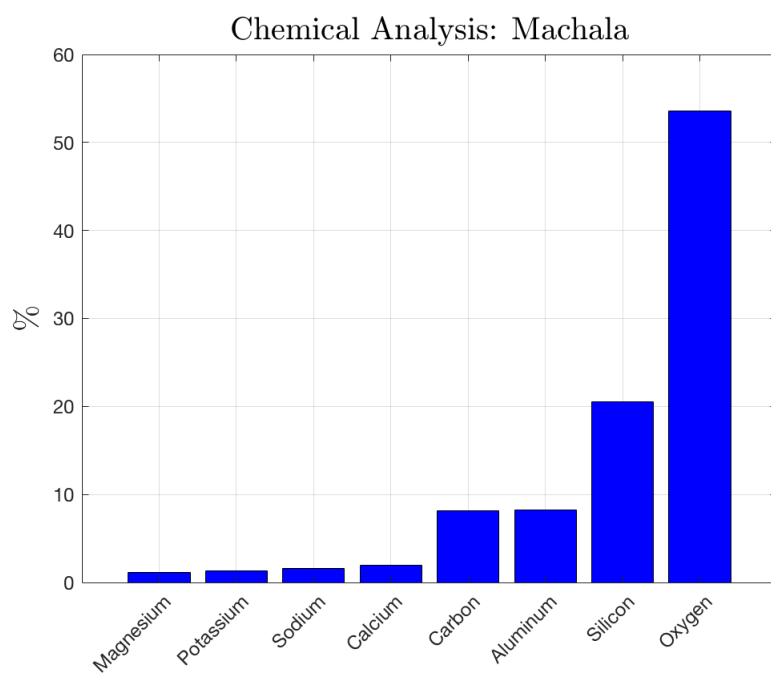
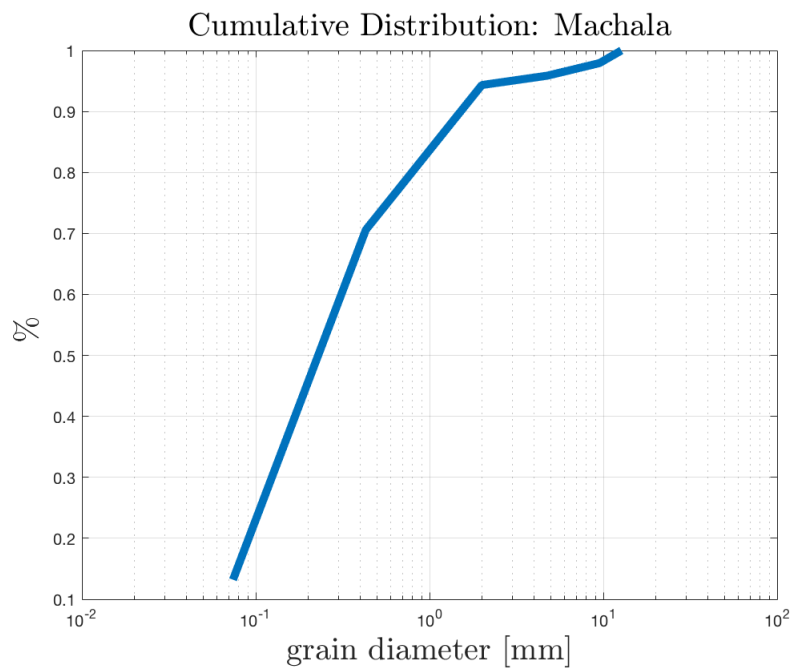
## A.7 Cotopaxi



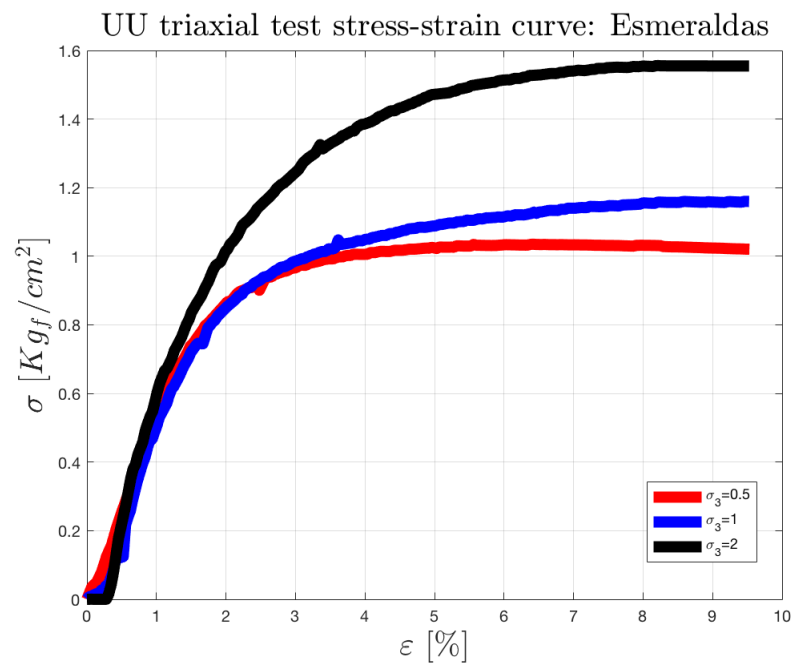
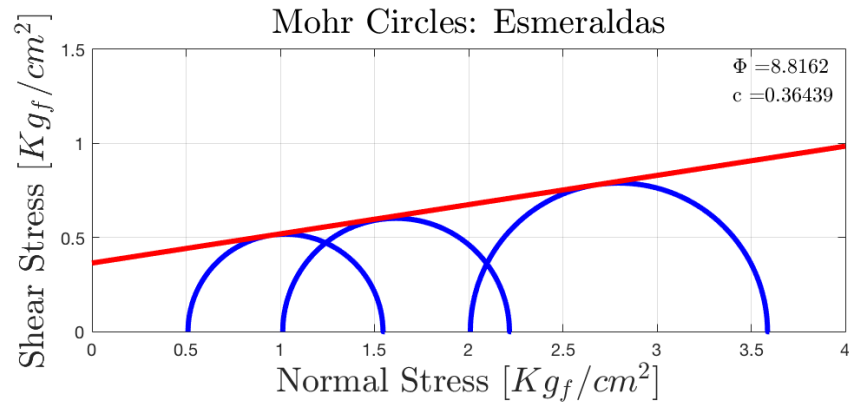


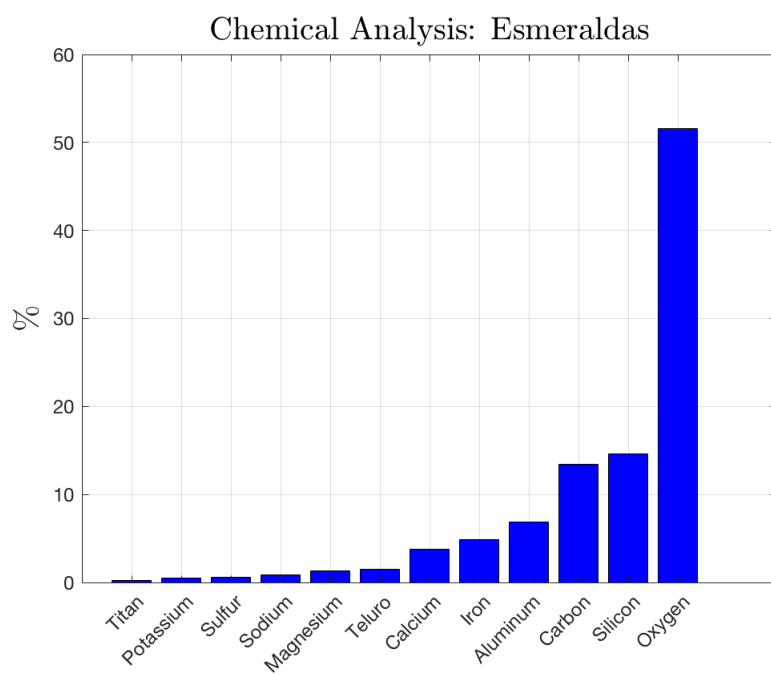
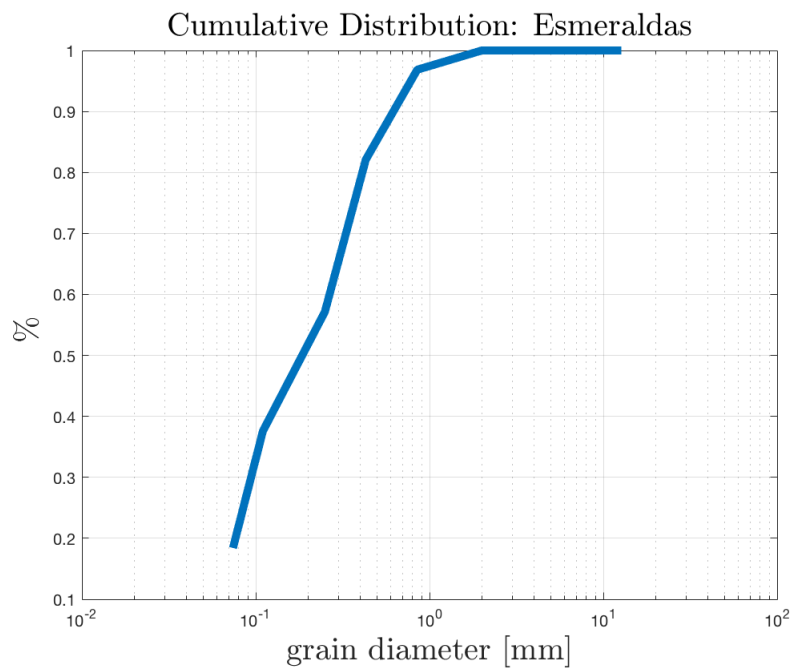
## A.8 Machala



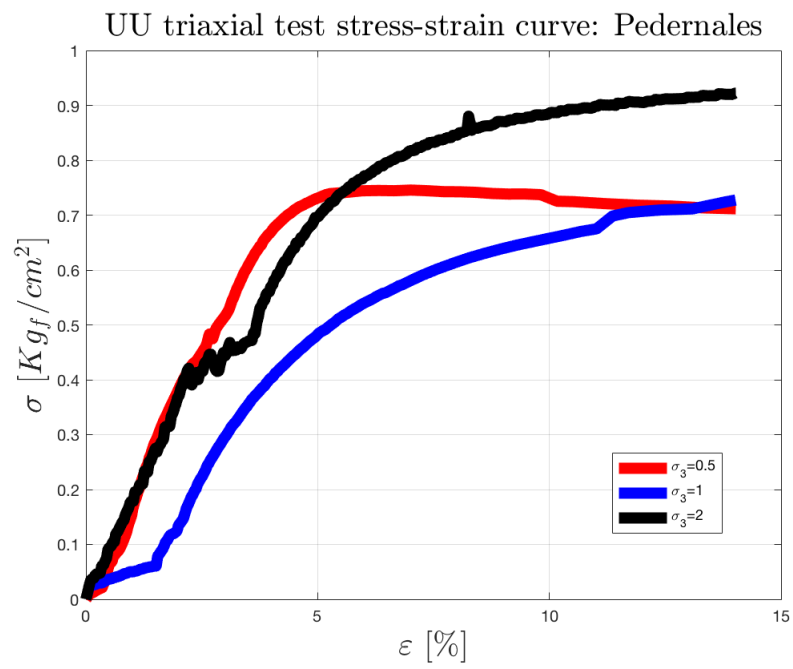
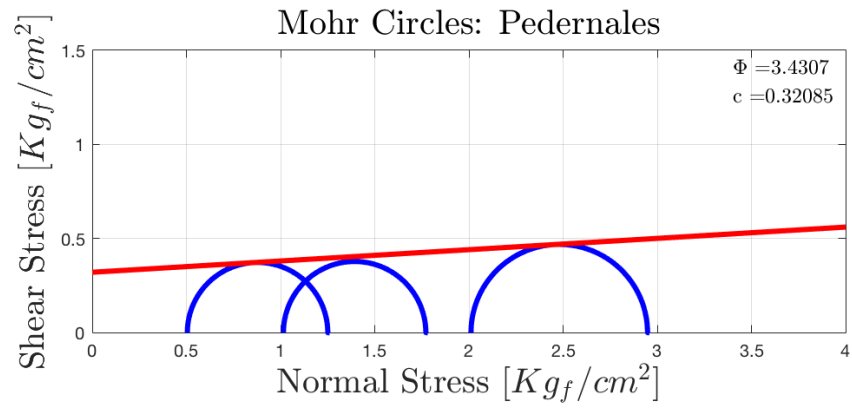


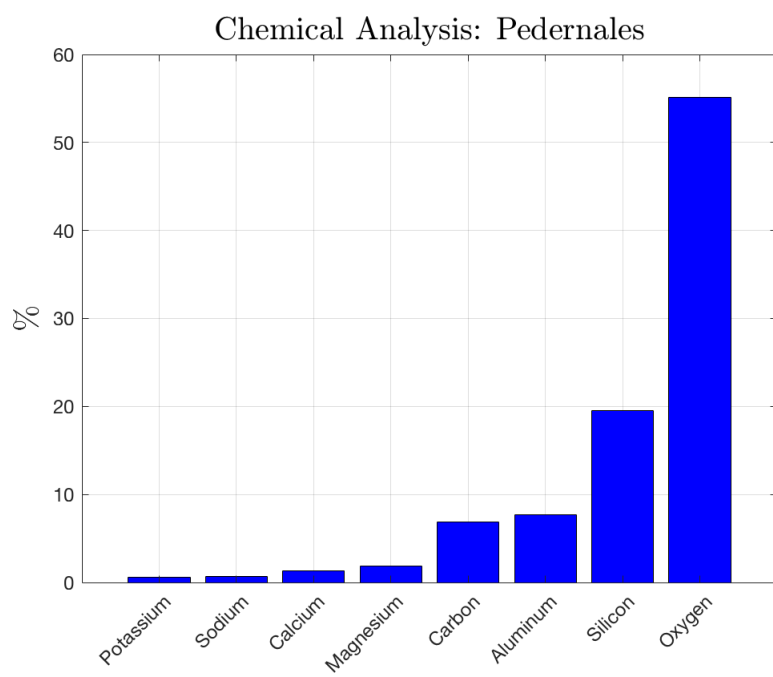
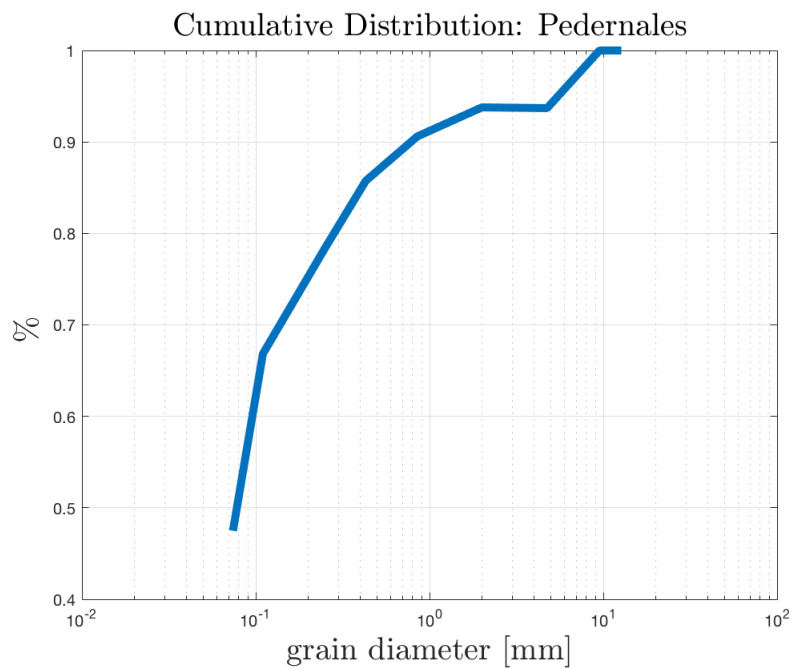
## A.9 Esmeraldas





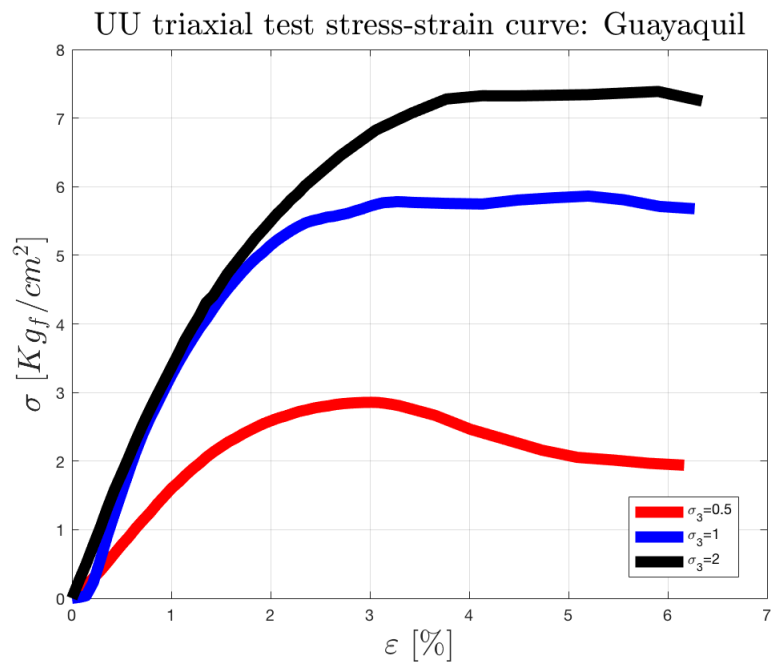
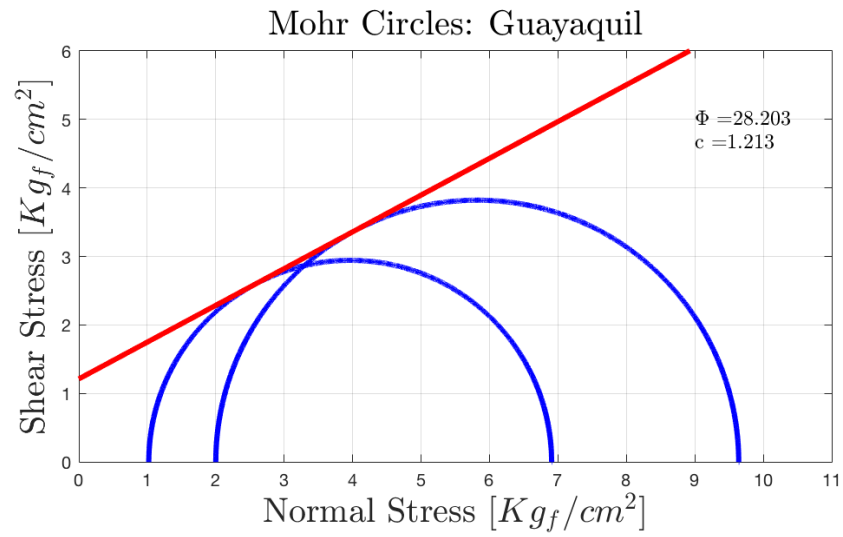
## A.10 Pedernales

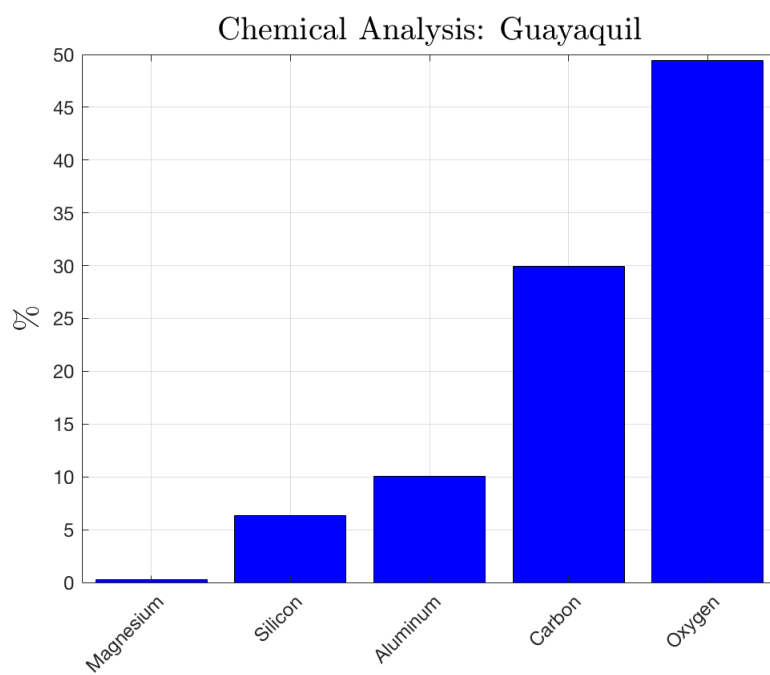
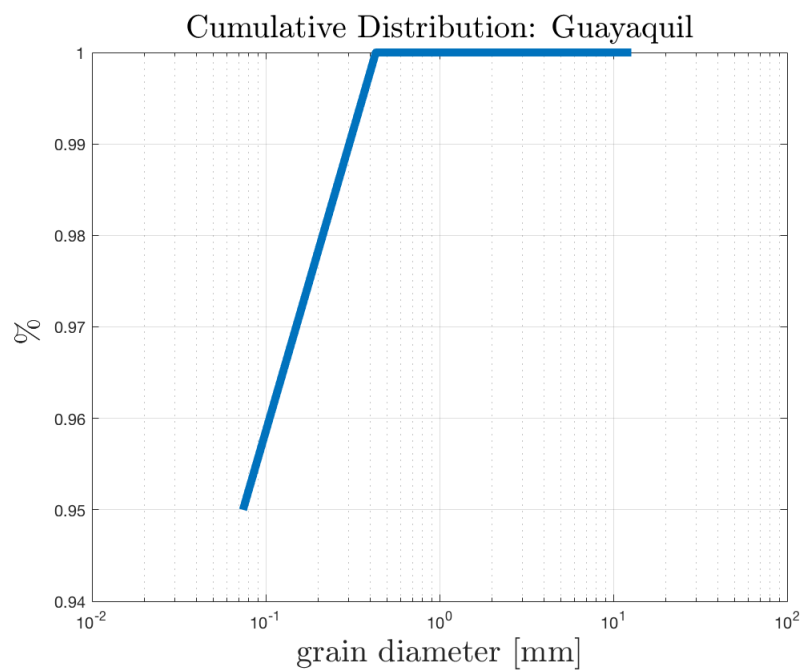




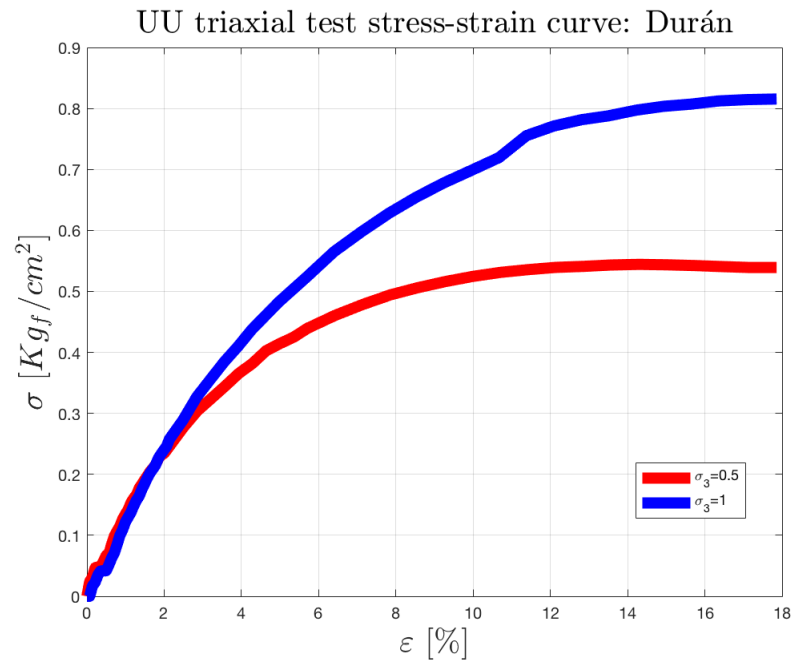
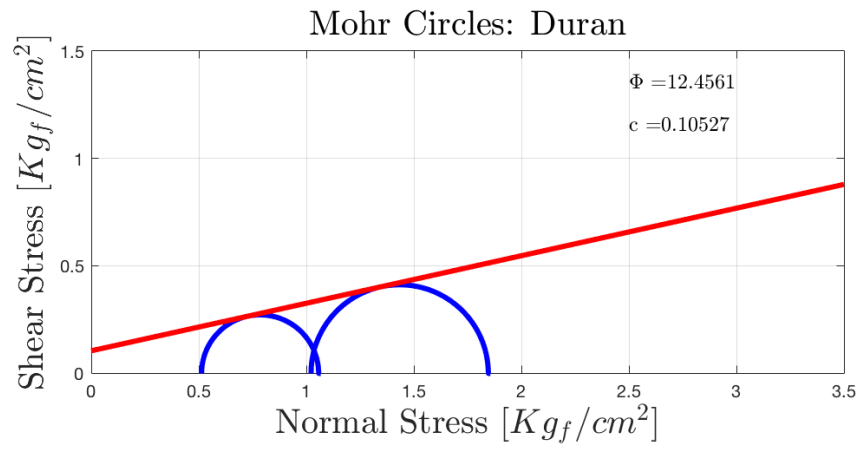


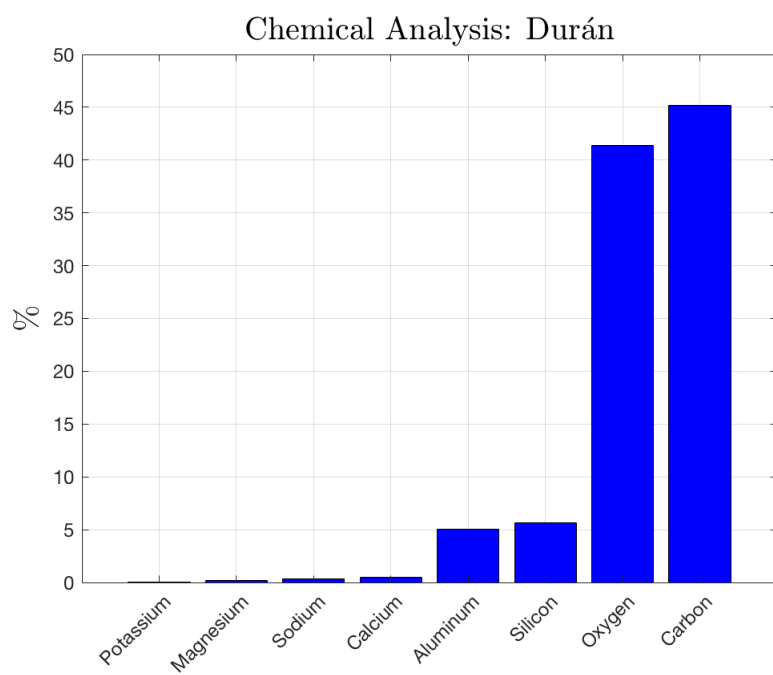
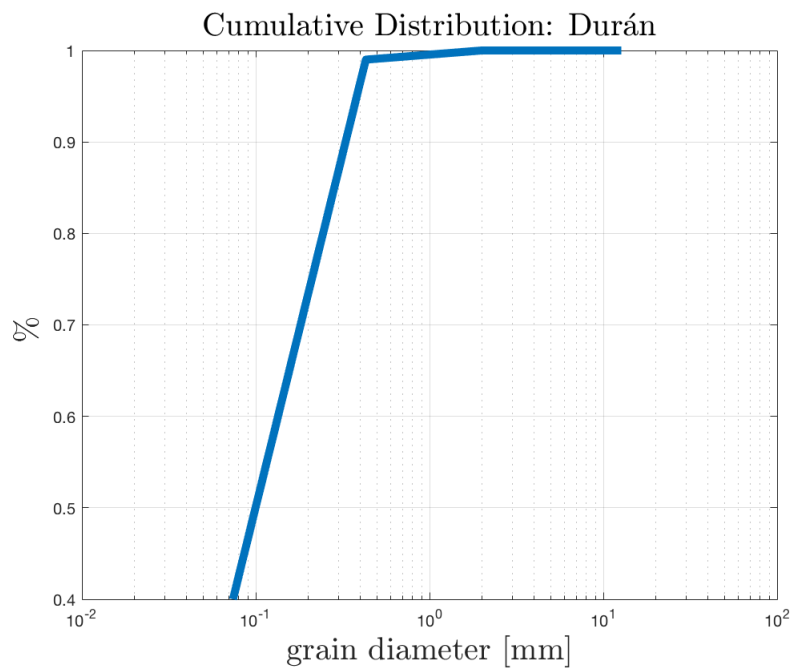
## A.11 Guayaquil



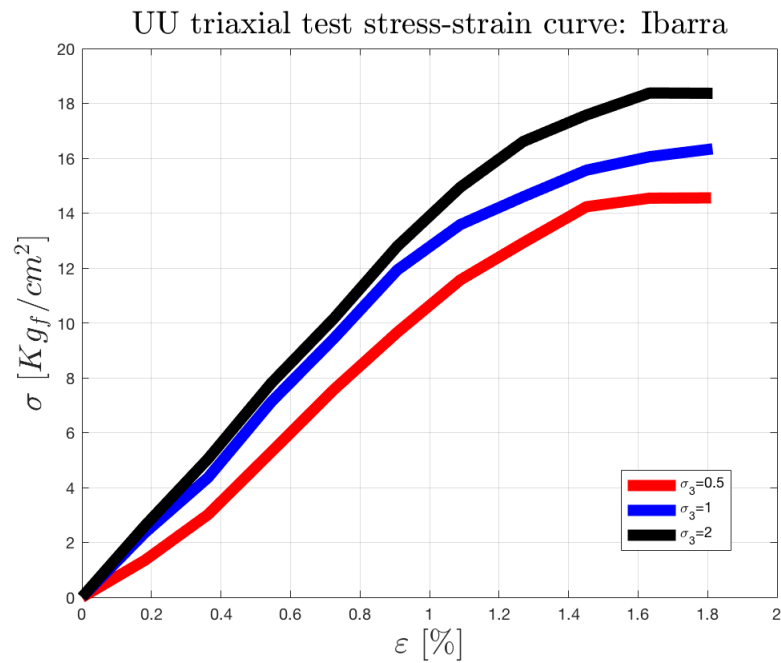
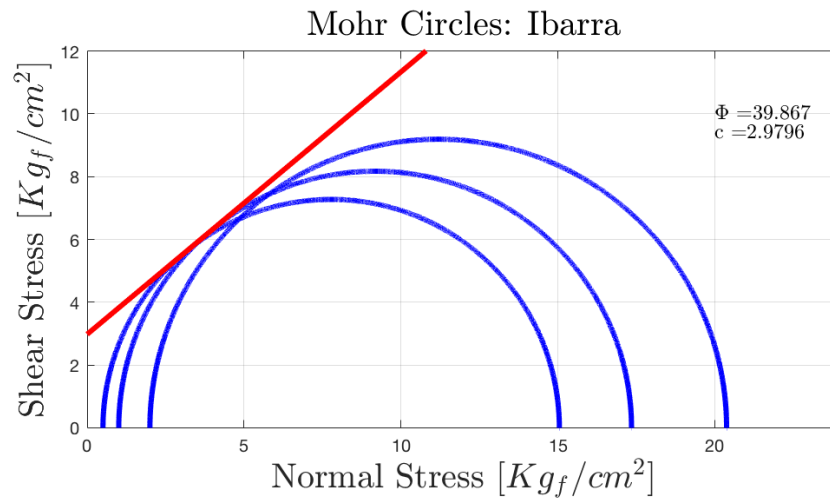


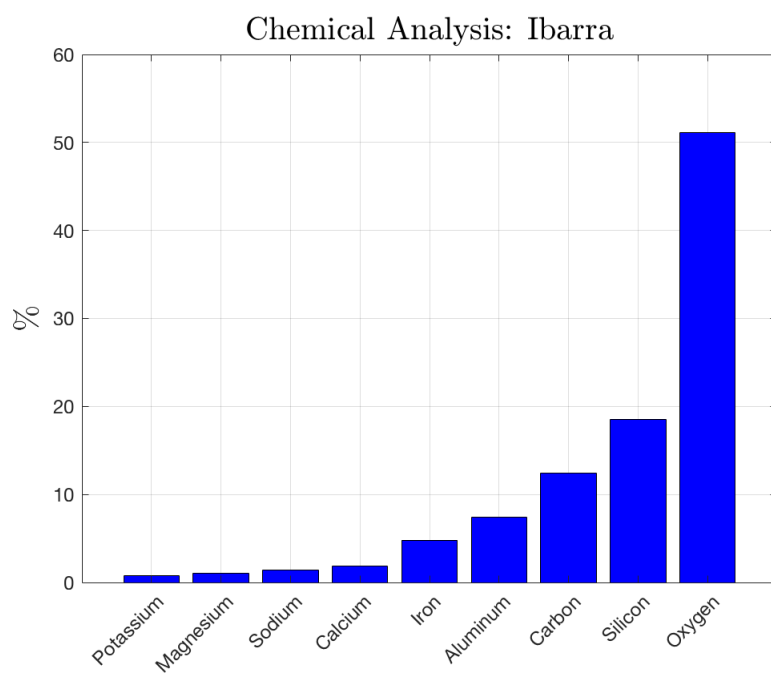
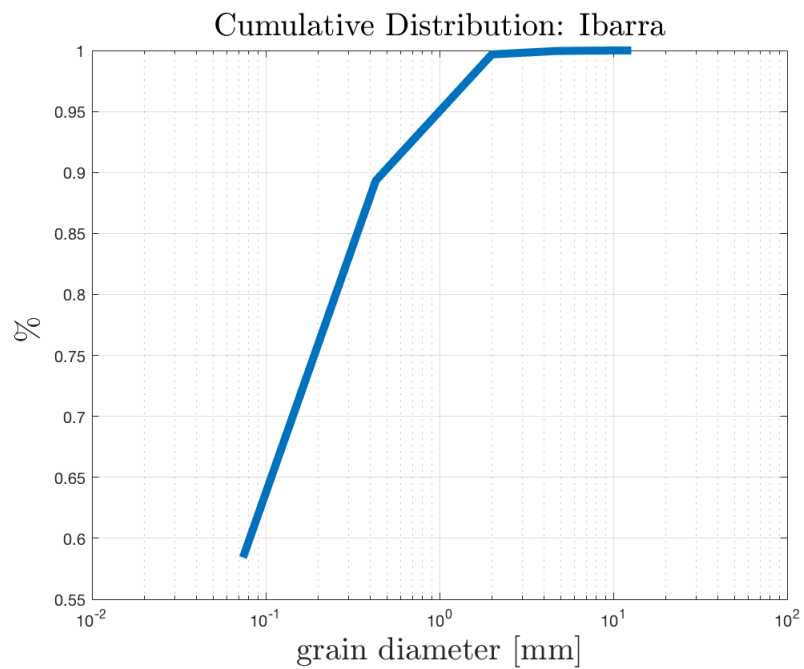
## A.12 Durán



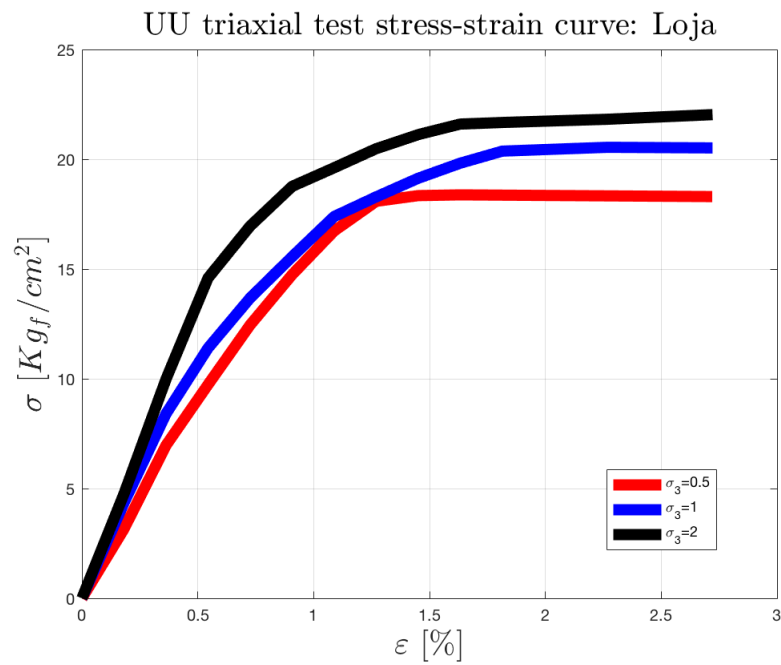
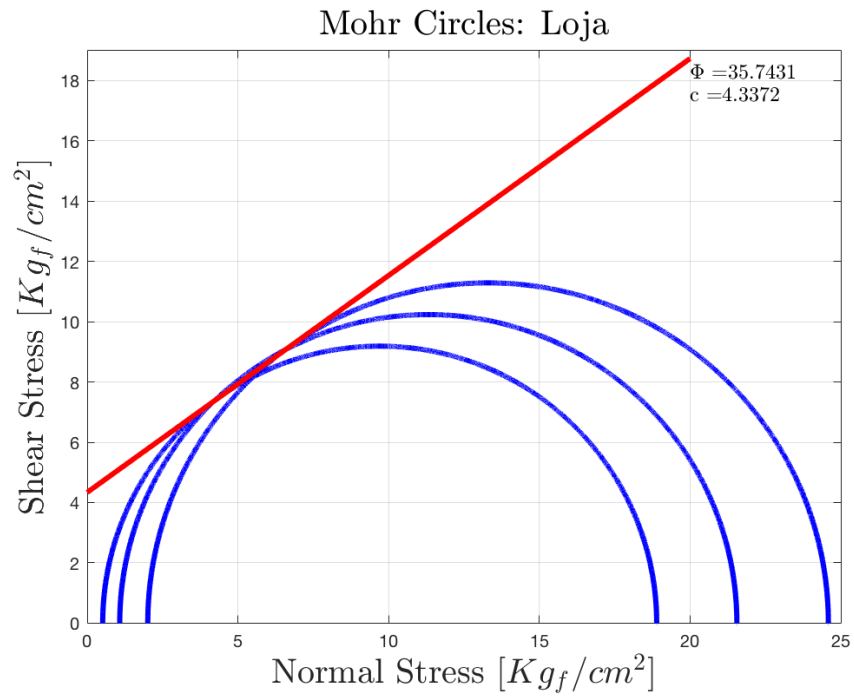


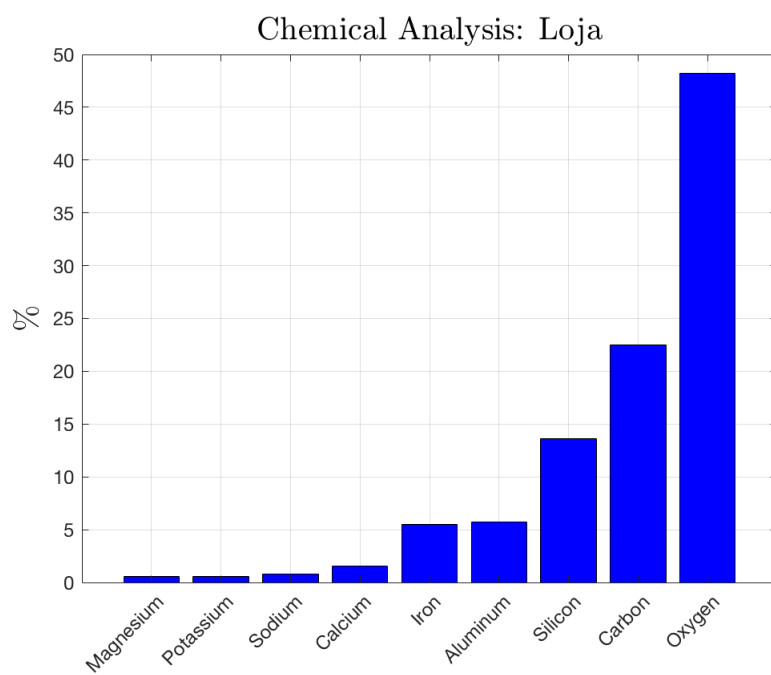
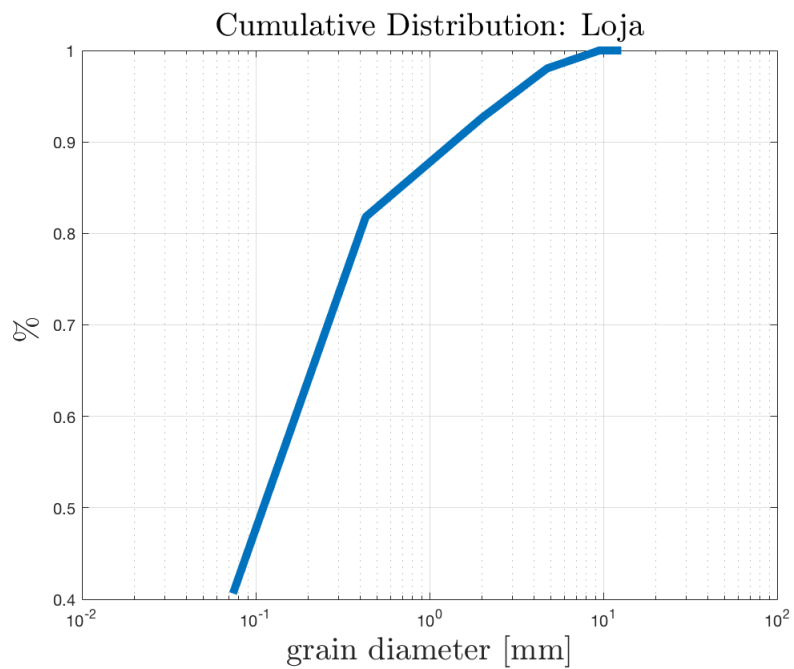
## A.13 Ibarra





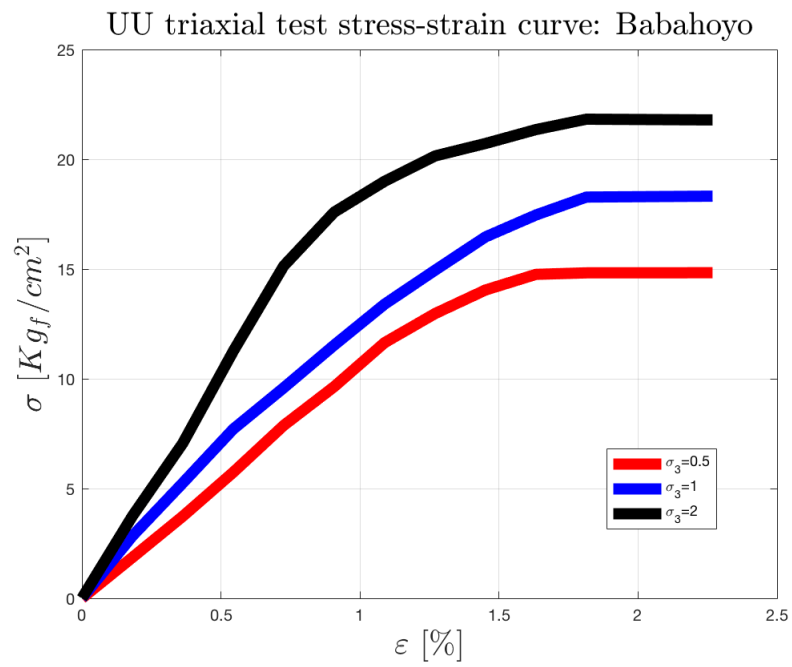
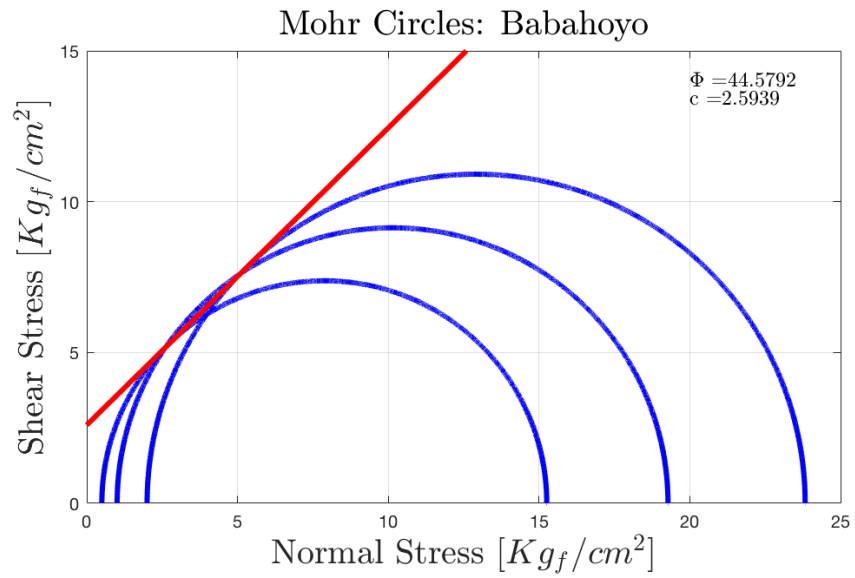
## A.14 Loja

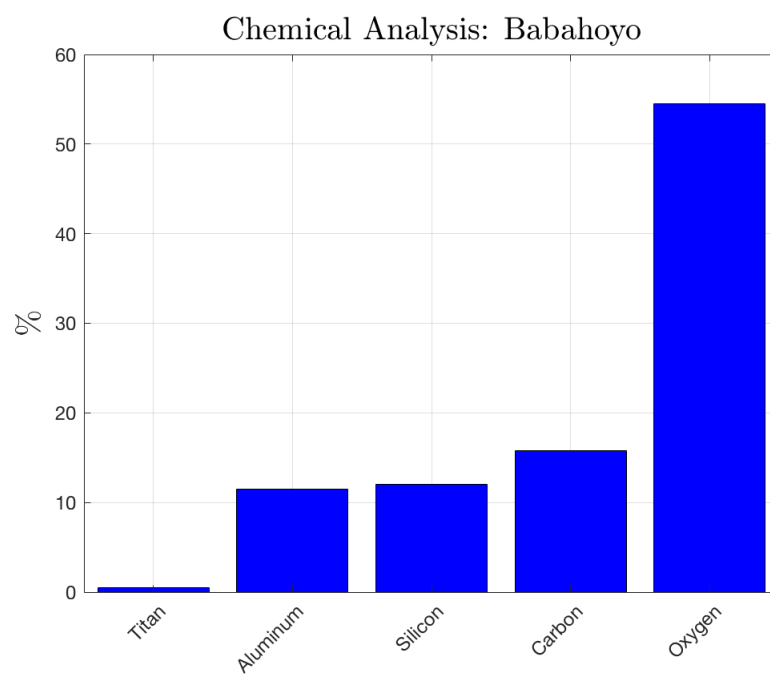
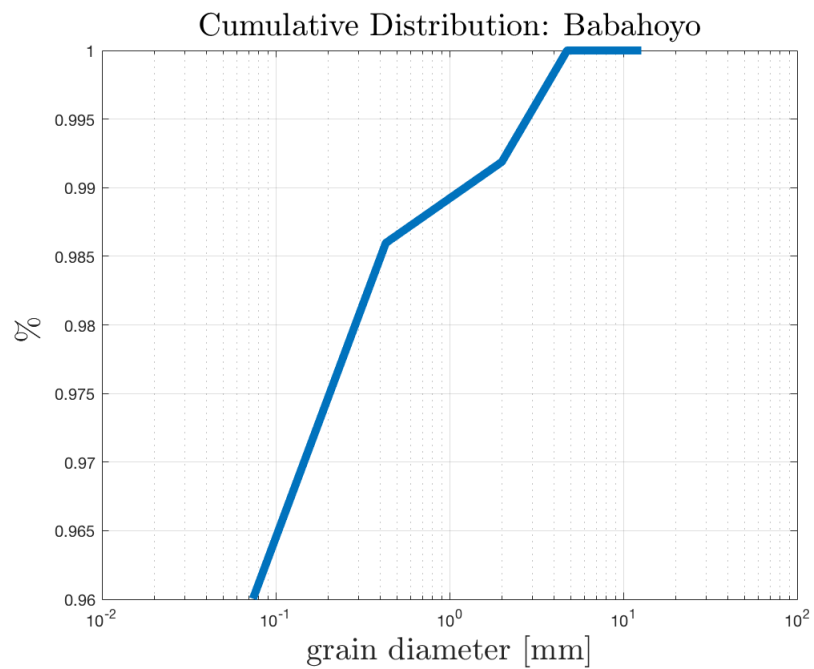




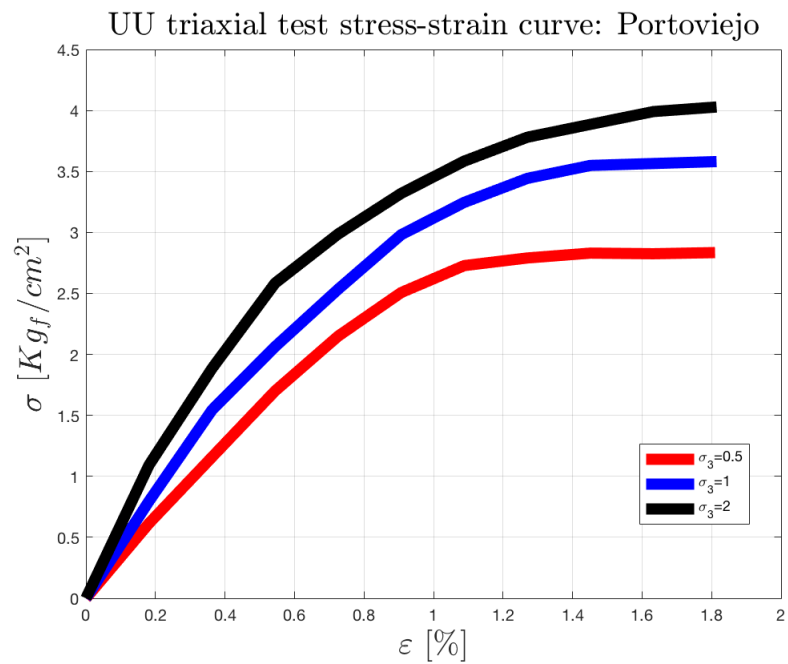
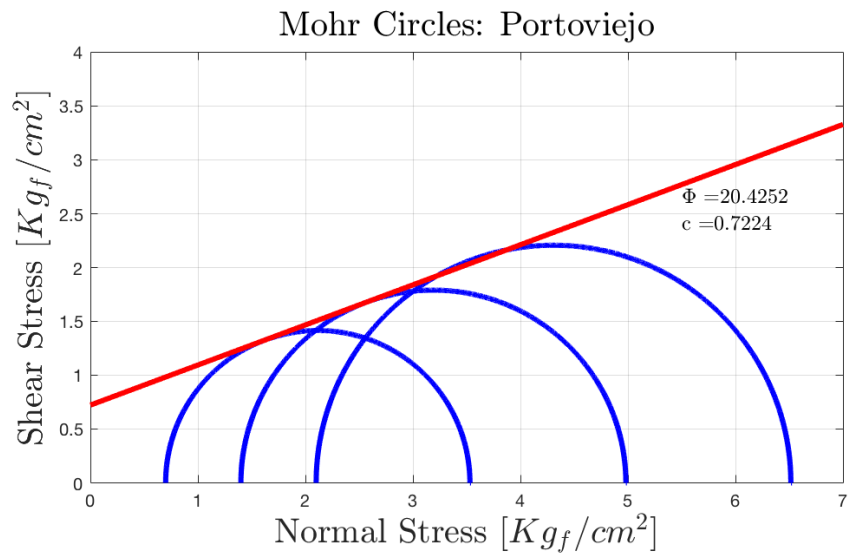


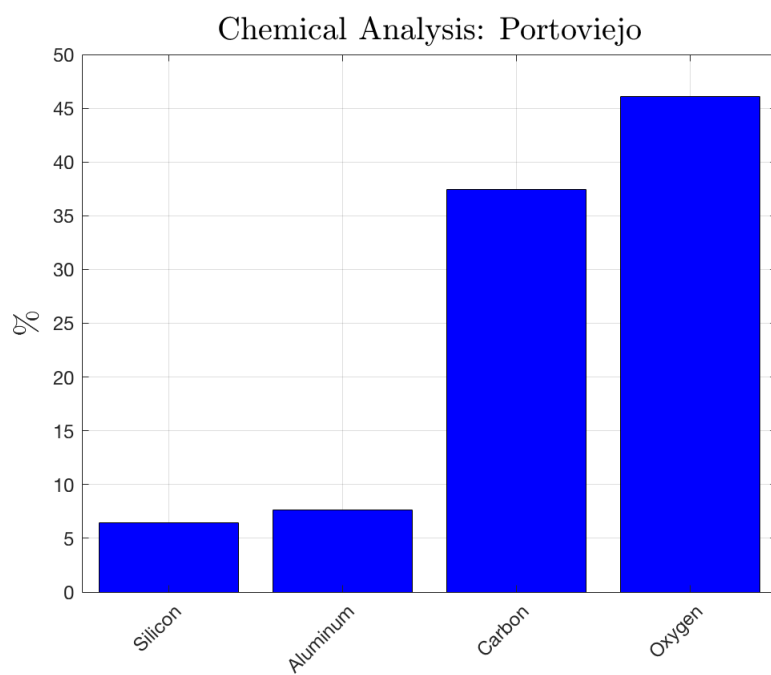
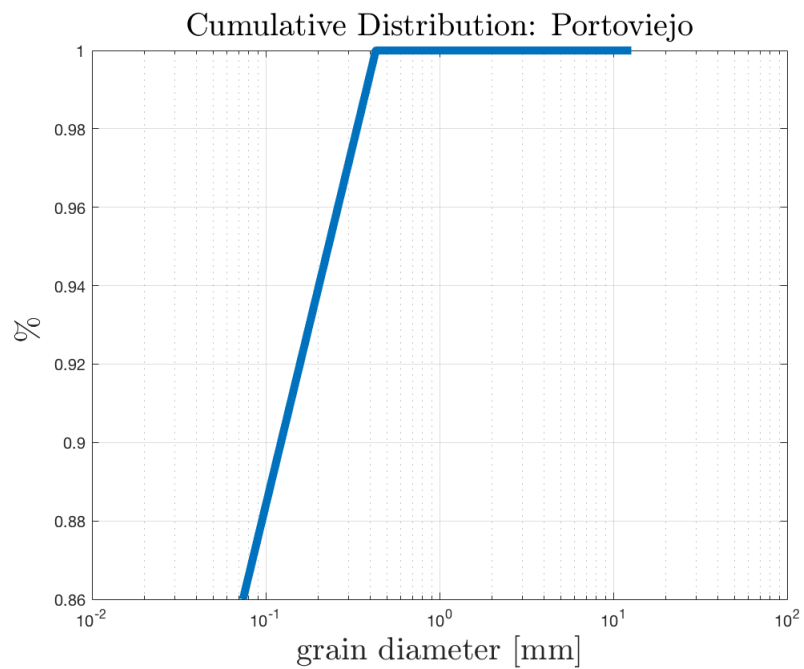
## A.15 Babahoyo



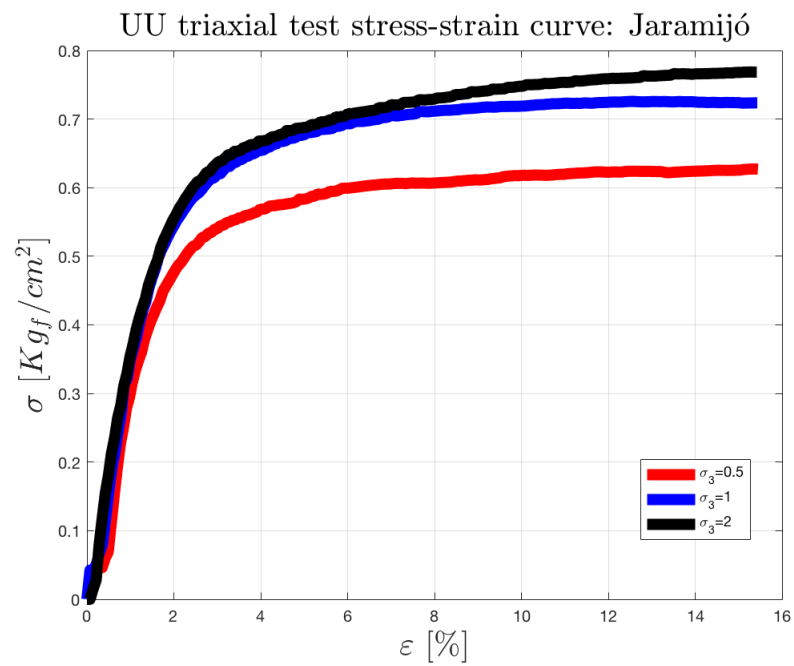
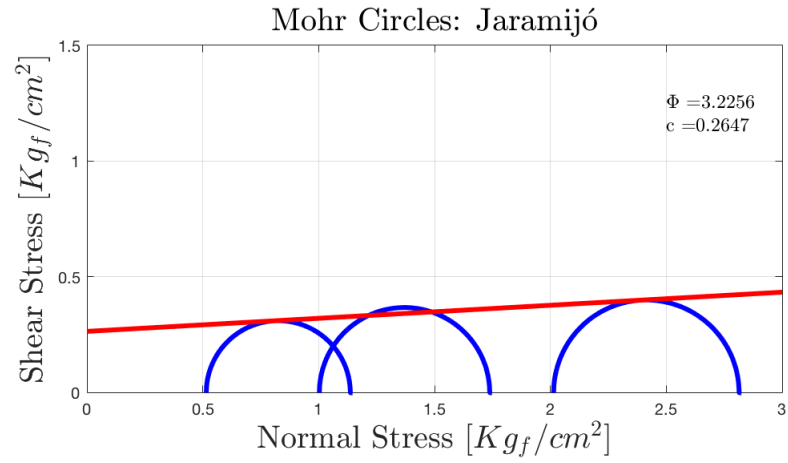


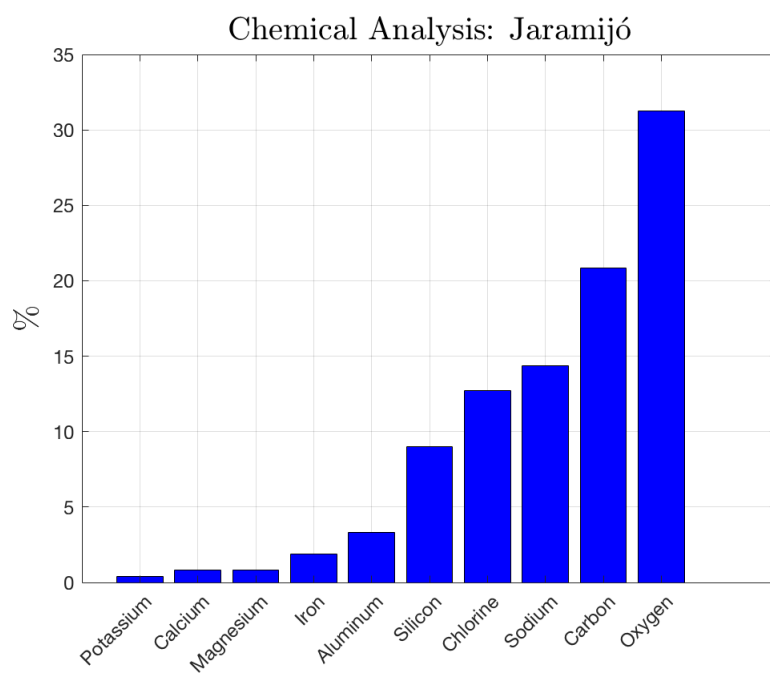
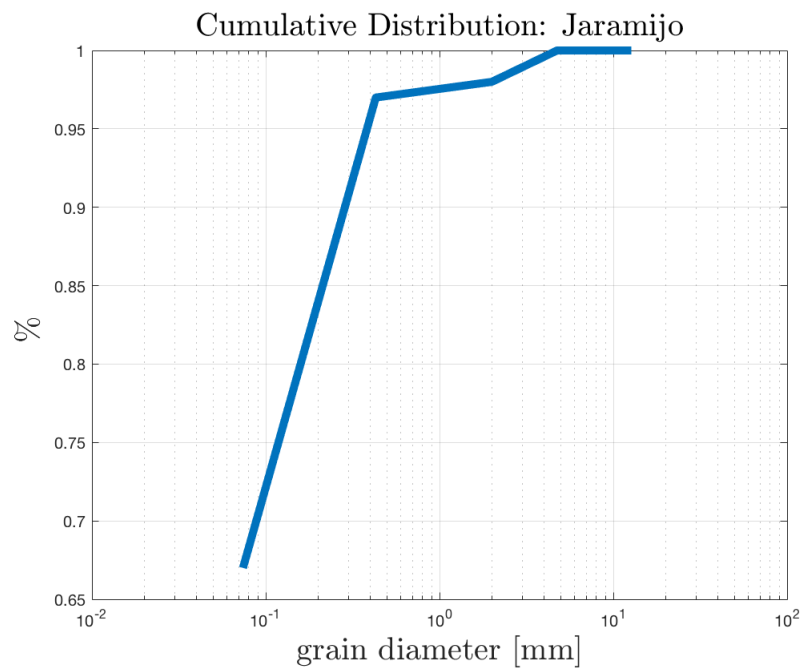
## A.16 Portoviejo



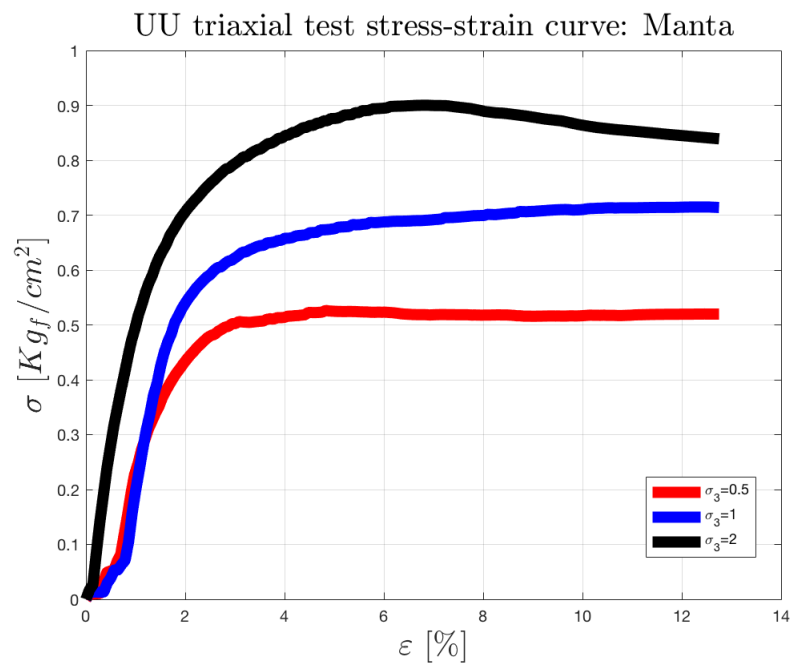
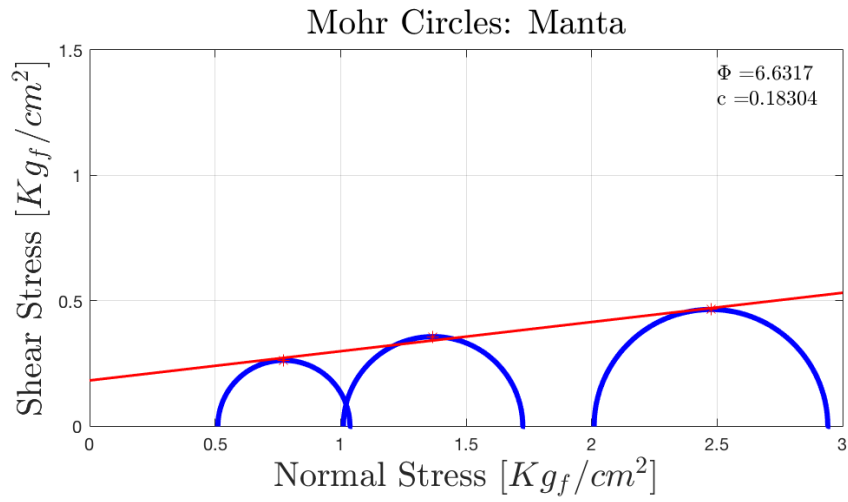


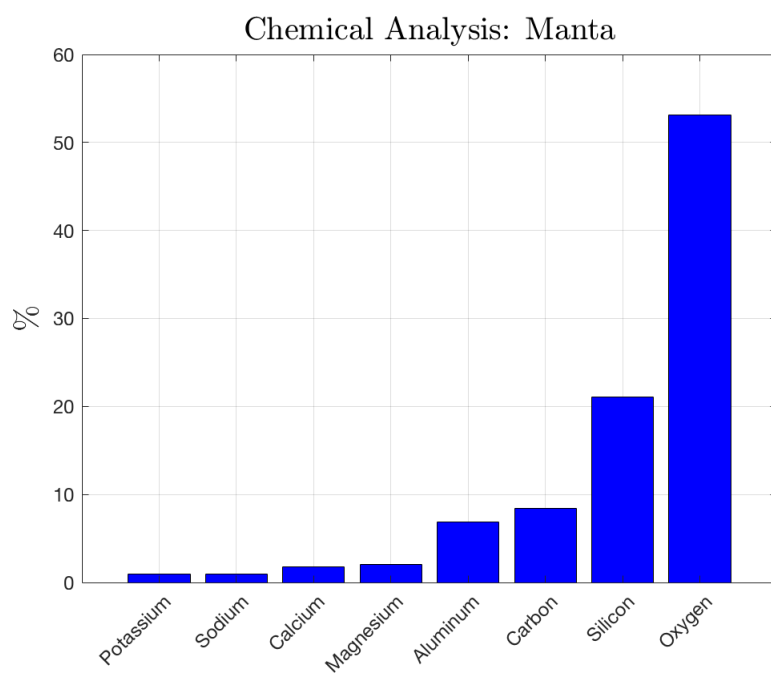
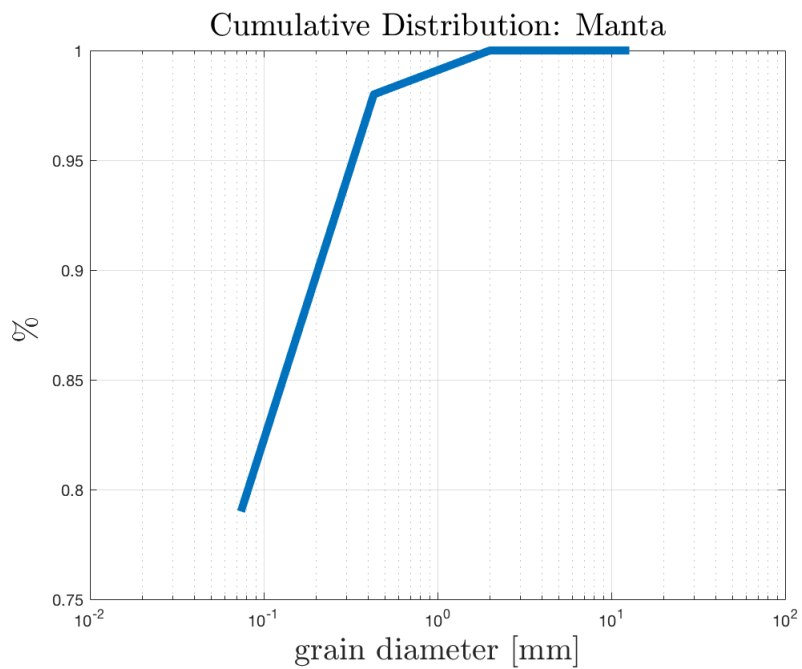
## A.17 Jaramijó





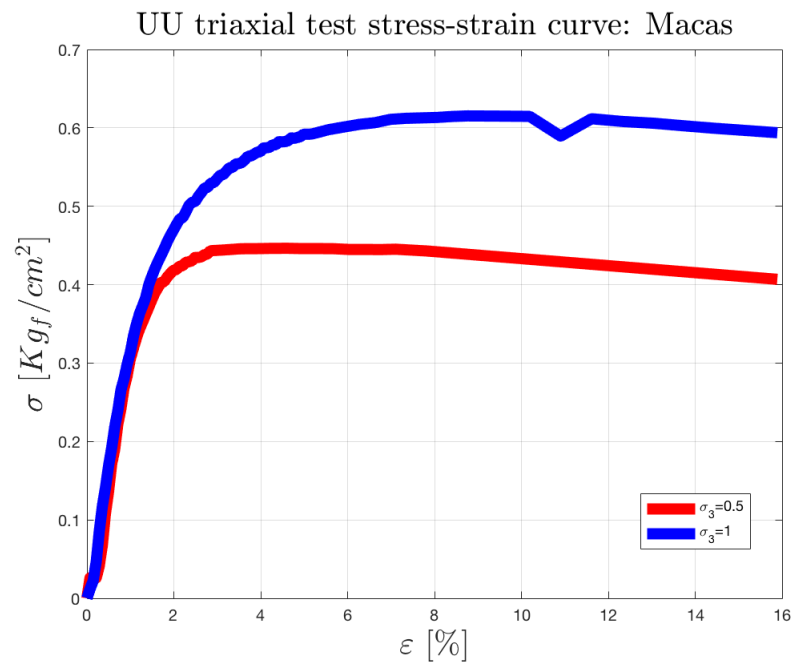
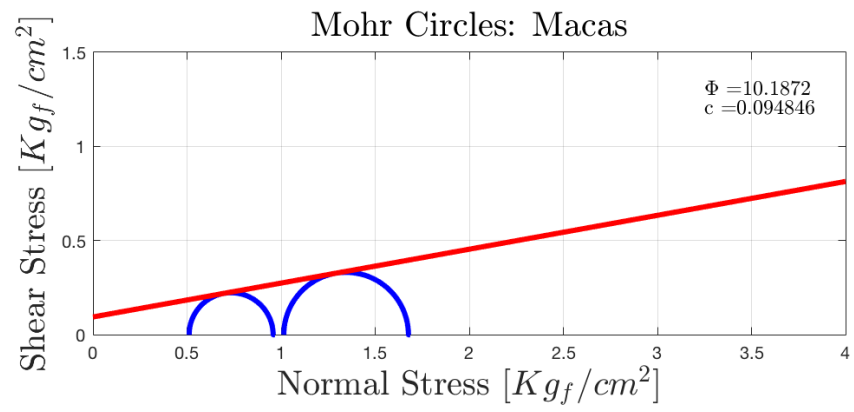
## A.18 Manta

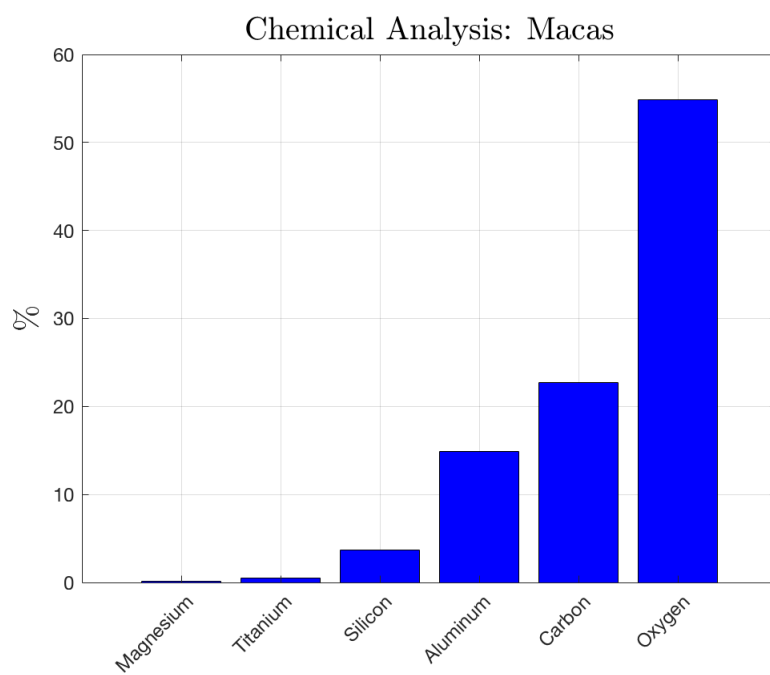
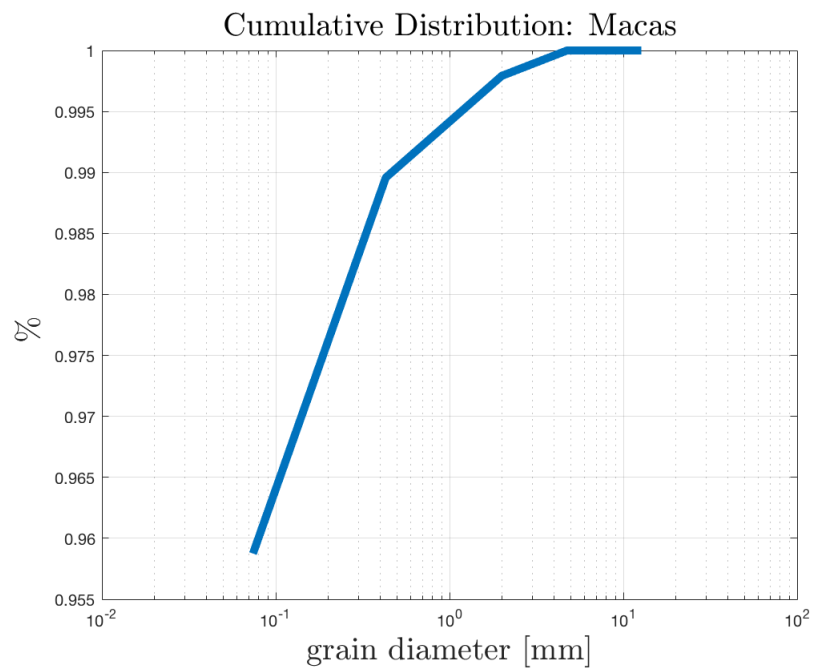




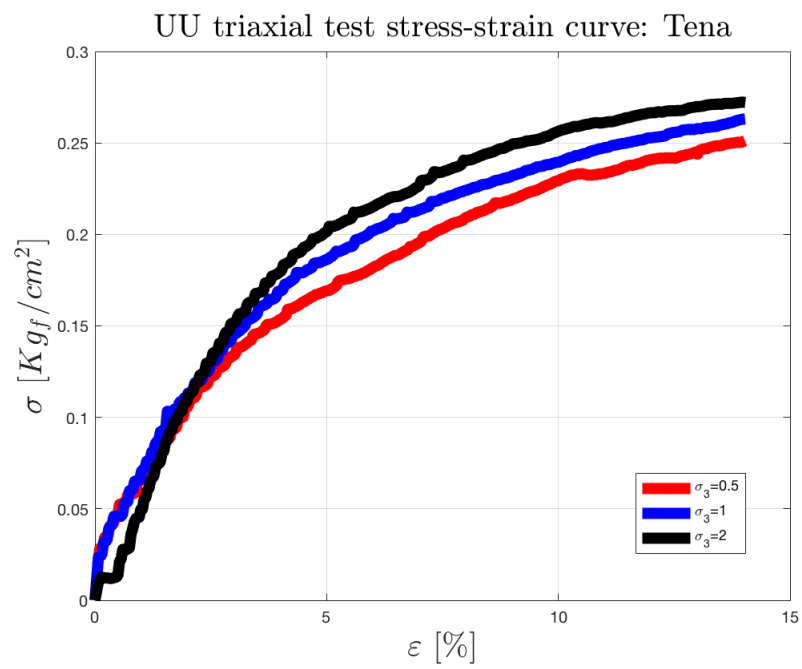
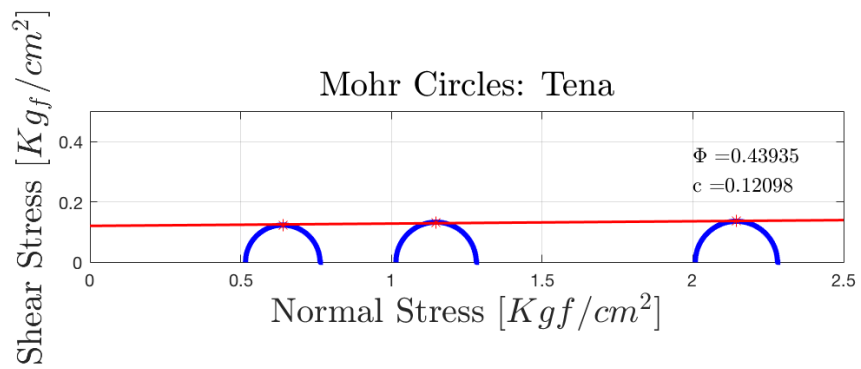


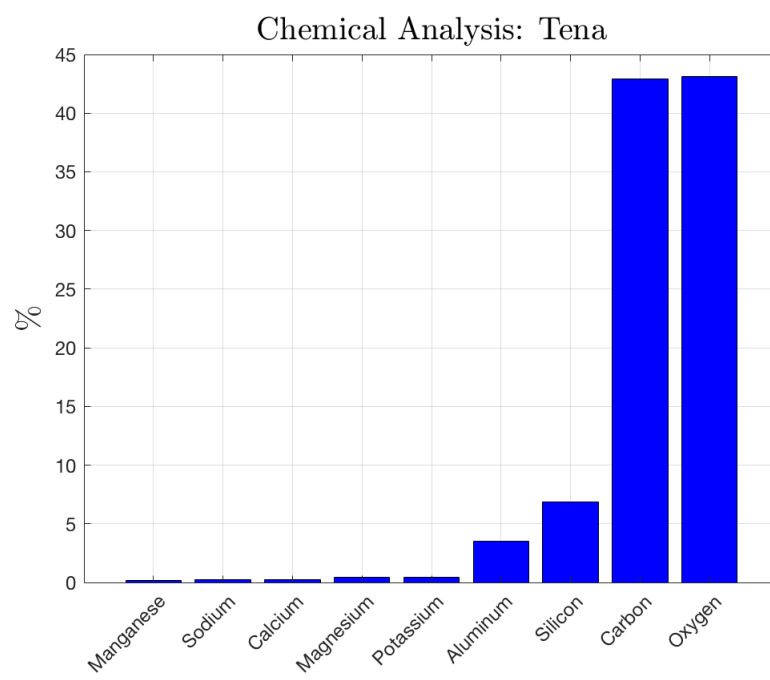
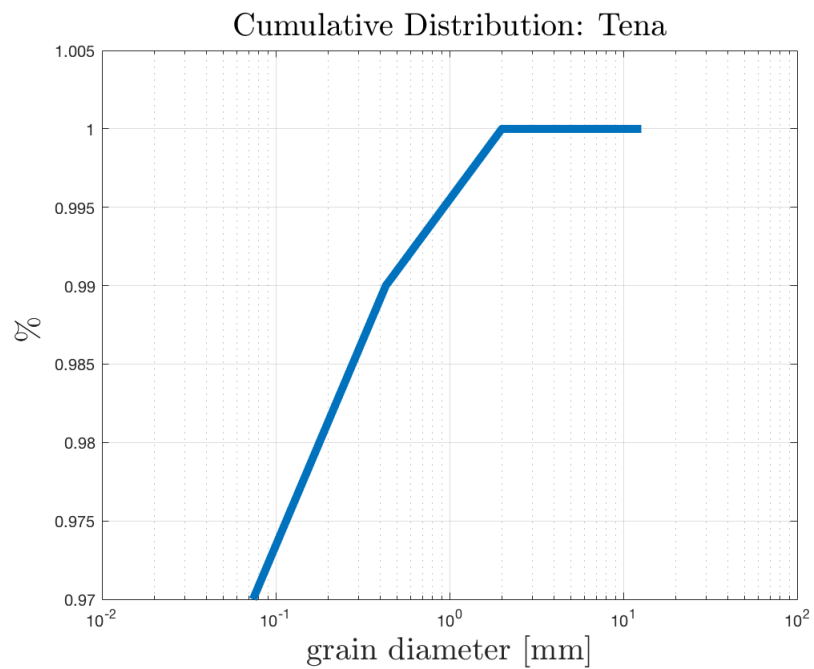
## A.19 Macas





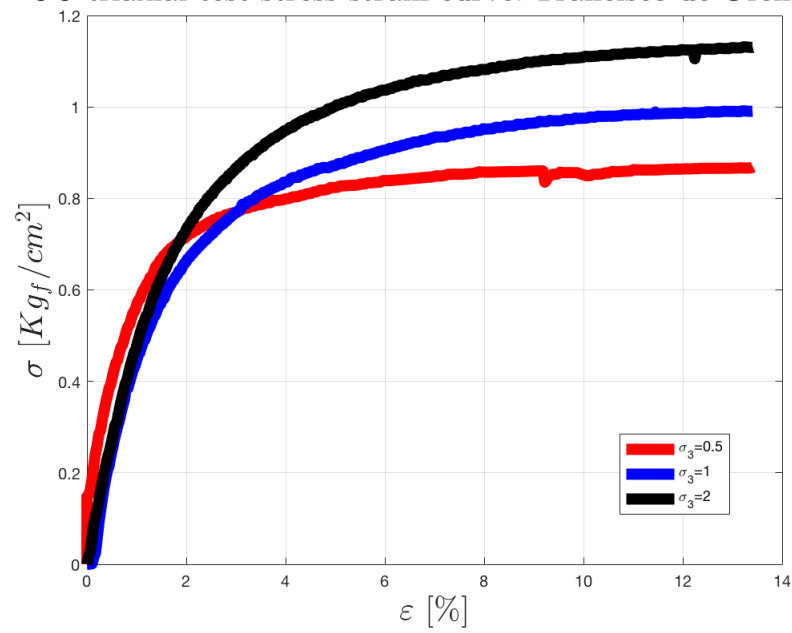
## A.20 Tena



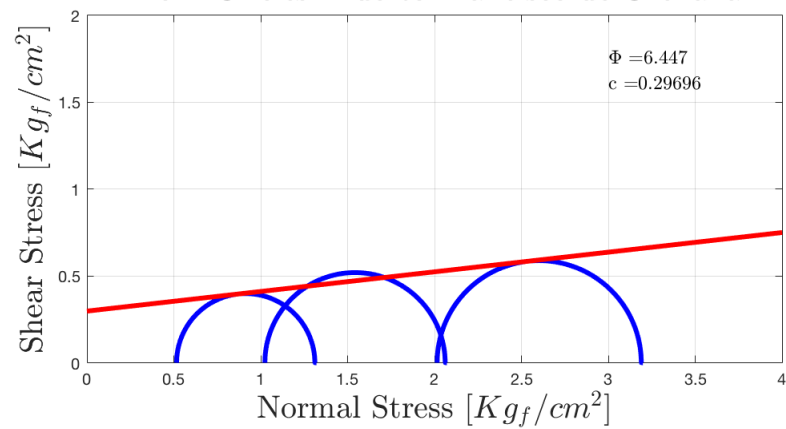


## A.21 Puerto Franciso de Orellana

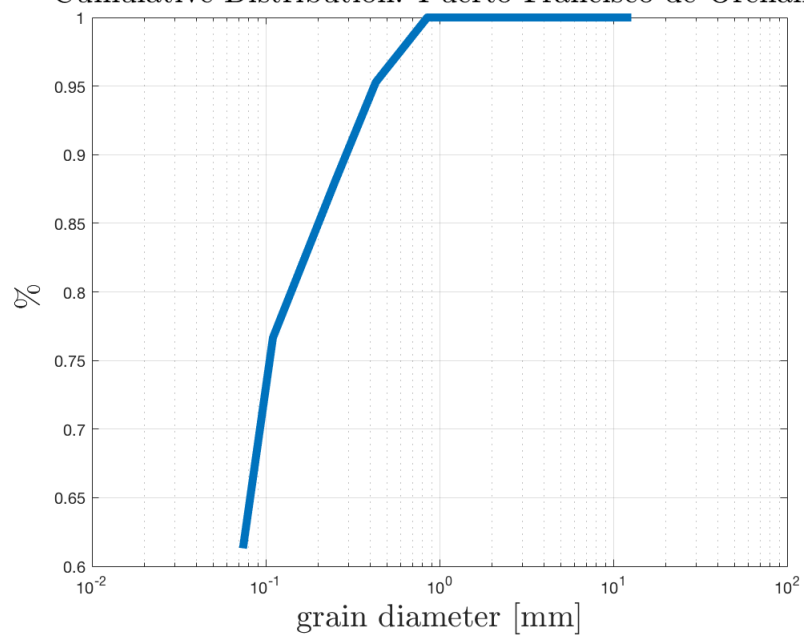
UU triaxial test stress-strain curve: Francisco de Orellana



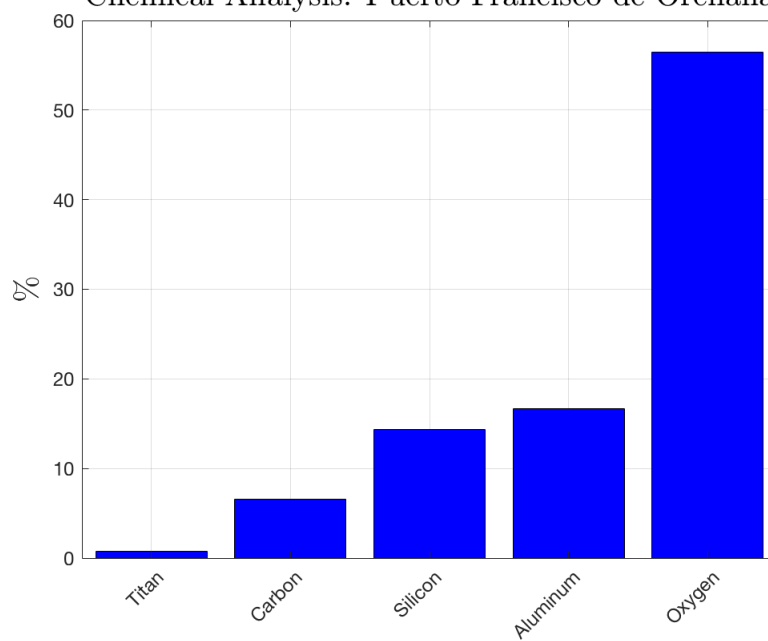
Mohr Circles: Puerto Franciso de Orellana



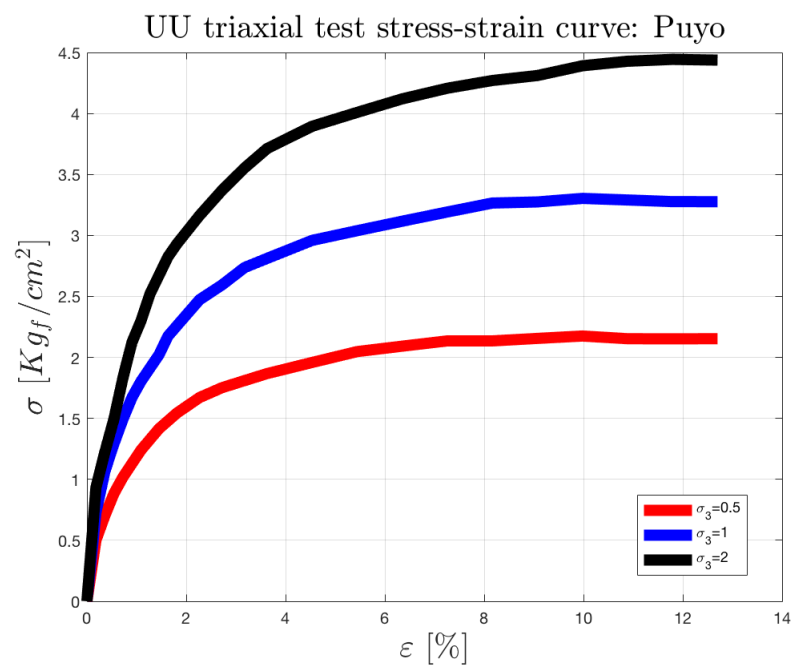
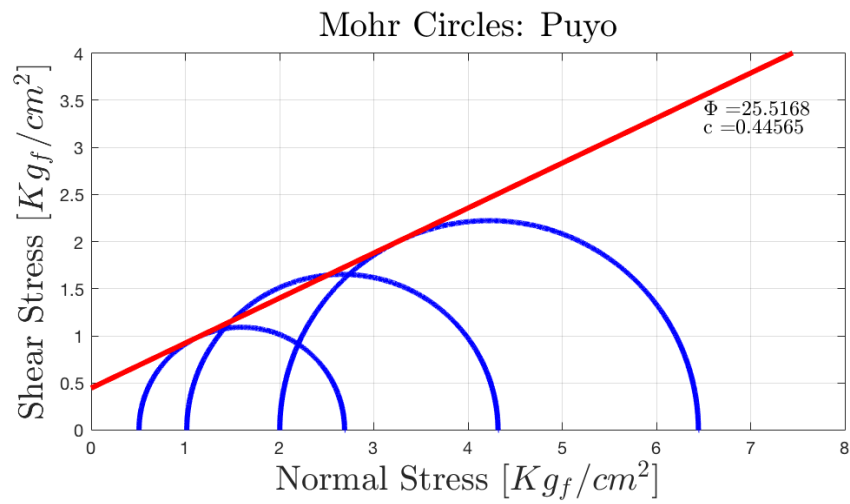
Cumulative Distribution: Puerto Francisco de Orellana

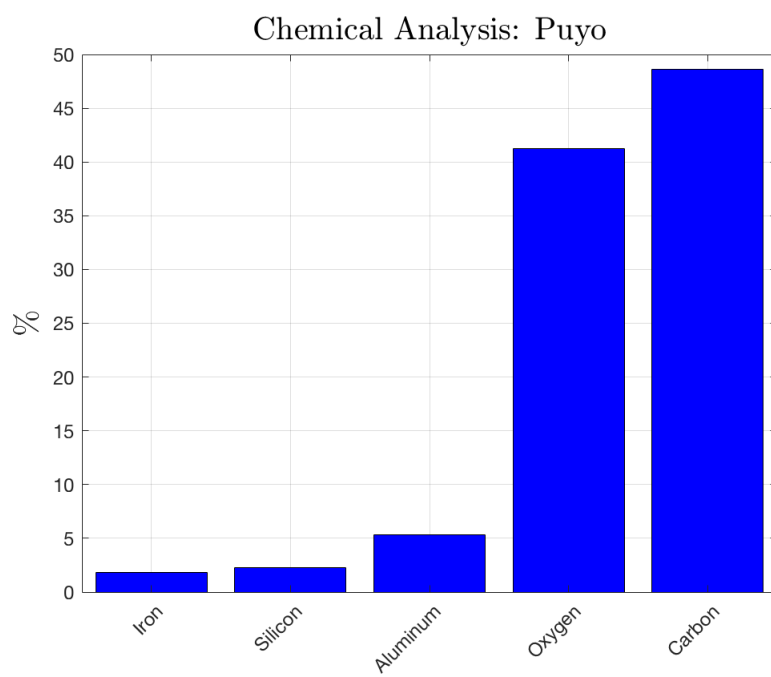
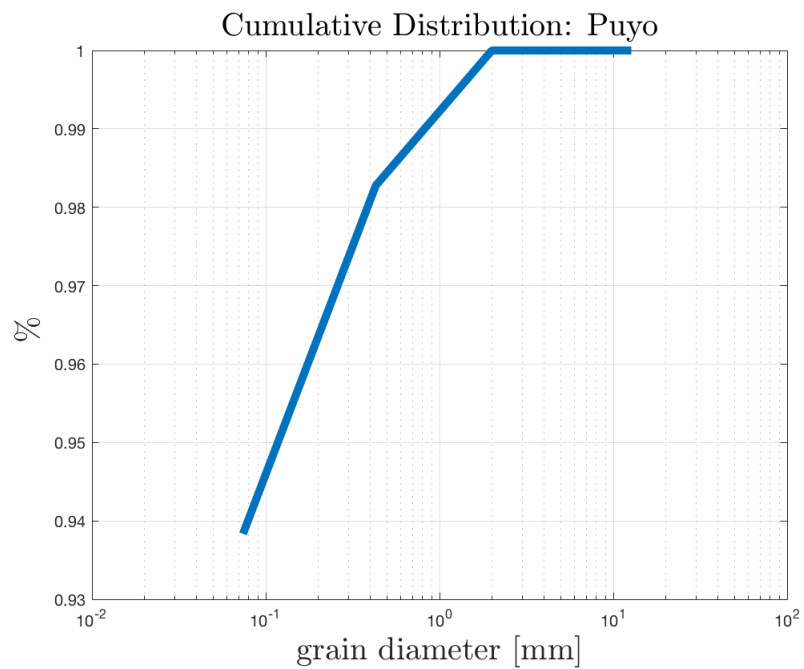


Chemical Analysis: Puerto Francisco de Orellana



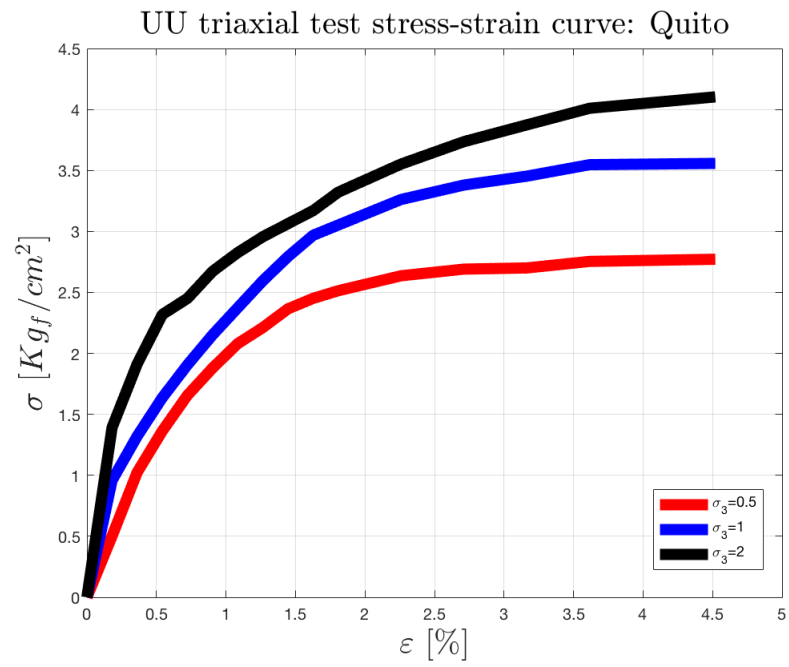
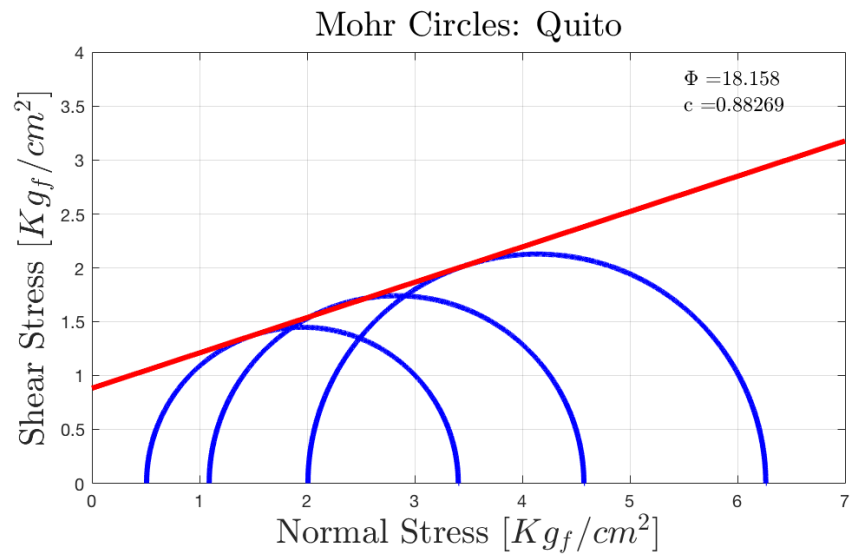
## A.22 Puyo

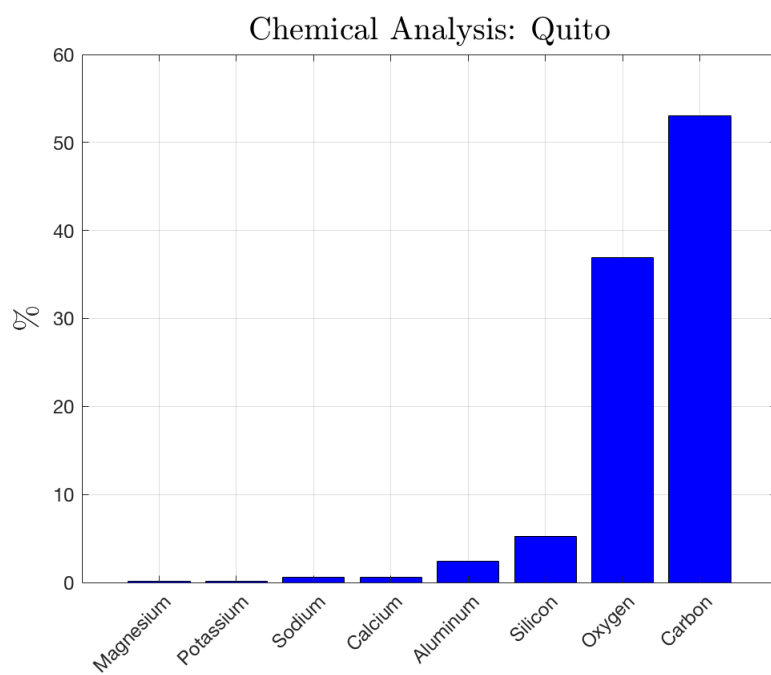
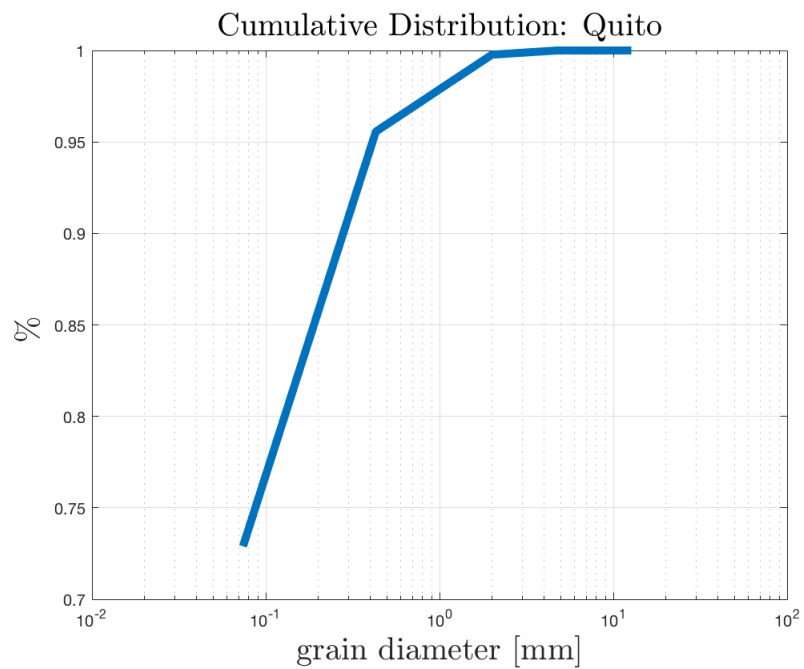




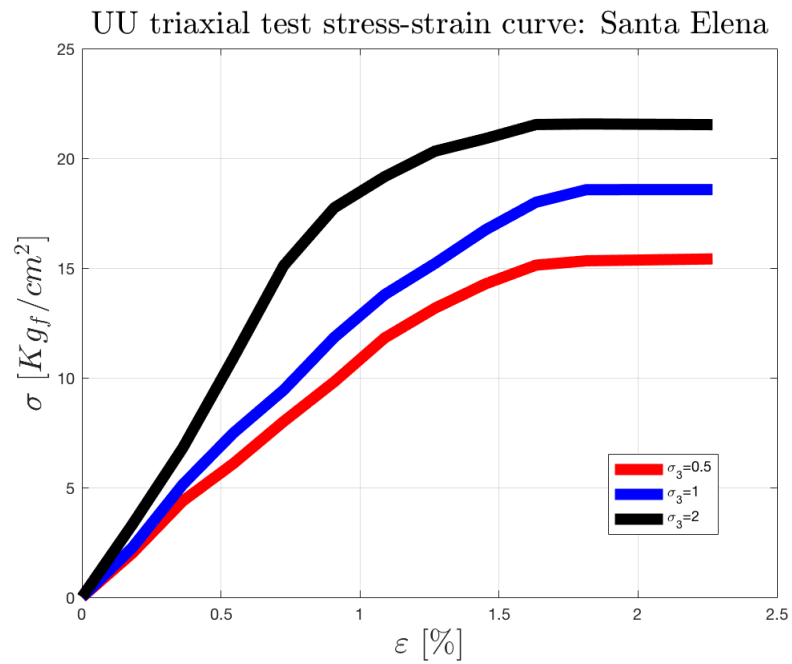
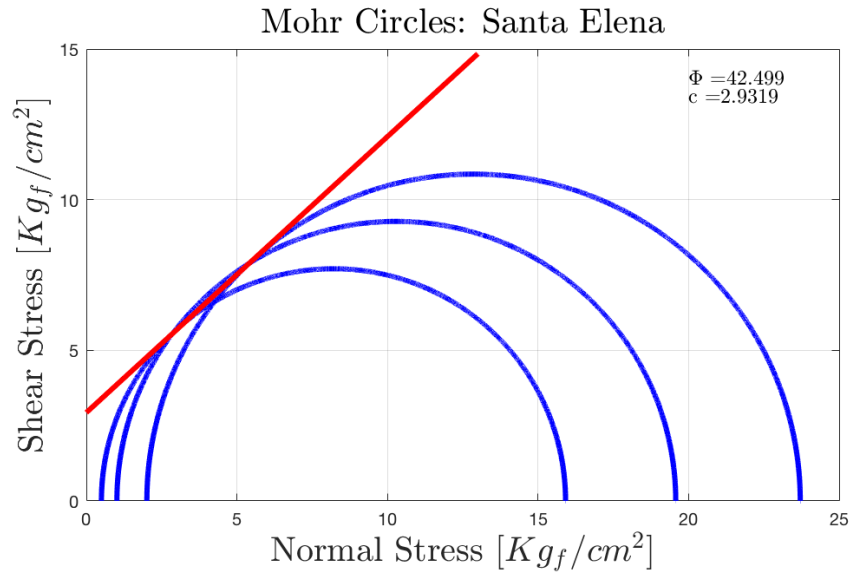


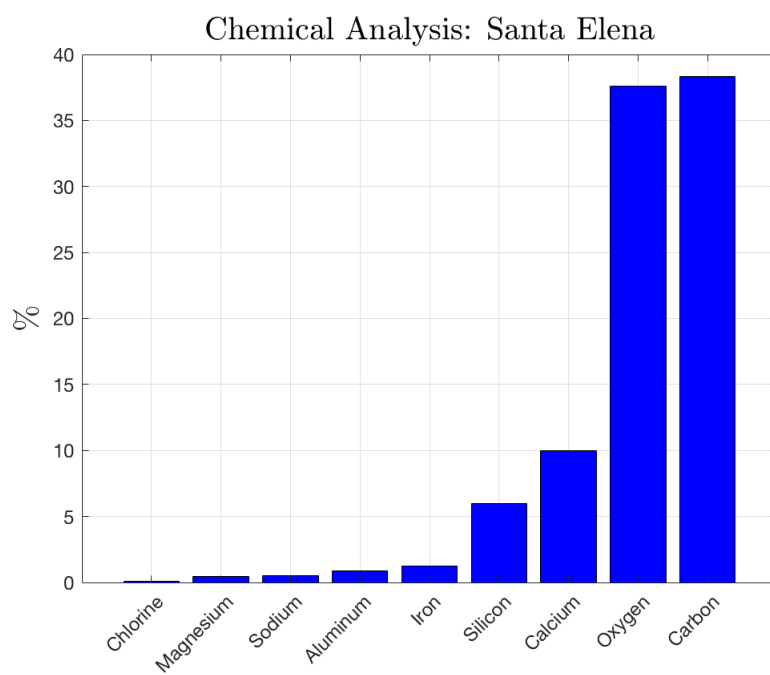
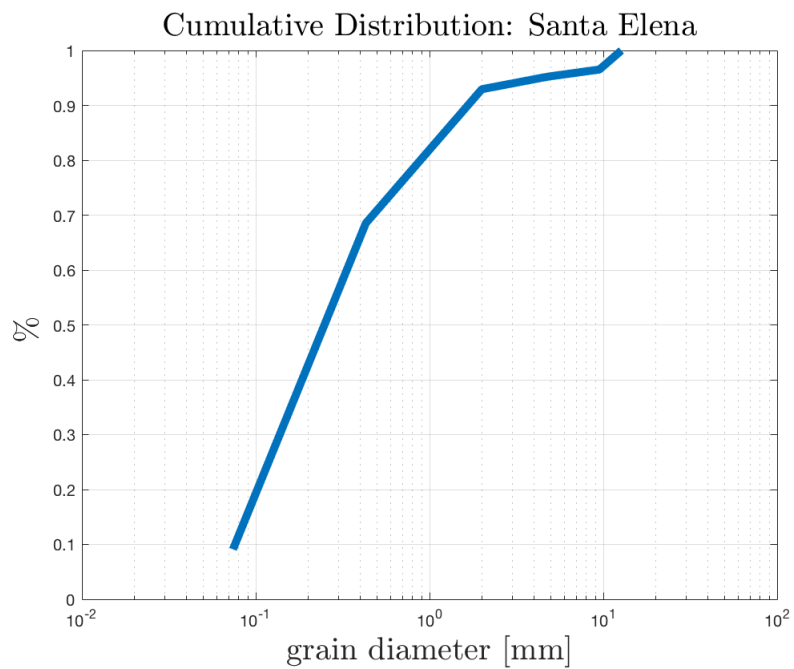
## A.23 Quito



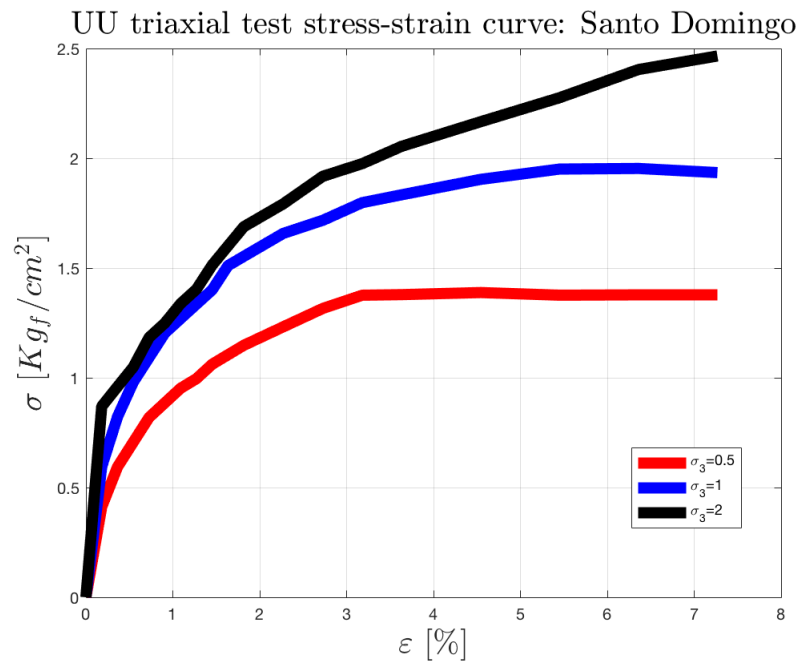
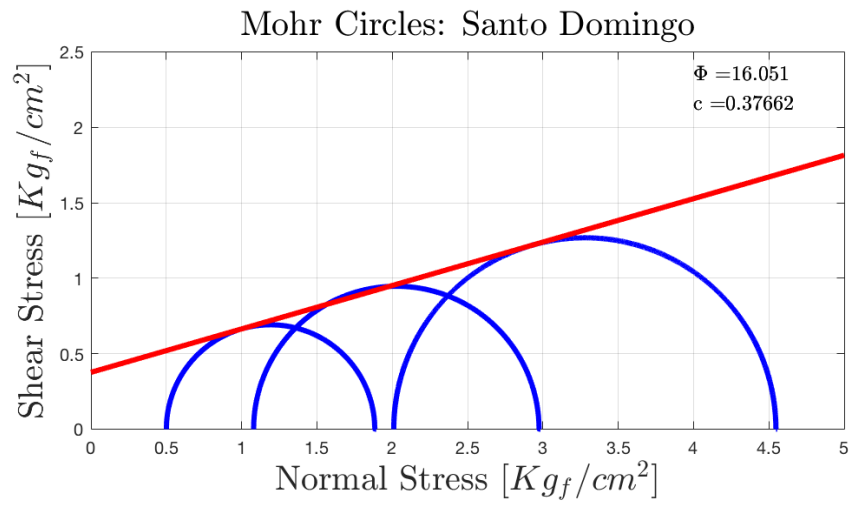


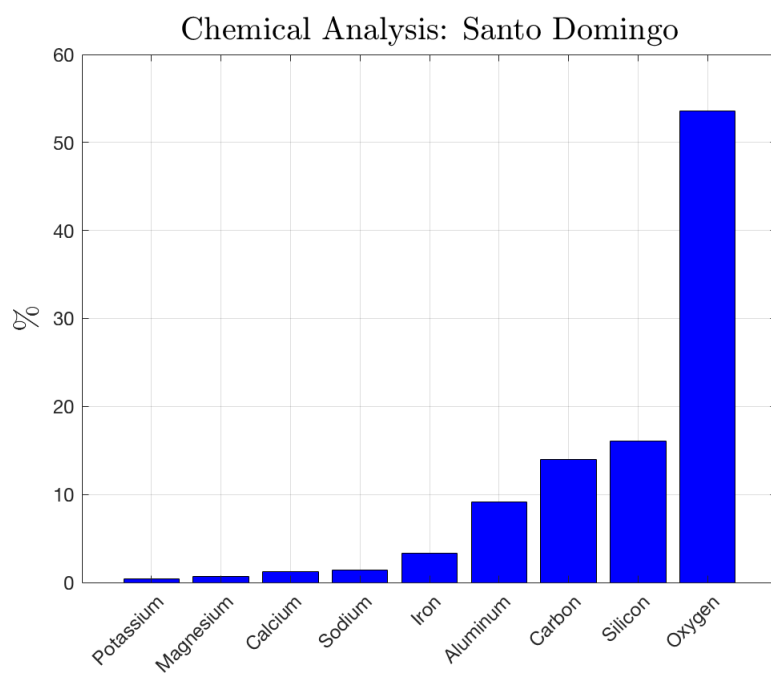
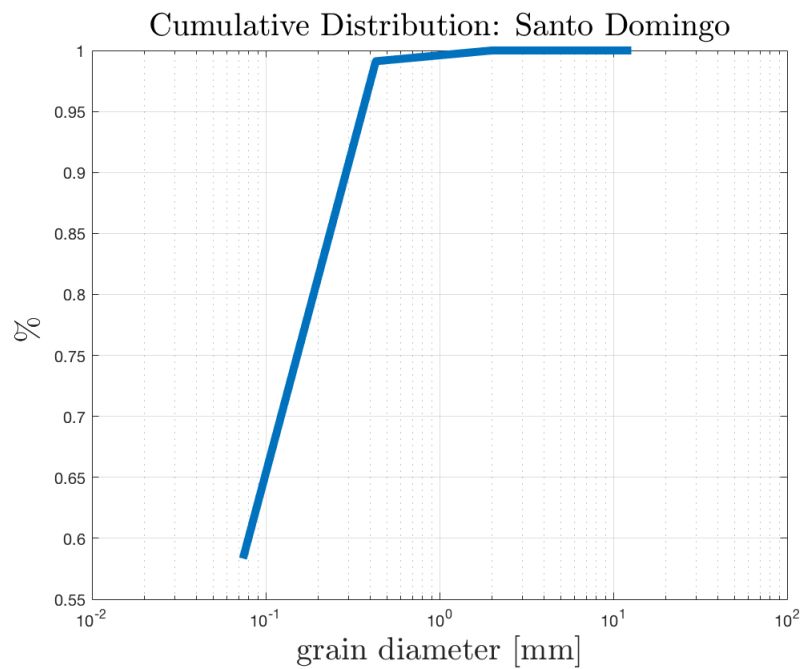
## A.24 Santa Elena



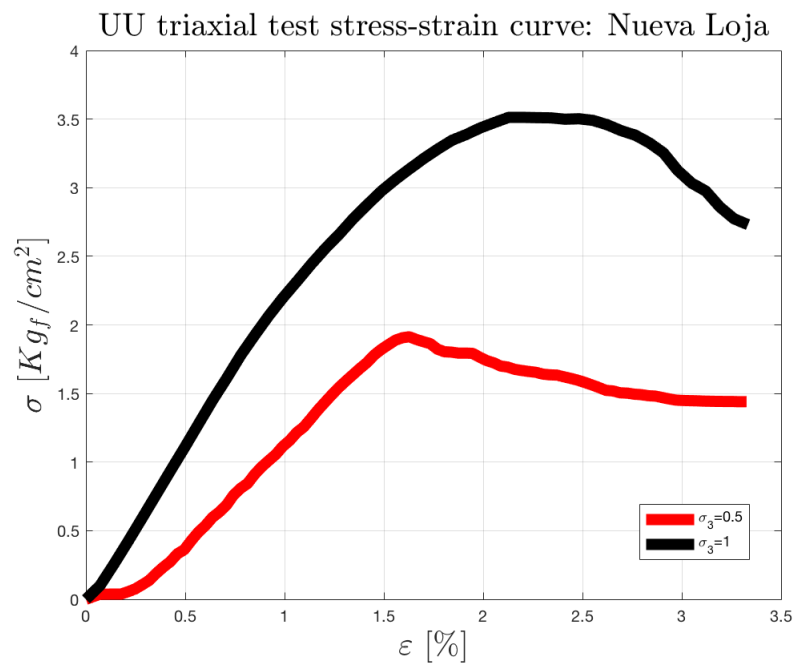
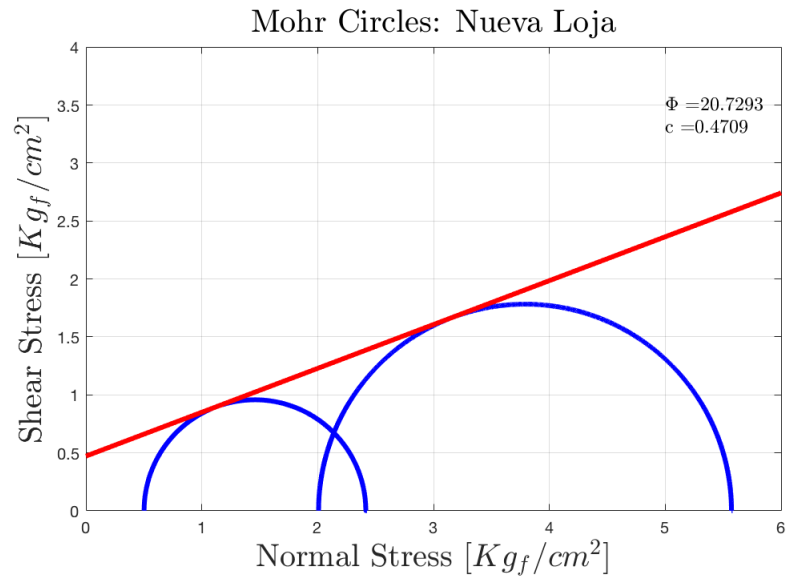


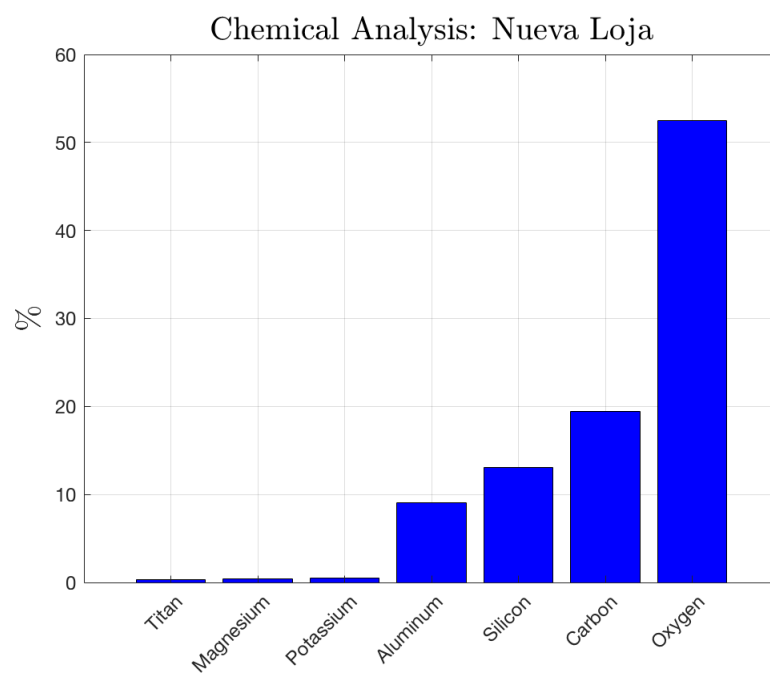
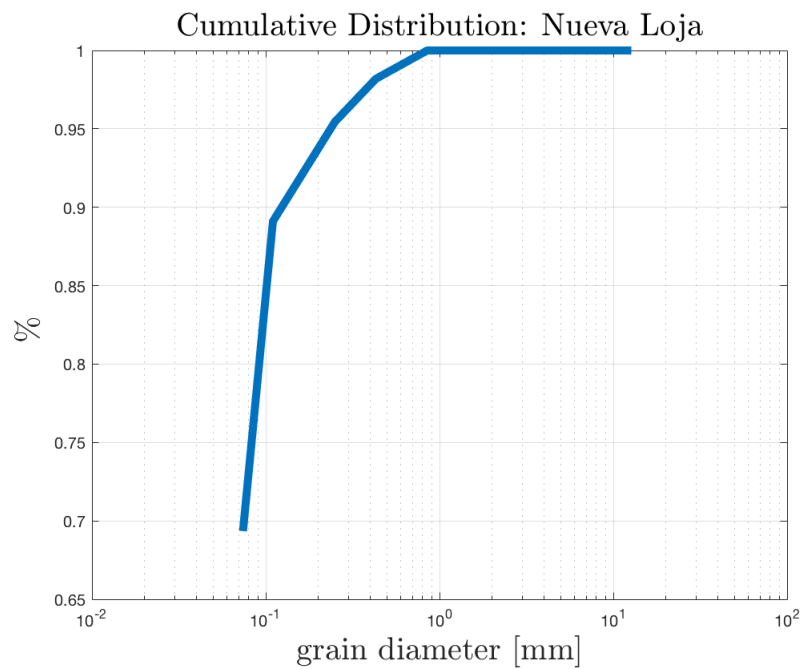
## A.25 Santo Domingo





## A.26 Nueva Loja

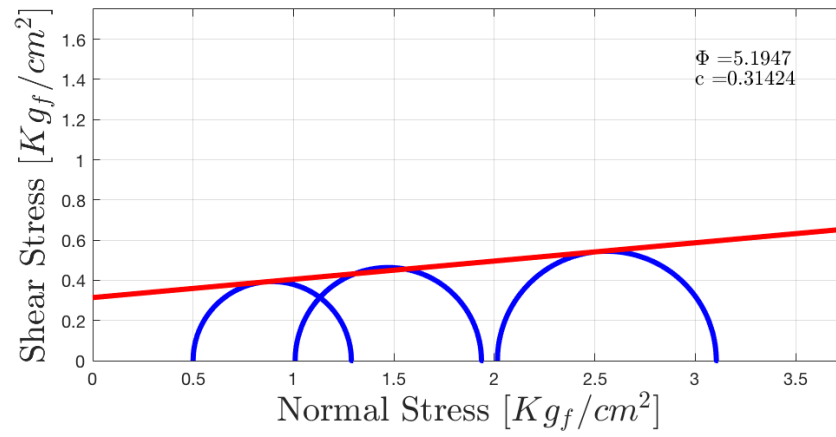




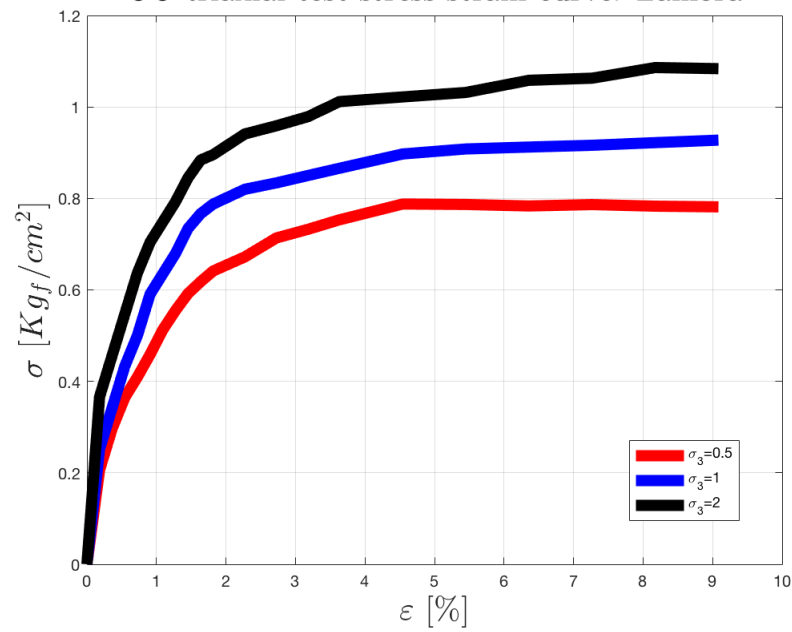


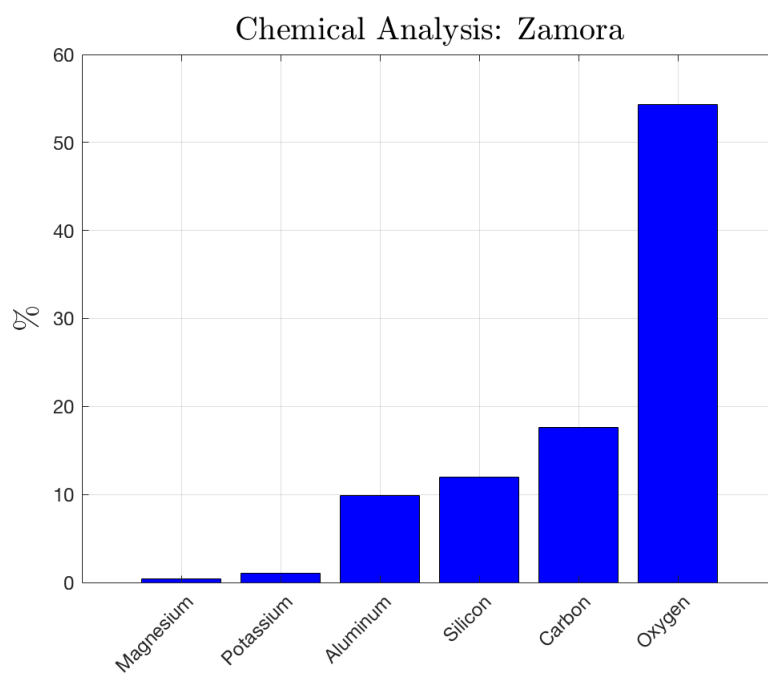
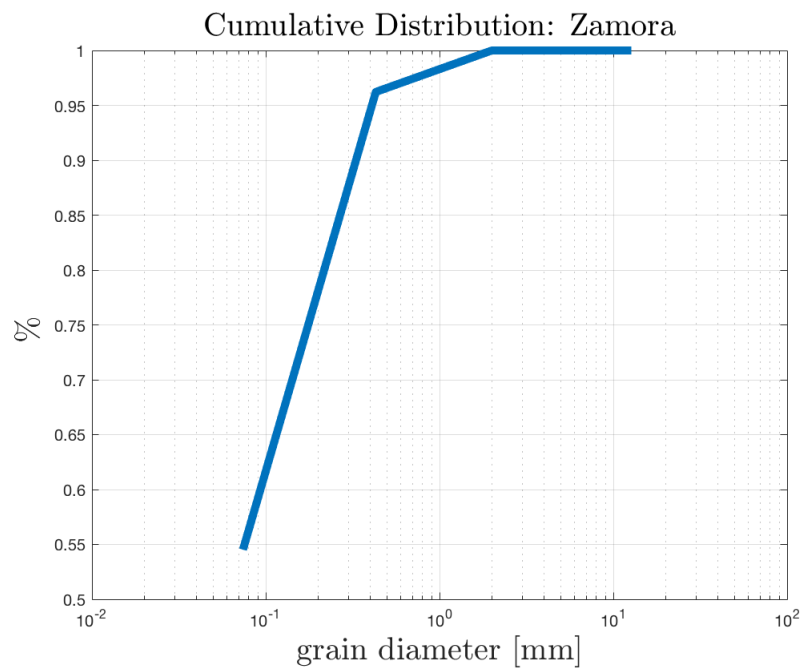
## A.27 Zamora

Mohr Circles: Zamora

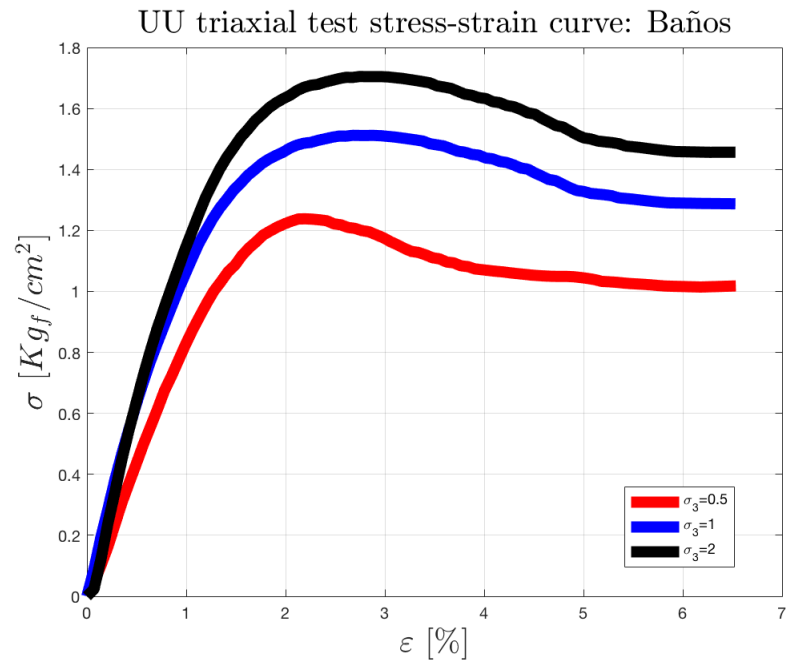
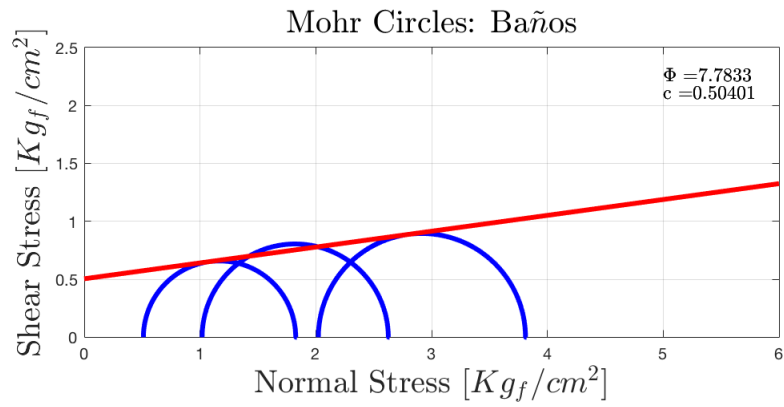


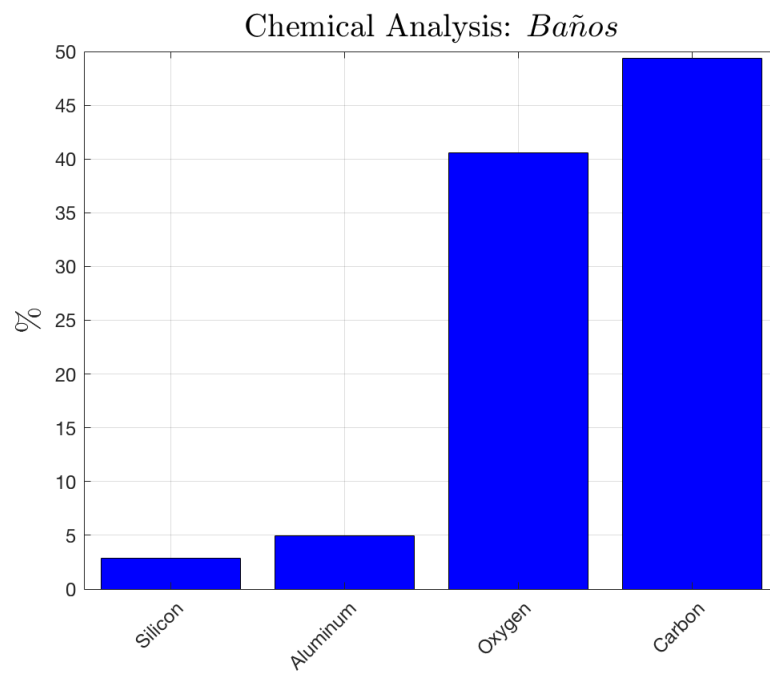
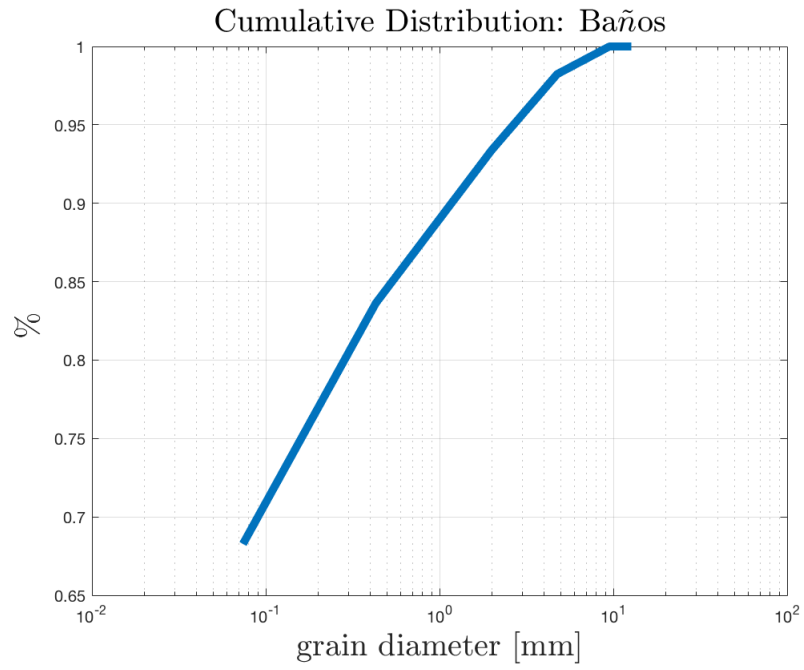
UU triaxial test stress-strain curve: Zamora





## A.28 Baños





## A.29 Ambato

